Pullout Capacity of Reinforced Concrete Deadman Anchors in Cohesionless Soil

by

Riley Padron

A Report Submitted to the Faculty of the

Milwaukee School of Engineering

in Partial Fulfillment of the

Requirements for the Degree of

Master of Science in Civil Engineering

Milwaukee, Wisconsin

May 2021

Abstract

Reinforced concrete deadman anchors are used by the nonprofit humanitarian organization Bridges to Prosperity (B2P) to arrest the suspension cables of pedestrian bridges they build in developing countries. The design methodology they use to determine the pullout capacity of these anchors relies on considering failure either in uplift or sliding, but not both in tandem. The focus of this research was to investigate the failure mechanics of a concrete anchor buried in dry, cohesionless soil as it is pulled by cables resisting the load of a pedestrian bridge. The research employed two major methods: a theoretical pullout capacity based on the limit equilibrium theorems of Meyerhof; and two-dimensional finite element modeling that was verified by quantitative and qualitative scale model testing. The results of the finite element modeling were used to create design charts based on anchor length, anchor height, soil density, soil internal friction angle, embedment depth, and the pullout angle of the cables. The results showed good correlation with what is predicted by Meyerhof's limit equilibrium equation but show that B2P's design methodology is overly conservative. The results of this research should be verified by full-scale or partial-scale model testing before any changes are adopted by B2P or their members, but it appears that limit equilibrium could be used as a working theoretical solution. Other variables that affect anchor pullout and are not covered in this research also need to be investigated for a more complete understanding of deadman anchor pullout capacity, including soil angle of dilatancy, cohesion, moisture content, sloping ground surfaces, modulus of elasticity, Poisson's ratio, and end effects.

Acknowledgments

There are many individuals and organizations who have contributed to this research and deserve acknowledgment.

Engineers without Borders, a fantastic organization that is a force of good abroad and at home. The inspiration for this research is due entirely to my life-changing experiences in Guatemala and the motivation to keep building infrastructure where it is most needed.

Bridges to Prosperity for being another fantastic organization and a guiding force in the development, design, and construction of these bridges. In particular, thanks to Alan Kreisa, Director of Engineering, for providing insight, information, and a focused scope.

GEOSLOPE International, in particular thanks to Curtis Kelln, PhD, P.Eng, for arranging a free license of SIGMA/W for use in this research.

Dr. Douglas Stahl and Dr. Richard DeVries for serving on my committee.

Dr. Christopher Raebel and Dr. Blake Wentz, for persistence.

Mr. Gary Shimek, M.L.I.S, for assistance and much-needed support.

Dr. Todd Davis, for guidance and patience.

Table of Contents

List of Figures

List of Tables

Nomenclature

Symbols

B = width of deadman anchor[1]

c = soil cohesion

D = depth from ground surface to bottom of deadman anchor[2]

E = Young's modulus of elasticity

F_f = frictional force developed between the bottom of the anchor and the soil

F'_q = Meyerhof's breakout factor

F'^{*}_q = Meyerhof's breakout factor for deep anchors beyond critical embedment ratios

F_x = forces acting on deadman anchor in horizontal direction

F_y = forces acting on deadman anchor in vertical direction[3]

H = height of deadman anchor[4]

K_a = active earth pressure coefficient

K_b = dimensionless earth pressure coefficient by Meyerhof

K_p = passive earth pressure coefficient

L = length of deadman anchor

P = pullout force[5]

P_{active} = resultant force of active earth pressure

$P_{friction}$ = pullout capacity of deadman anchor due to the limit state of friction

---

[1] This symbol, in either lowercase or uppercase form, also appears in this paper representing other variables in the Literature Review. Those uses are defined in each instance by the author of the literature referenced and are defined as needed by occurrence. The definition shown here is per the Problem Definition of the research subject as illustrated in Figure 30 and is the de facto definition.
[2] See footnote 1.
[3] See footnote 1.
[4] See footnote 1.
[5] See footnote 1.

$P_{Meyerhof}$ = pullout capacity of deadman anchor based on Meyerhof's limit equilibrium

$P_{passive}$ = resultant force of passive earth pressure

P_{uplift} = pullout capacity of deadman anchor due to the limit state of uplift

P_{ult} = ultimate pullout capacity of deadman anchor

P_x = horizontal component of pullout force based on angle θ

P_y = vertical component of pullout force based on angle θ

Q'_u = Meyerhof's net ultimate holding capacity of shallow inclined rectangular anchors

R = Oveson's modifier

S = anchor spacing for three-dimensional end-effects

w = soil moisture content[6]

W_{anchor} = self-weight of deadman anchor

W_{soil} = self-weight of soil above the deadman anchor

$W_{overburden}$ = self-weight of overburden material above anchor (trapezoidal shape)

δ = angle of friction for deadman anchor-soil interface

γ_a = unit weight of deadman anchor material

γ_s = unit weight of soil material

ν = Poisson's ratio

∑ = sum of included variable

φ = soil internal angle of friction[7]

Ψ = angle of dilatancy of soil[8]

θ = pullout angle of deadman anchor measured from the horizontal plane

---

[6] See footnote 1.
[7] See footnote 1.
[8] See footnote 1.

Abbreviations

AASHTO	American Association of State Highway and Transportation Officials
B2P	Bridges to Prosperity
EWB	Engineers without Borders
LRFD	Load and Resistance Factor Design
LVDT	Linear Variable Differential Transformer
MSOE	Milwaukee School of Engineering

Glossary

Apex: Of an isosceles triangle, the included angle between the two sides having the same length.

Actuator screw: A rotating screw mechanism that drives linear motion via a threaded nut around the screw shaft.

Catenary: The curved shape that an idealized wire rope cable will form when hanging under its own weight as well as the weight of a uniformly distributed load in the case of the cable-suspension style bridges.

Centroid: The geometric center of a physical shape or body.

Cohesion: An engineering property of soil used to describe a component of the soil's shear strength due to interparticle attraction.

Cohesionless (soils): Used to refer to soils that have negligible cohesion in their natural state, i.e., sands and gravels.

Cohesive (soils): Used to refer to soils that have a measurable cohesion in their natural state, i.e., clays and silts.

Deadman anchor: A buried object used to resist movement of an above-ground object, primarily through self-weight and soil weight resistance.

Dilatancy: The property of a granular soil describing its volume change when subjected to shear stress. In compacted dense granular soils, the change is typically expansive under shear, caused by the shifting and mobilizing grains moving around one another from their original compacted state.

Effective: In describing soil properties, the condition of having pore water pressure in an undrained soil mass that acts primarily to decrease strength.

Elastic: In soils, the linear portion of the stress-strain curve whereby the strains experienced by the soil are linearly related to the stresses applied.

Elastoplastic/Elastic-plastic: Having both elastic and plastic properties or conditions.

Factor of safety: A value indicating the multiplier by which a system is stronger than required to resist design loads.

Finite element model: In structural analysis, a model, typically computerized, used to calculate stresses and strains in a structural element or system by subdividing the element or system into smaller simpler parts called finite elements.

Internal friction angle of soil: An engineering property of soil used to describe a component of the soil's shear strength due to interparticle friction.

Limit equilibrium/analysis: A method of engineering investigation into the stability of a rock or soil mass using an assumed failure plane and calculating shear stresses and yield points. The equilibrium is found by balancing driving forces to resisting forces, and an iterative process is used to determine the controlling limit state and a resultant factor of safety against failure.

Mesh: The divided area of a finite element model made up of the finite elements themselves.

Modulus of elasticity: A soil parameter describing elastic soil behavior as a measure of soil stiffness. The modulus of elasticity of a soil is defined as the ratio of stress along an axis or plane over the strain along that axis or plane only in the range of elastic (linear) soil behavior.

Mohr-Coulomb failure criterion: The envelope of the elastic/linear portion of a material's behavior under normal stress and the resulting shear strength.

Moisture content: The ratio by weight of the amount of water to the amount of solids in a soil mass.

Node: The connection points of finite elements in a finite element model that characterize movement and deformation based on the applied stresses and strains to the particular nodes as defined by shape functions.

Plastic: In soils, the non-linear portion of the stress-strain curve whereby the strains experienced by the soil cannot be linearly related to the stresses imparted to it. In the plastic zone of deformation, permanent strain is observed after reaching the yield strength of the material.

Poisson's ratio: A dimensionless ratio used to describe the behavior of a stressed material in the direction perpendicular to the direction of loading. The value of Poisson's ratio is the negative ratio of transverse strain to axial strain.

Qualitative: Describing research or data that is performed or collected through observation of non-numerical data.

Quantitative: Describing research or data that is performed or collected through systematic empirical investigation and measurement of numerical data.

Rankine's theory: Specifically relating to earth pressures, the theory of assuming no wall friction, cohesionless soil, a vertical soil-wall interface, a planar failure surface, and the resultant earth pressure force is parallel to the backfill surface.

Shear: Force applied parallel to a plane that acts against a force in the opposite direction that is offset to the other side of the plane. These unaligned forces cause shear stress along the plane.

Shear Strength: The ability of a material to resist failure by shear.

Body of Report

Chapter 1: Introduction, Background, and Literature Review

1.0 Introduction

Bridges to Prosperity (B2P) is a United States-based nonprofit organization that is committed to providing reliable footbridges over impassable crossings in developing countries. B2P builds these bridges as well as trains communities to build them independently using primarily locally-sourced materials. The footbridges for which B2P provides design and construction resources are of two types: suspended-cable and suspension-cable. The suspended-cable bridges are built by constructing large, short, and heavy stone-masonry towers on either side of the river that support cables hung between them upon which a walking surface is built (Figure 1). The cables are cast into concrete anchors built into each of the stone-masonry towers, with the design intention being that the entire tower resists the cable tension as the bridge is loaded.

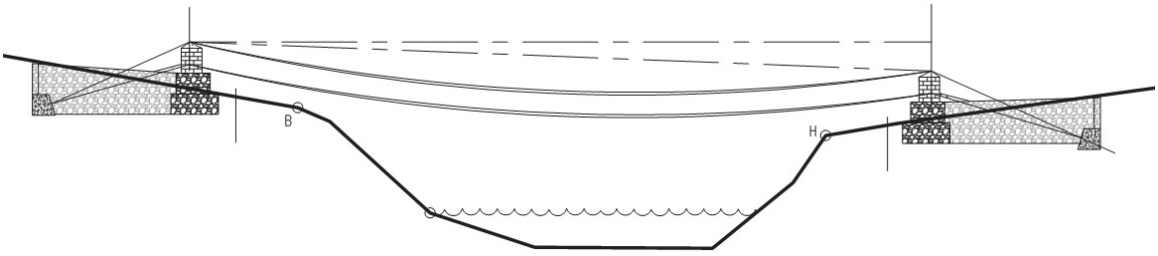

Figure 1 – Typical Geometry of a B2P Suspended-Cable Footbridge (Bridges to Prosperity, 2016).

The suspension-cable bridges follow a more conventional suspension bridge geometry, with a walkway supported by overhead cables with a larger curvature that cross over tall,

slender steel or concrete towers and are cast into a deadman concrete anchor buried below the ground behind the towers (Figure 2). Because of a larger curvature or "sag" the cable tension is intended to be much lower than in the suspended-cable version and the deadman anchor resists this tension alone. This suspension-cable bridge deadman anchor is the subject of this report and therefore the towers and/or anchors of the suspended-cable bridges will not be discussed, and it is not intended that the results of this research be applied to their design in any capacity. The subject of this report is an investigation of concrete deadman anchors used in B2P suspension-cable bridges, to more accurately predict pullout capacity and possibly improve upon the existing B2P design methodology.

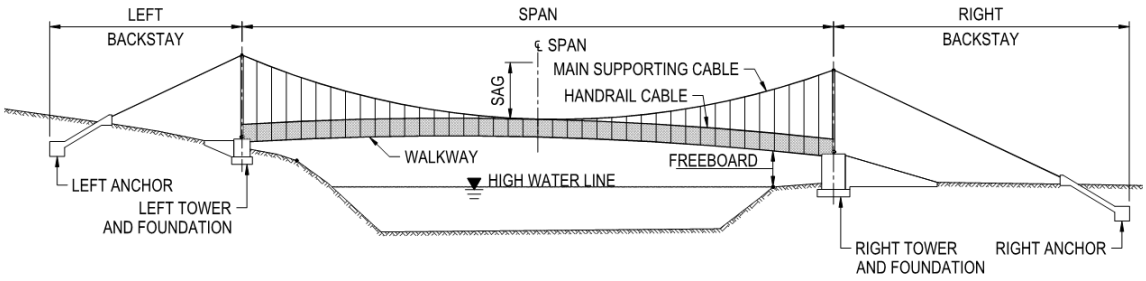

Figure 2 – Typical Geometry of a B2P Suspension-Cable Footbridge (Bridges to Prosperity, 2016).

1.1 Background – Bridges to Prosperity Design Methodology

B2P publishes its own *Bridge Builder Manual* (Bridges to Prosperity, 2016) that details the design and construction of their two bridge styles; Volume 3 contains a full design example of a suspension-cable bridge. The capacity of the deadman anchor to resist the cable tension in their design example is separated into two components based on two

possible assumed failure modes: by forces in the horizontal direction (sliding resistance) and vertical direction (uplift resistance).

1.1.1 Horizontal Forces

The horizontal forces are active and passive earth pressure, the horizontal component of the cable tension, and friction force between the concrete anchor and the soil below. The B2P design example shows the earth pressures acting over the height of the anchor and a portion the soil above, which is shown as one-half the height of the anchor in Figure 3.

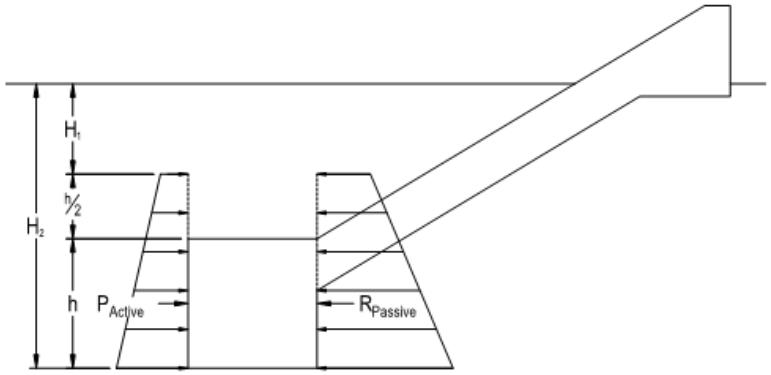

Figure 3 – Free-Body Diagram Showing Horizontal Earth Pressure Forces Acting on Deadman Anchor and Soil Above Anchor (Bridges to Prosperity, 2016).

The passive earth pressure and soil friction provide sliding resistance against the sum of the horizontal component of the cable tension and the active earth pressure. The soil friction force is determined by multiplying the weight of the anchor plus the weight of a column of soil above the anchor minus the vertical component of the cable force by a coefficient of friction for concrete on soil, as shown in the free-body diagram in Figure 4.

1.1.2 Vertical Forces

The weight of a trapezoidal soil mass above the anchor and the weight of the anchor itself are uplift resistance against the vertical component of the cable tension (Figure 5). The capacity of the entire deadman anchor system is controlled by the lesser failure force in either the horizontal or vertical direction. B2P recommends applying a minimum factor of safety of 1.5 for both limit states.

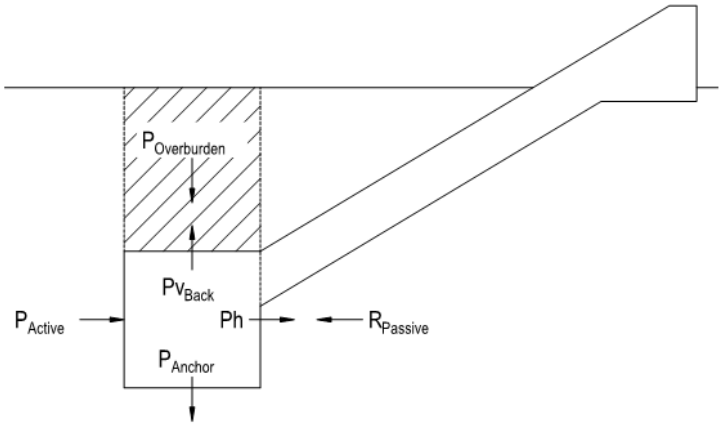

Figure 4 – Free-Body Diagram of Forces Acting on Deadman Anchor for Horizontal Pullout Component (Bridges to Prosperity, 2016).

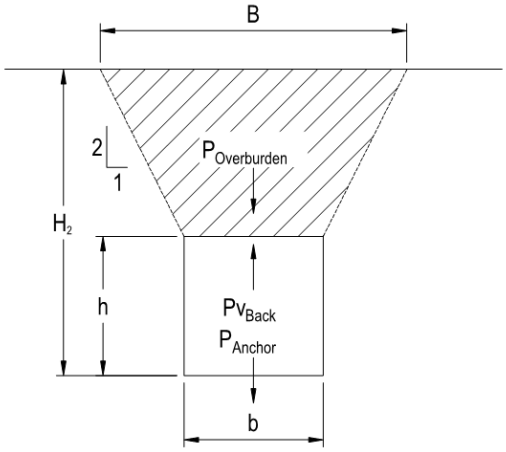

Figure 5 – Free-Body Diagram of Forces Acting on Deadman Anchor for Vertical Pullout Component (Bridges to Prosperity, 2016).

1.1.3 Research Objective (Improvements to B2P Design Methodology)

The intention of this report is to provide a more comprehensive design methodology for deadman anchors to be used with B2P bridges that better reflects the ultimate pullout capacity of an anchor buried in soil. While this methodology is based on more complex soil mechanics than currently used in B2P's manual, the end result of this research is design charts and simple equations based on the following variables:

(1) embedment depth

(2) soil internal friction angle

(3) pullout angle

(4) anchor size (height and length)

(5) soil unit weight

For simplicity, this report features only an analysis of dry, loose cohesionless soils as an embedment medium, as well as assuming a level ground surface above the anchor. Additional variables that may affect pullout capacity but are not considered in this research, include, but are not limited to, moisture content, dilatancy, and cohesion. These variables are discussed in more detail in the Recommendations section of this report as the subject of future research.

In the early months of this research, the Director of Engineering at B2P was contacted to help focus the scope of what the organization wanted to investigate. One of their recommendations was that the embedment ratios (depth divided by height of anchor) analyzed in this research range only from 2 to 5. The heights of the anchors are on the order of one meter, so embedment beyond 5 meters is unrealistic given available construction technologies in the often-rural areas of developing countries. The pullout angle was also recommended to be between 25 and 45 degrees from the horizontal. B2P's recommended practice for setting this angle is to match the angle of the cable going over the span as it passes over top of the tower. This is recommended to ensure there is no net moment created by unequal horizontal force components about the base of the bridge towers, which in the B2P-recommended design are constructed with steel posts with pinned bases free to rotate. Pullout angles shallower than 25 degrees and steeper than 45 degrees would not match the cable angles within the recommended spans and sag amounts. Finally, a consensus was reached that this particular research would only look at cohesionless, dry soils with a level ground surface and that the effects of cohesion, moisture content, and a sloping ground surface should be examined at a later date.

Dilatancy was not discussed as it was not known at the time the considerable effect it can have on anchor pullout capacity.

1.1.4 Research Methods

This research used multiple means of assessing anchor pullout capacity. First, a theoretical solution using the B2P design procedures establishes a baseline from which increases or decreases in capacity can be observed. Another theoretical solution using a modified limit equilibrium equation from the literature was analyzed to see if it gives a reasonable estimate of pullout capacity. Second, computer modeling using the finite element program GEOSLOPE SIGMA/W modeled the deadman anchor and found its pullout capacity by analyzing the stresses and strains of the soil medium mobilized by the anchor. Third, a qualitative scale model was built to show a cross-section of a deadman anchor pulled to failure. This model showed the deformation of soil around a scaled-down anchor as it was pulled out of the ground by hand. The deformation of the soil at different embedment depths and pullout angles was compared to the finite element model stress results to verify that the finite element model was returning realistic results. Finally, a quantitative scale model was built and tested to measure pullout force and displacement for a limited number of configurations of embedment depth and pullout angle. Together, these four research methods provide a comprehensive understanding of deadman anchor pullout capacity as it is calculated today and how it could be improved to design bridges with greater capacity or less material.

1.2 Literature Review

Various forms of earth anchors have been thoroughly researched since the mid-20th century. These include deadman anchors, or anchors that resist uplift or pullout primarily due to their self-weight and the weight of soil above them. Modern applications of these anchor types are guy wire anchors for electrical transmission towers or mooring of offshore floating structures, and tieback anchors behind retaining walls. Both usually rely on a large surface area to increase the soil weight resistance and are oriented such that this area is orthogonal to the direction of pullout. These anchors are more commonly referred to as plate anchors. These differ from the B2P style anchor not only in shape and orientation but in that the self-weight of the B2P anchor contributes greatly to its resistance. Nevertheless, the results of the investigation of plate anchor pullout capacity are relevant to this research and provide clarity into the failure mechanics of an embedded deadman anchor.

1.2.1 Anchors to Resist Uplift

Experimental research began in 1961 by Balla for uplift resistance of bell-end foundations using model tests of small circular plates in medium-dense sand (Goel *et al.*, 2006). Sutherland performed similar research in 1965 on larger plates in dense sand, as did Kananyan in 1966 (Goel *et al.*, 2006). When comparing experimental data to a theoretical capacity, literature at this time provided two widely accepted options[9]: that the

[9] The authors of most of the papers that performed experimental research also usually created their own theoretical solutions, none of which became generally accepted or used elsewhere in literature. These solutions mostly differed in the assumption of the shape of the failure surface, ranging from circular (Balla, 1961) to parabolic (Macdonald, 1963) to cylindrical (Sutherland, 1965).

plate or footing be resisted by either a vertical surface or an outwardly-angled surface. The vertical-surface theory describes uplift capacity as the sum of shear resistance along a slip surface extending vertically from the edges of the plate or footing as well as the weight of soil bounded by this plane, as shown in Figure 6. Conversely, there were two methods that used an outwardly-angled slip surface. Mors in 1959 proposed that a plate anchor or footing would resist uplift due to the weight of soil in an inverted cone or rectangular pyramid above the circular or rectangular footing, respectively (Figure 7). The surface of this cone or pyramid was defined by an apex angle of $90 + \phi/2$ and was truncated at the top face of the plate or footing. Downs and Chieurzzi in 1966 proposed a similar theory, but that the apex angle of the cone or pyramid was 60 degrees (Figure 8). In both theories, shear resistance along the surface of the cone or pyramid is neglected and the plate or footing resisted solely by the weight of soil contained within (Das & Shukla, 2013). These theories are the basis for how Bridges to Prosperity recommends

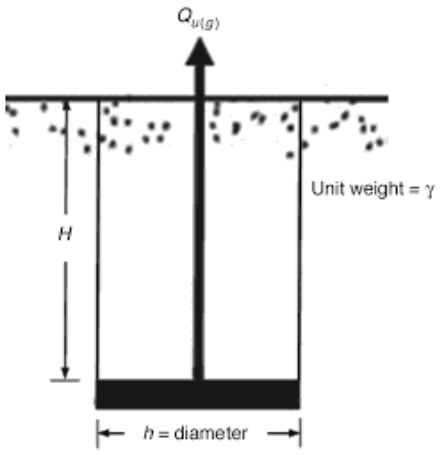

Figure 6 – Vertical-Surface Uplift Resistance Theory (Das & Shukla, 2013).

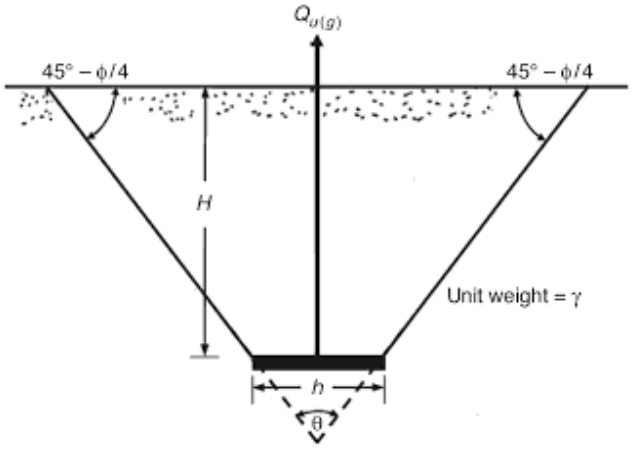

Figure 7 – Mors' Theory of Uplift Resistance (Das & Shukla, 2013).

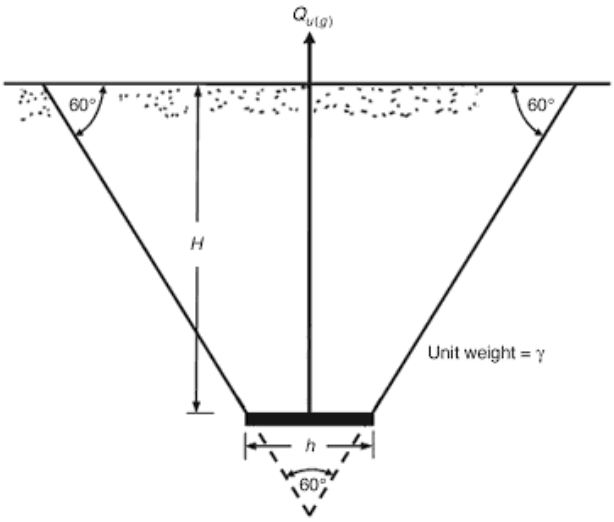

Figure 8 – Downs and Chieurzzi Theory of Uplift Resistance (Das & Shukla, 2013).

calculating the uplift resistance of their deadman anchors, particularly as proposed by Downs and Chieurzzi because their apex angle is independent of the soil internal friction

angle, and the 2:1 slope from the vertical in the B2P diagram is similar to the 30 degrees from the vertical that would be provided using an apex angle of 60 degrees. Meyerhof and Adams in 1968 stated that neither the vertical nor cone/pyramid surface provide reliable uplift resistance estimation based on experimental research, particularly for deeper foundations. They developed separate failure surfaces for shallow and deep footings (Figure 9), with the conclusion that shallow footings are resisted in uplift by a soil mass extending to the ground surface as well as a cohesive force and shearing force that develop along the failure surface. They also concluded that deep footings are resisted by the same forces, but the soil mass does not reach the ground surface and instead an overburden pressure is imparted to the soil mass due to the weight of soil not mobilized above the footing. The extent of the soil mobilization, H, was determined through experimental testing and reported by Meyerhof and Adams as dependent on soil internal friction angle and footing size, B. They found good correlation in experimental and theoretical results for denser sands, but weaker correlation for loose sands.

1.2.2 Plate Anchors Pulled Horizontally or Vertically

Rowe and Davis (1982) greatly expanded the scope of previous research to include additional variables such as surface roughness of the plate, initial stress state, and soil dilatancy. They also performed theoretical and experimental analysis of both horizontal anchors pulled vertically and vertical anchors pulled horizontally. Finally, unlike previous theoretical research, they considered an elastoplastic finite element analysis as opposed to a purely elastic response of the surrounding soil medium. The finite element analysis utilized an approach to soil-structure interaction detailed in another paper

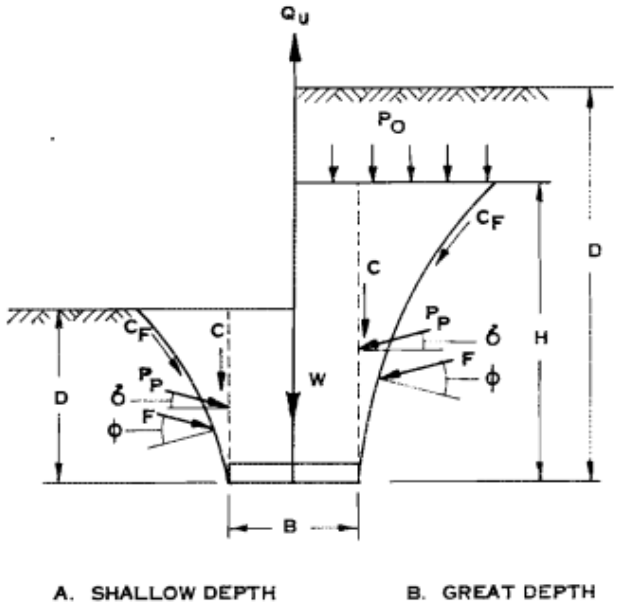

Figure 9 – Failure Modes for Shallow and Deep Footings in Uplift (Meyerhof & Adams, 1968).

featuring failure within the surrounding soil medium, anchor breakaway from the soil behind the anchor, and shear failure at a frictional, dilatant soil structure interface without having to define specific joints or interface elements (Rowe & Davis, 1982). The anchor was assumed to be perfectly rigid and the soil was assumed to have a Mohr-Coulomb failure criterion that included the effects of soil dilation as defined by an angle of dilatancy, ψ. The presence of dilatancy in this analysis provided the ability to include plastic volume strain as a function of major principal strain, thereby tracking the extent of plastic failure within the soil medium. The finite element analysis returned load-displacement curves for varying embedment ratios based on inputs of Poisson's ratio, angle of internal friction, and angle of dilatancy (Figure 10). The results from the full extent of finite element analyses were found to be in reasonable agreement with available

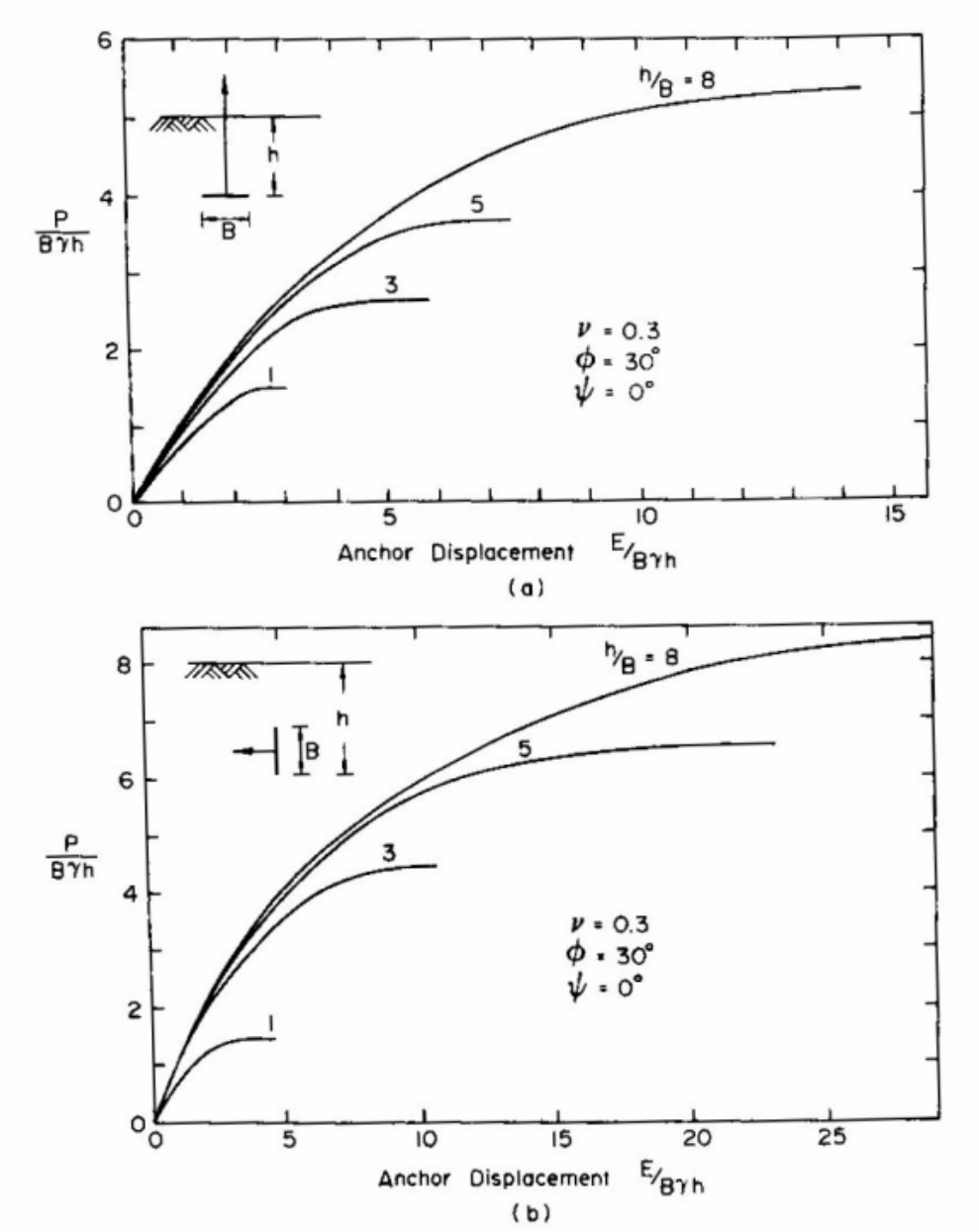

Figure 10 – Load-Displacement Curves Generated by Finite Element Analysis of Horizontal or Vertical Plate Anchors (Rowe & Davis, 1982).

elastic solutions and classical plasticity solutions as they relate to what was termed a "collapse load."

Rowe and Davis organized much of the analysis around the determination of this ultimate collapse load, but also identified a "yield" load, or what was called the k_4 failure load (Figure 11). This is the load which produces four times the displacement that would have occurred had the soil remained elastic, which Rowe and Davis suggest is a more adequate description of failure than local shear failure for this type of application. This failure is most noticeable for deep embedment where the deformations before collapse are so large that a practical failure would have already occurred. Limiting the recommended capacity of these deep anchors to this k_4 failure load would ensure structures with a factor of safety between 2.5 and 3 would not experience working loads in the highly non-linear range and result in displacements much larger than could be predicted from an elastic analysis.

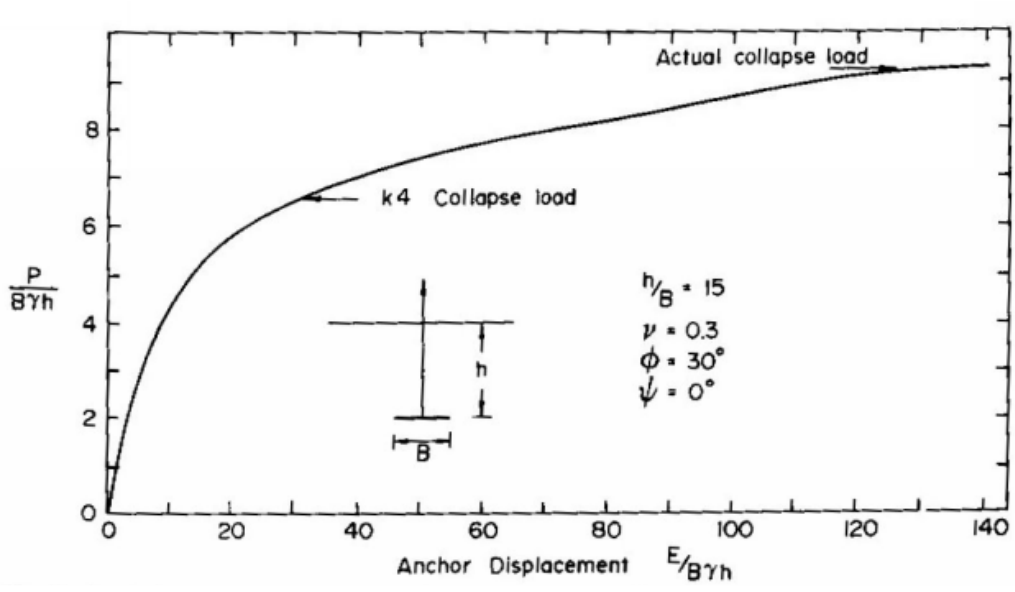

Figure 11 – Load-Displacement Curve Illustrating k_4 Collapse Load versus Ultimate or Actual Collapse Load for Deep Embedment (Rowe & Davis, 1982).

For more normal embedment ratios, the finite element analysis was able to define a basic anchor capacity to which the researchers applied correction factors for soil dilatancy, anchor roughness, and initial stress state. This means that the derivation of basic anchor capacity, F_y, was based on a soil with $\psi = 0$, or, a soil that deforms plastically with zero volume change, which is a reasonable assumption for loose sands (Figure 12). For denser sands, plastic behavior begins to exhibit when collapse is about to occur, which is a result of soil dilatancy. Similarly, initial stress state is shown to have an effect on collapse load, though the authors state that for increasing levels of dilatancy this effect becomes

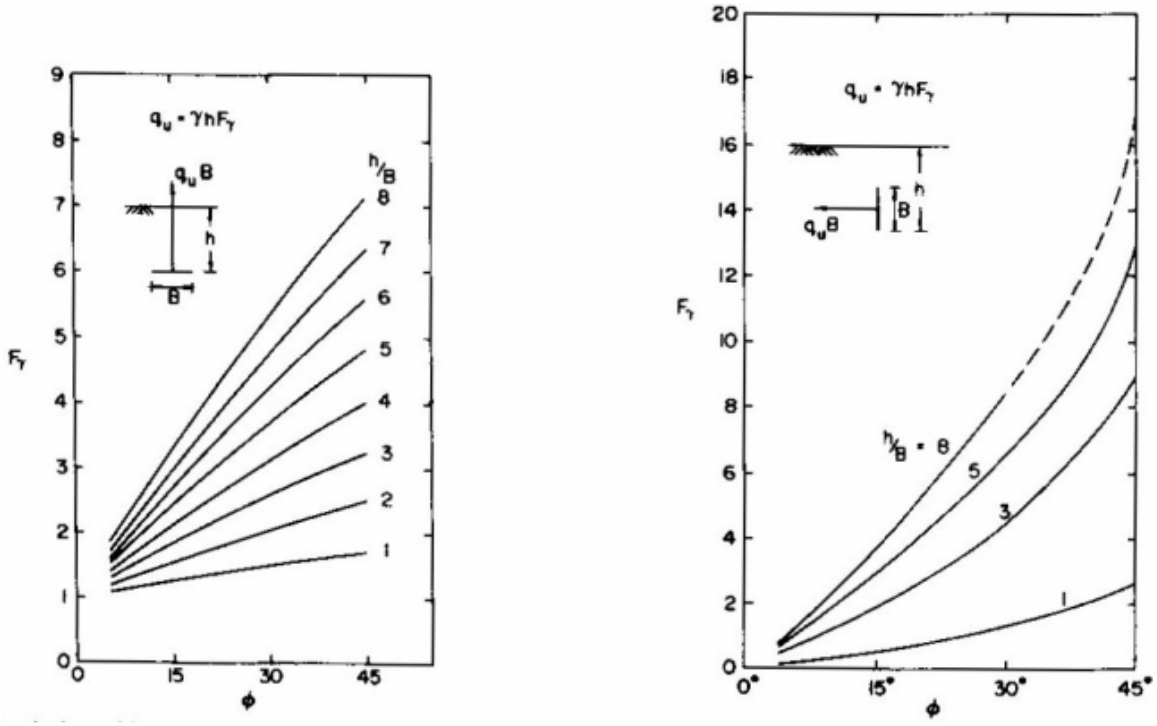

Figure 12 – Values of F_y for Varying Soil Internal Friction Angles and Embedment Ratios (Rowe & Davis, 1982).

negligible. As for anchor roughness, the correction only seems to be significant in cases where embedment is small: at greater embedment the effect of roughness is negligible. Rowe and Davis also performed several experimental trials (Figure 13) where these variables were controlled or measured afterwards. They found good correlation between the theoretical and experimental results (Figure 14), as well as reasonable precision amongst experimental trials (Figure 15). Rowe and Davis also compared their theoretical solutions to the experimental results of previous researchers and found similarly promising correlation (Figure 16). Notably, the experimental results of previous researchers were found to be higher than theoretical predictions for sands in which the angle of dilatancy was held at zero. This supports the importance of dilatancy, or volume

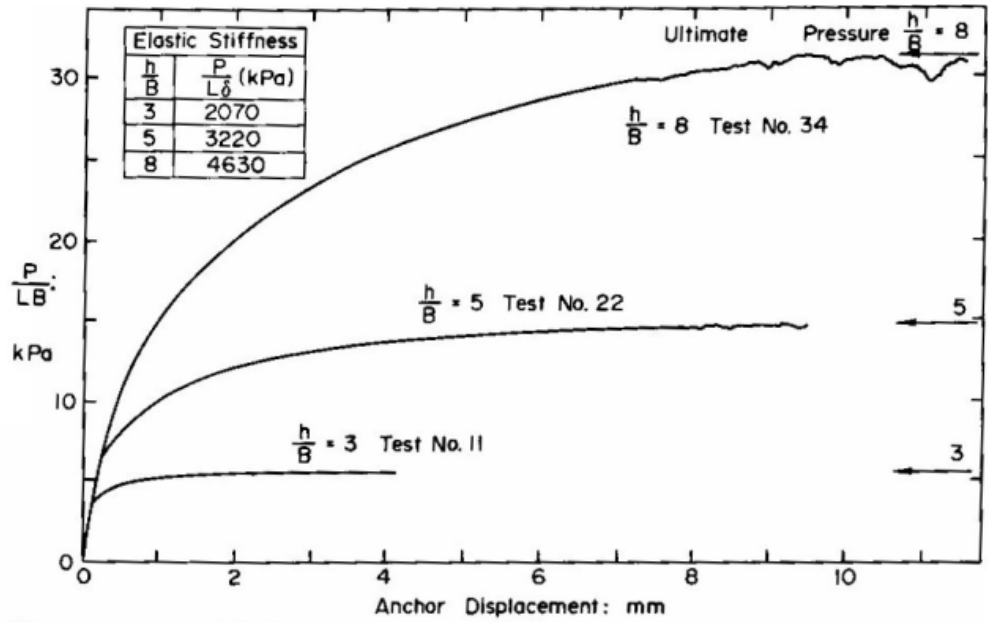

Figure 13 – Typical Load-Displacement Curves Generated by Experimental Trials for Varying Embedment Ratios (Rowe & Davis, 1982).

changes under shear strain, when considering these types of anchors. Major capacity gains can be observed when dilatancy can be increased or controlled for. Rowe and Davis compiled by far the most comprehensive investigation into the failure of embedded plate anchors, and particularly regarding soil dilatancy and elastoplastic response that goes into much greater depth than explained here. Other researchers, including Murray and Geddes in 1987, attempted to predict ultimate uplift resistance using more complex theoretical methods such as equilibrium and limit analysis and found mixed results,

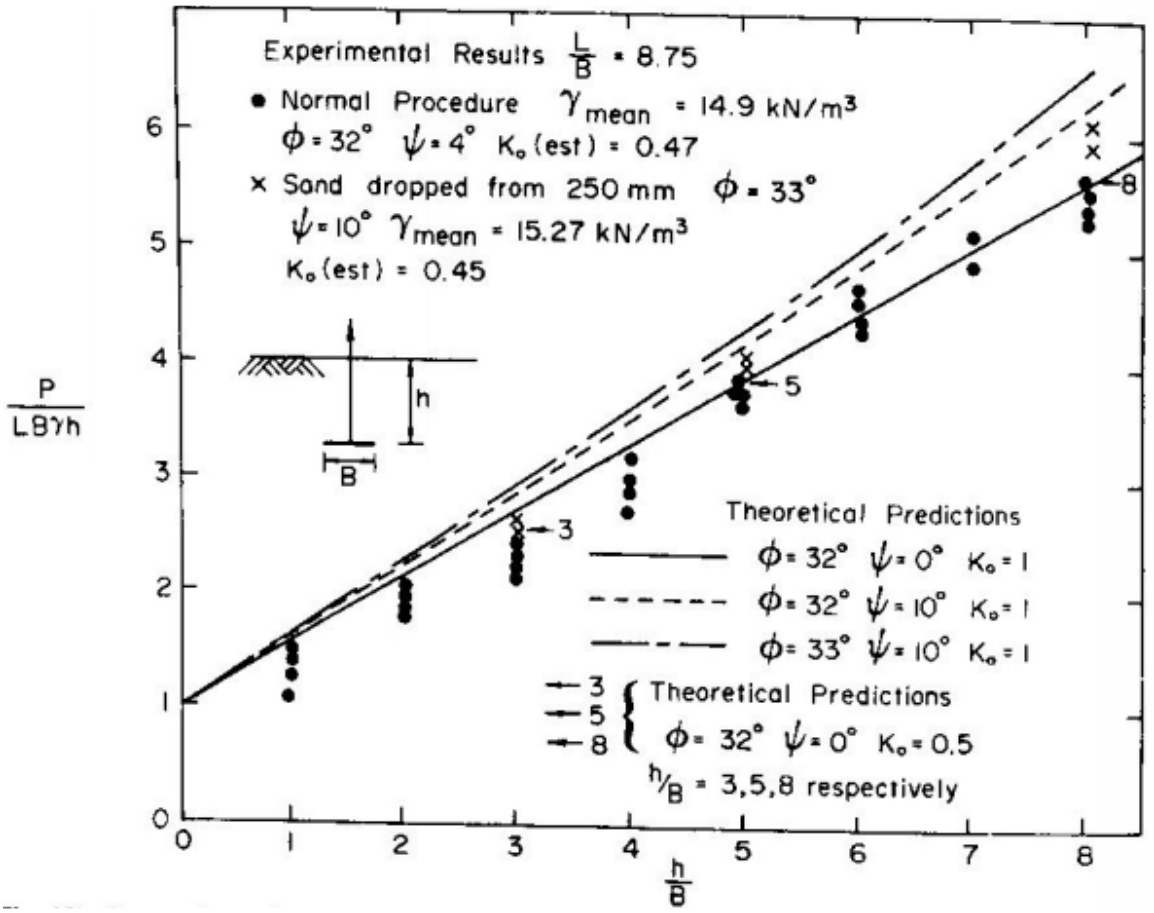

Figure 14 – Comparison of Experimental and Theoretical Collapse Loads (Rowe & Davis, 1982).

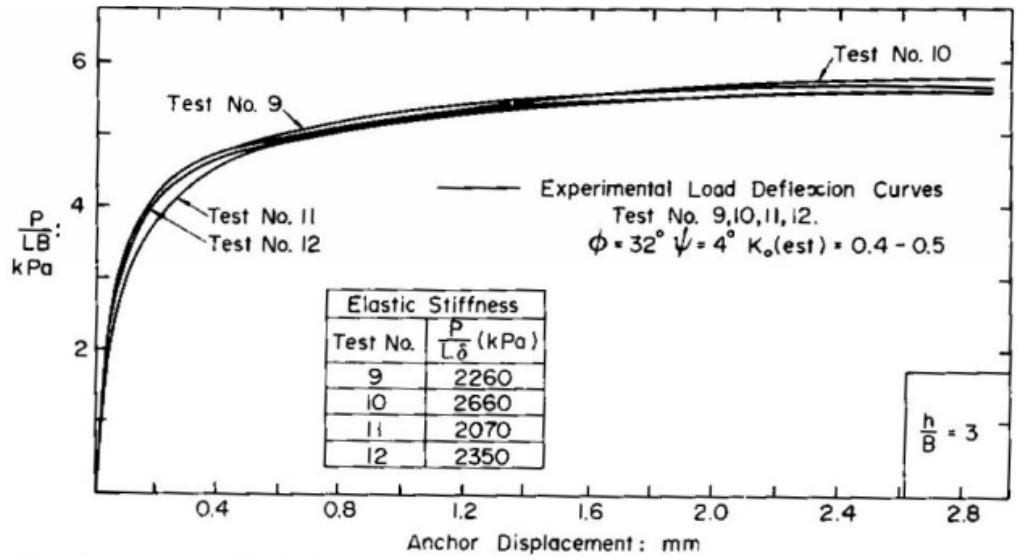

Figure 15 – Load-Displacement Curves Generated by Experimental Trials for the Same Embedment and Other Controlled Variables (Rowe & Davis, 1982).

particularly for varying shapes and soil densities. Further research in more recent years that used upper and lower bound limit analysis complemented by or implemented through numerical finite element analysis have produced more promising correlations with past or recreated experimental data.

1.2.3 Inclined Anchors

Research into the uplift capacity of horizontal plate anchors and footings was important to establish a general understanding of the failure mechanics involved in the pullout of embedded anchors. Further research has investigated the pullout capacity of inclined anchors, which is much more pertinent to this research. In a manner similar to their predecessors, different theories were proposed and tested with varying results. One

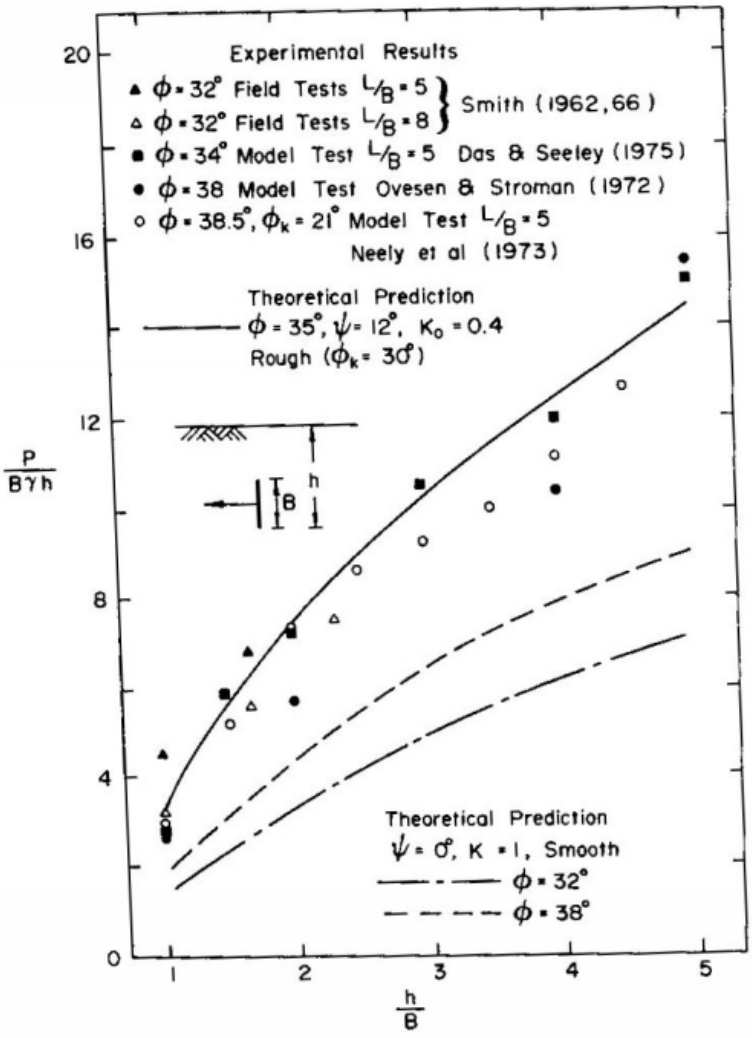

Figure 16 – Comparison of Experimental and Theoretical Collapse Loads from Previous Researchers (Rowe & Davis, 1982).

researcher's work, however, has maintained its status as the most accurate in predicting model test results, and that is the work done by Meyerhof in 1973 on the uplift resistance of inclined anchors and piles. The conclusion of his work was an equation to estimate the pullout capacity of an inclined anchor of configuration shown in Figure 17. Note that the symbol ψ is now being used to signify the angle of inclination, not the angle of dilatancy.

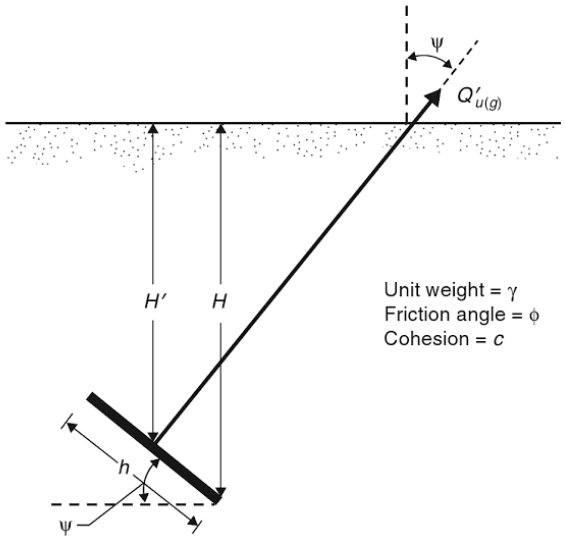

Figure 17 – Inclined Anchor Geometry for Meyerhof Method (Das & Shukla, 2013).

Meyerhof found that for a shallow inclined rectangular anchor, the net ultimate holding capacity Q'_u per unit width was determined to be (for cohesionless soil, c = 0)

$$Q'_u = \frac{1}{2} K_b \gamma H^2 + \gamma h H \cos^2 \Psi , \tag{1}$$

where K_b is an earth pressure coefficient determined by Meyerhof for varying soil friction angles and inclination angles, similar to the earth pressure coefficients for an inclined retaining wall. Meyerhof also expressed this capacity as an average breakout factor F'_q, a dimensionless coefficient similar to the work of other researchers. For a shallow anchor in cohesionless soil and eliminating the variable H to replace with H' and h such that it could be compared to other researchers' embedment ratios:

$$F'_q = \frac{Q'_u}{\gamma h H'} = \frac{1}{2} K_b \left(\frac{H'}{h} \right) \left(1 + \frac{h}{2H'} \sin \Psi \right)^2 + \left(1 + \frac{h}{2H'} \sin \Psi \right) \cos^2 \Psi . \tag{2}$$

Meyerhof determined that for shallow anchors this breakout factor can be used to describe failure, but there is a critical embedment ratio $(H'/h)_{cr}$ beyond which the average breakout factor remains constant for a single inclination angle. Meyerhof asserted that beyond the critical embedment ratio, deep anchor behavior is observed, where local shear failure of the surrounding soil controls. For these cases, the breakout factor $F'_q{}^*$ was graphed by Meyerhof (Figure 18) based on soil internal friction angle and anchor inclination angle only.

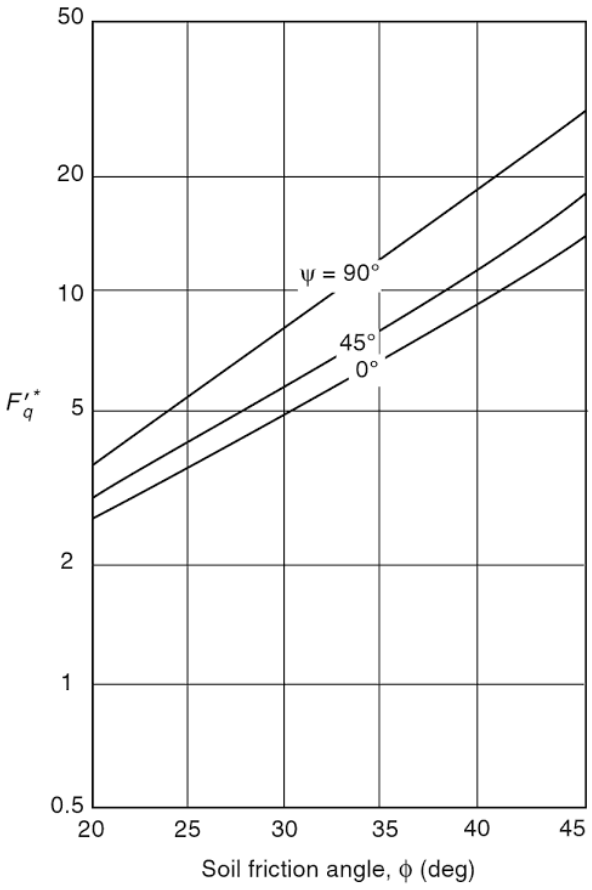

Figure 18 – Graph of Breakout Factor for Deep Anchors by Meyerhof Method (Das & Shukla, 2013).

Research by Emirler, Tolun, and Laman (2016) have verified the accuracy of the Meyerhof method by comparing theoretical results for a given geometry to the results given by a finite element analysis in PLAXIS 3D (Figures 19 and 20). Their finite element results show good correlation with Meyerhof's theory, particularly for greater angles of inclination from the vertical (Figure 21).

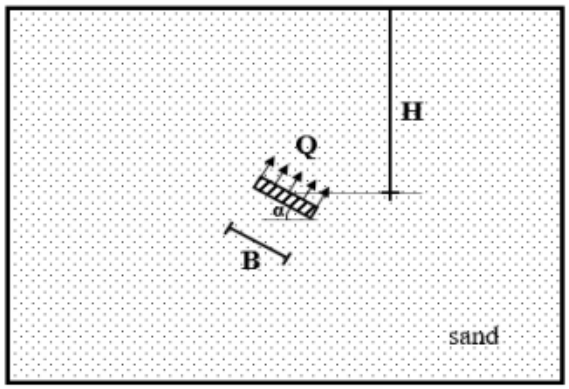

Figure 19 – Problem Definition for Finite Element Modeling (Emirler *et al.*, 2016).

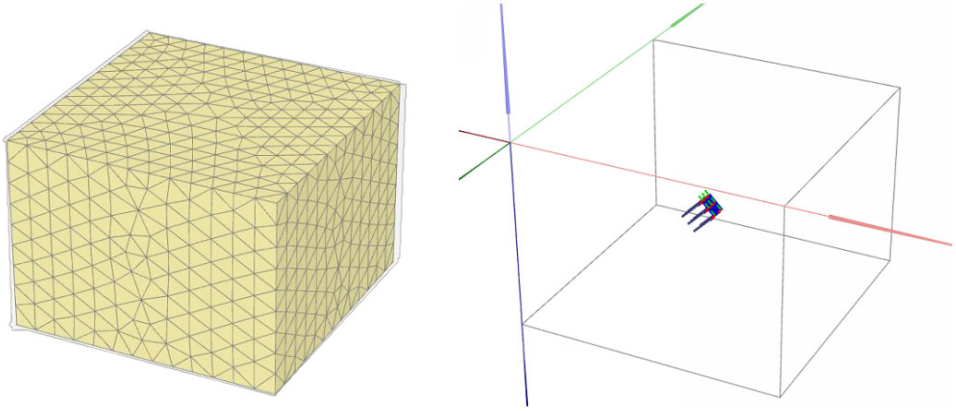

Figure 20 – PLAXIS 3D Modeling of Inclined Soil Anchor (Emirler *et al.*, 2016).

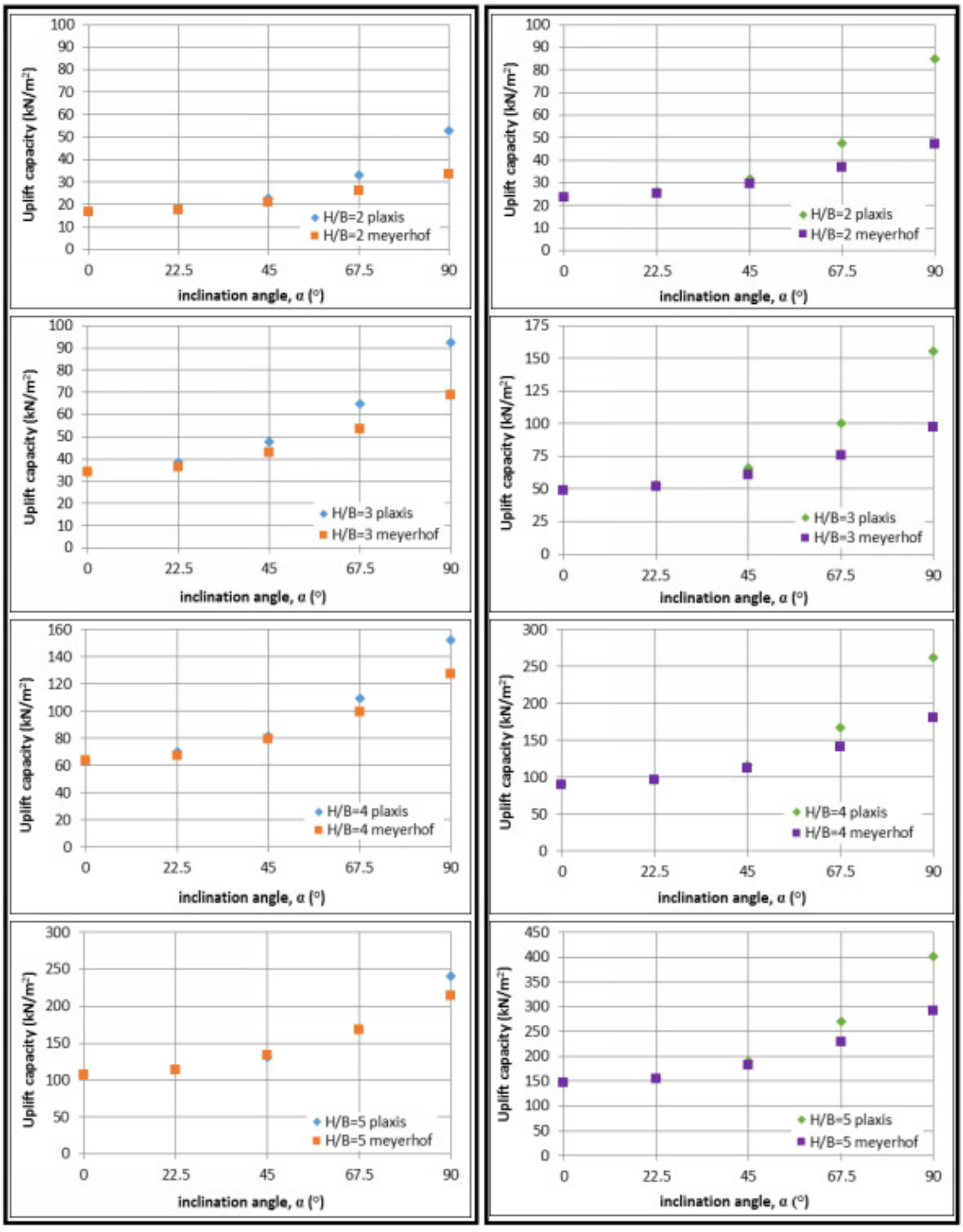

Figure 21 – Comparison of PLAXIS 3D Results with Meyerhof Method Theoretical Results for Loose Sand (left) and Dense Sand (right) (Emirler *et al.*, 2016).

1.2.4 Displacements

The deadman anchor system used by B2P to arrest the cables of their suspension bridges is highly displacement-sensitive. The construction of the bridges is such that the suspension cables are continuous from one deadman anchor, up over top of one tower, across the bridge span, up over the opposite tower, and into the opposite deadman anchor. Thus, pullout displacement of a deadman anchor will directly change cable geometry or tension and have progressively worsening effects across the bridge superstructure.

The work of researchers in the past has shown that anchors of this type can resist pullout while displacing a considerable amount, particularly for deeper embedment, before reaching an ultimate load and the surrounding soil experiencing plastic deformation. This is illustrated particularly well in the work of Murray and Geddes in 1989 in their research into inclined plate anchors in a cohesionless medium. Their experimental data using rectangular steel plate anchors (with anchor width B = 50 mm) consistently showed two correlations: higher pullout capacity for shallower pullout angles at the same embedment and larger displacements required to fail each anchor at deeper embedment (Figures 22 and 23). Both correlations are consistent with the findings of other researchers and point towards an embedment ratio beyond which failure mechanics can be labeled “deep anchor behavior,” though Murray and Geddes never use such terminology or determine it in their results. However, a slope change is visible in many of the graphs in Figures 22 and 23 beyond a certain ratio. Deep anchor behavior is not a focus of this research as a simple matter of constructability in developing countries. A worthwhile observation would instead be that for shallower embedment ratios, the failure displacement is relatively constant and only varies on the order of 0.5 mm.

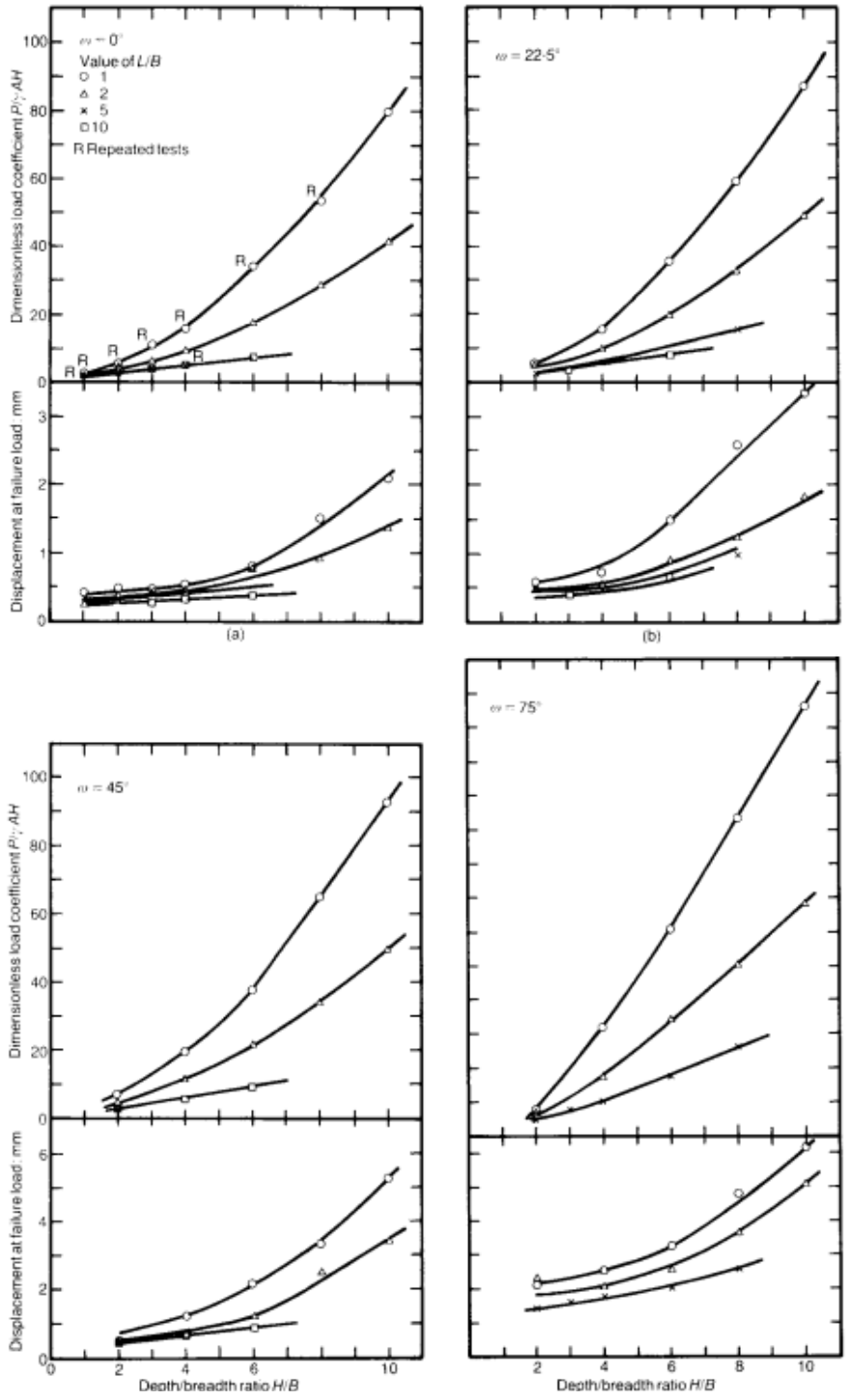

Figure 22 – Experimental Results for Inclined Plate Anchors in Sand. Inclination Angle ω is Measured from the Vertical (Murray & Geddes, 1989).

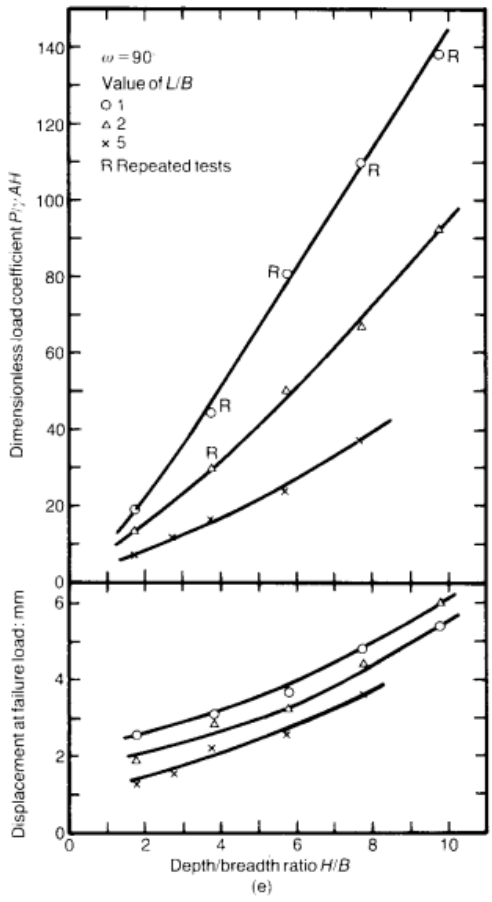

Figure 23 – Experimental Results (cont.) for Inclined Plate Anchors in Sand. Inclination Angle ω is Measured from the Vertical (Murray & Geddes, 1989).

In the case of B2P anchors, displacement in-line with the cables eventually leads to structural failure of the bridge deck and its inability to support load. The cables are not fixed at the top of the towers as they pass over and are free to slip as the anchor displaces under higher-than-anticipated loads. The amount of displacement required to reach structural failure is highly dependent on bridge geometry, and most notably cable sag. In their *Bridge Builder Manual*, B2P suggests a maximum cable sag of 9.09% for suspension-cable bridges. Calculations using a catenary relationship for cable shape show

that for sag of 5% to 9%, constant span, and constant tower height (the bridge towers do not deflect or rotate about their base), the anchor displacement required to lower the bridge deck one foot range from 3 to 5 inches, respectively. This relationship demonstrates that even at this large sag, small in-line cable displacement leads to larger vertical cable displacement over the span. However, as sag increases with anchor displacement under load, cable force will also decrease. As cable force decreases the anchor displacement will most likely eventually be arrested so long as additional load is not added to the bridge. It is important to note that the magnitude of displacement before arresting, as well as the resulting changes in cable sag and tension, is highly dependent on bridge geometry and loading and cannot be sufficiently analyzed under the scope of this research. The Recommendations section of this report covers in greater detail the variables involved in the relationship between anchor capacity and bridge loading, and how they can be investigated in future research.

1.2.5 End Effects (Three-Dimensional Effects)

Most of the former research with plate anchors focused on finding a dimensionless pullout load coefficient as well as factors to account for anchor shape, surface roughness, or other such variables that could be changed between trials. The shape factors described the variability between square or circular anchors but also the difference between sizes of square anchors or circular anchors. For example, these factors helped to define the changes in pullout capacity that happened when changing the anchor from a 10 mm x 20 mm plate to a 10 mm x 50 mm plate, and the results of modifying these factors were highly variable between researchers. Given their variability as well as their inapplicability

to the shape of B2P anchors, they cannot be used to help estimate changes in capacity due to varying anchor lengths. However, the *Trenching and Shoring Manual* published by the California Department of Transportation (2011) presents the findings of Ovesen on the effects of varying length in deadman anchor blocks used behind retaining walls as tiebacks. In this configuration, the blocks are pulled entirely horizontally but the shape is highly similar to the B2P anchor. They are normally large concrete blocks buried in shallow embedments outside of the active wedge of the retaining wall and used to resist wall displacement (Figure 24). Given their orientation, the only forces acting on the anchor blocks as a result of the tieback force are active and passive earth pressure. The active wedge behind the anchor block, similar to that behind a retaining wall, together with the tieback force helps to create a passive wedge in front of the anchor block that resists the pullout (Figure 25). The manual presents Ovesen's theory as a way to describe

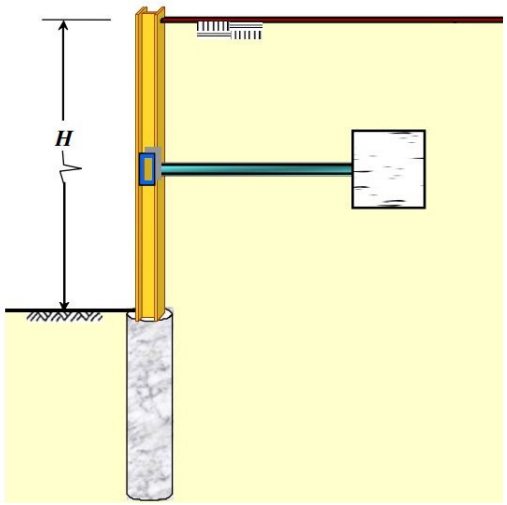

Figure 24 – Typical Configuration for Deadman Anchor Blocks Used as Tiebacks in Retaining Walls (California Department of Transportation, 2011).

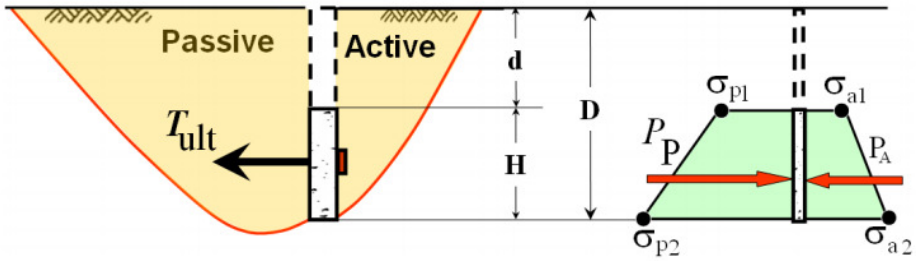

Figure 25 – Forces Acting on Deadman Anchor Blocks per Ovesen's Theory (California Department of Transportation, 2011).

the behavior of soil within the passive wedge on the ends of the anchor as it is pulled to failure (Figure 26). This behavior is quantified as a modifier to an anchor capacity calculated per unit length, similar to the work of other researchers. Unlike the B2P calculation for horizontal capacity, the active and passive pressure act only on the anchor block and not a portion of the soil above. However, given the geometry of the anchors used by Ovesen it appears to be the most applicable to this research. These deadman anchor blocks are commonly used as discrete anchor points along the length of a retaining wall, and therefore spacing S is a variable used in the calculation of three-dimensional effects and is used to calculate an unnamed variable, B. B approaches a value of 1 for larger and larger spacings (Equation 4), so for isolated anchors such as B2P, B can be considered equal to 1.

Ovesen's modifier, R, can be expressed as:

$$R = 1 + \Delta K^{2/3}\left[1.1E^{4} + \frac{1.6B}{1+5\frac{L}{D}} + \frac{0.4\Delta K E^{3}B^{2}}{1+0.05\frac{L}{D}}\right], \quad (3)$$

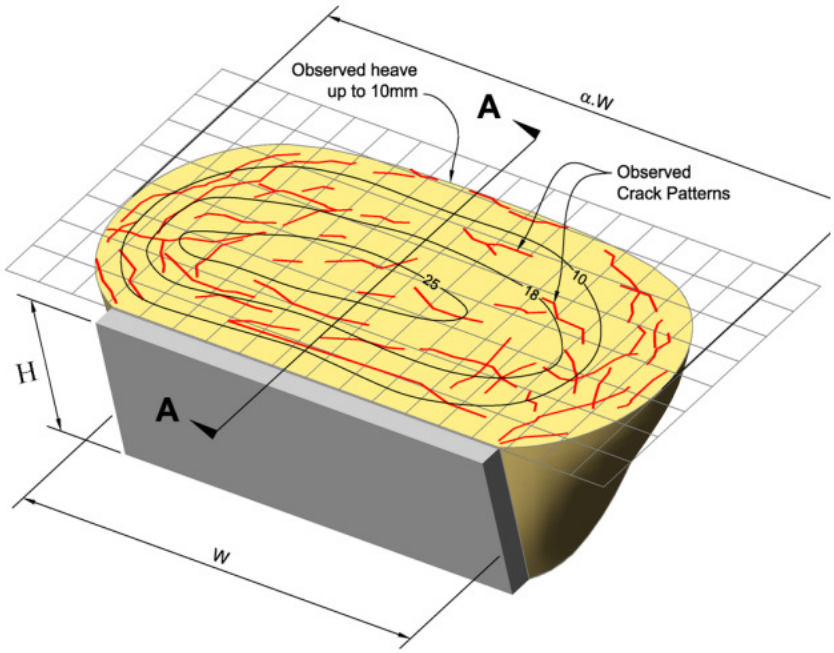

Figure 26 – Observed Soil Deformation Within Passive Wedge During Horizontal Pullout That is Quantified in Ovesen's Three-Dimensional Factor (California Department of Transportation, 2011).

where

$$B = 1 - \frac{L}{S}, \tag{4}$$

$$E = 1 - \frac{H}{d + H}, \tag{5}$$

$$\Delta K = (K_p - K_a)\cos\delta, \tag{6}$$

L is anchor length, D is the depth to the bottom of the anchor block, H is the height of the anchor block, d is the difference between H and D as shown in Figure 25, K_p and K_a are the coefficients of passive and active earth pressure, respectively, and δ is the friction angle of the anchor material against the soil medium.

The relationship between anchor length and the modification for end effects is graphed in Figures 27 through 29 for varying soil internal friction angles and a constant interface friction angle of $\delta = 29°$ for concrete poured against clean sand. The factor decreases for longer lengths, which is intuitive given that the capacity over the length of the anchor becomes more dominant than the effects of soil movement at the ends. The factor increases with anchor embedment, which is also intuitive given the propagation of the passive wedge up to the surface of the ground. Finally, it increases with the angle of friction, which directly affects only the ΔK value but is much larger for increasing friction angles as K_a decreases and K_p increases.

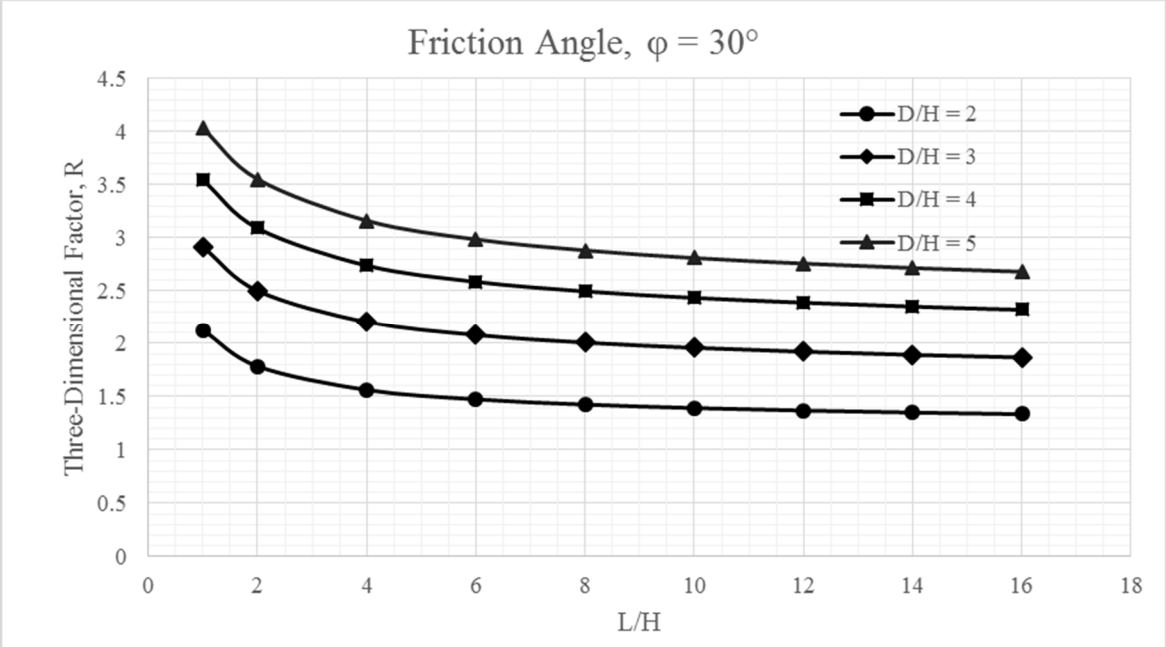

Figure 27 – Ovesen's Factor for Three-Dimensional Effects Based on Anchor Length for a Surrounding Soil Medium with an Angle of Internal Friction of 30 Degrees.

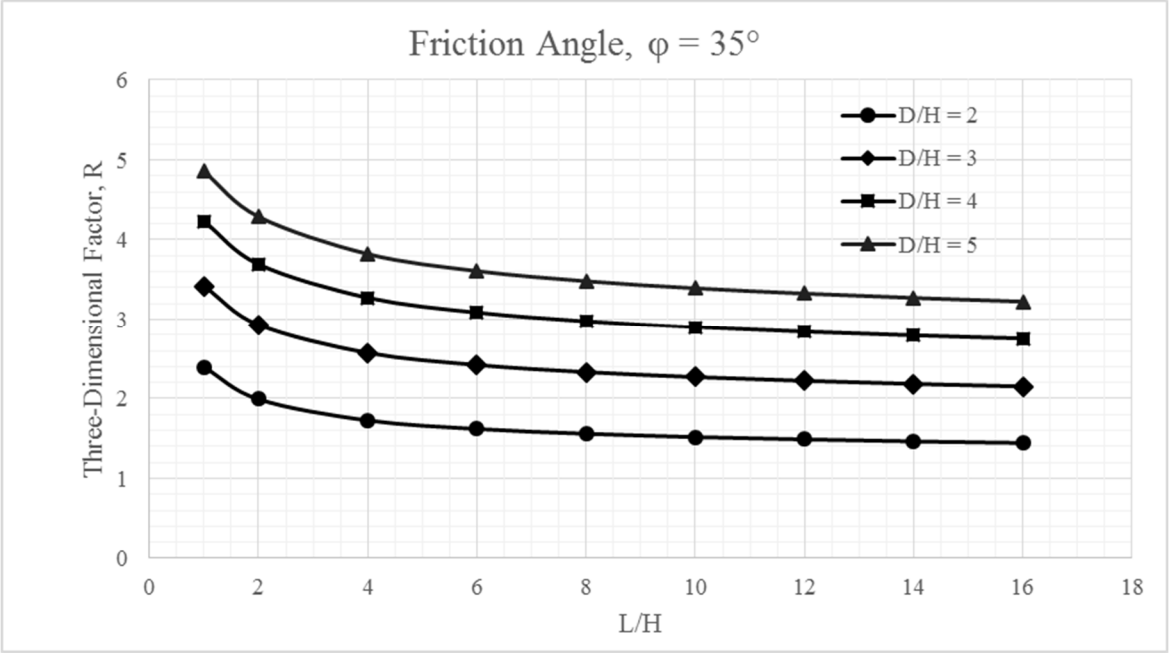

Figure 28 – Ovesen's Factor for Three-Dimensional Effects Based on Anchor Length for a Surrounding Soil Medium with an Angle of Internal Friction of 35 Degrees.

Because Ovesen developed this factor for deadman anchors pulled horizontally, the values taken from Figures 27 through 29 based on anchor length and height should be multiplied by the cosine of the pullout angle θ prior to multiplying by capacity determined for along the length of the anchor.

It should be noted that the California Department of Transportation recommends using a maximum three-dimensional factor of 2.0, so the capacity of an anchor is never more than doubled as a result of end effects. It is a reasonable attempt to conservatively estimate the effects of length on anchors and in the opinion of the author should be applied in the case of B2P anchors as well.

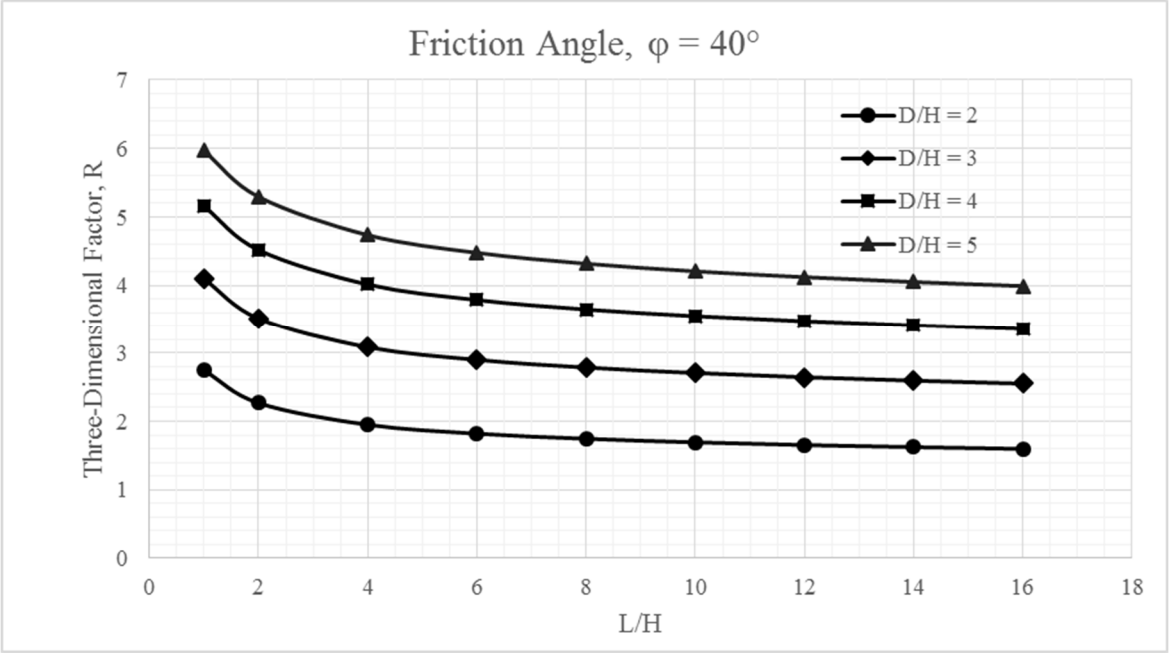

Figure 29 – Ovesen's Factor for Three-Dimensional Effects Based on Anchor Length for a Surrounding Soil Medium with an Angle of Internal Friction of 40 Degrees.

1.2.6 Literature Review Conclusions

With all the research conducted on embedded plate anchors, and how the soil and failure mechanics might relate to a B2P deadman anchor, there are many conclusions that are inapplicable and others that seem to disagree between model tests and theoretical solutions. However, there are a few general conclusions that are common in the literature and that are expected to hold true for the B2P anchors. These conclusions are that there are three variables that increase pullout capacity of an anchor in a cohesionless medium:

(1) an increase in soil internal friction angle

(2) an increase in pullout angle measured from the vertical

(3) an increase in embedment ratio

The effect of other factors such as soil dilatancy will be addressed only in the concern that soil density will be kept constant throughout all modeling and tests to normalize the effect of varying volume strain under loading. Further research to investigate the effects of soil density and dilatancy on anchors of the B2P configuration is certainly recommended. Other factors such as anchor roughness and initial stress state were also kept constant for all modeling and testing performed in this capstone project, though the literature would suggest their effects on pullout capacity are negligible and further research to include these variables is not as strongly recommended. Finally, none of the previous research encountered by the author has investigated anchor shapes other than flat plates. The B2P anchor geometry provides a particularly unique situation whereby the square edge could introduce an entirely new failure surface, particularly for shallow embedment. The failure would more likely be based on the anchor's leading edge acting as a wedge to separate the surrounding soil if the overburden stress is low enough. The lack of prior research in this area necessitates at least qualitative investigation.

Chapter 2: Experimental Methods and Modeling

2.0 Methods

The theoretical and experimental formulas and models detailed herein all conform to the geometry and variables as defined in Figure 30. The anchors analyzed all are square in cross-section and prismatic along their length. They were oriented as shown in Figure 30 with level, horizontal bottom and top edges and vertical front and back faces. The cable force P acts through the centroid of the anchor cross-section at an angle of θ from the horizontal. The anchor has height and width H and is buried to a depth D measured to the bottom of the anchor. The surrounding soil medium has an internal angle of friction φ, unit weight γ_s, modulus of elasticity E, Poisson's ratio ν, and a level ground surface. The soil properties of moisture content w, cohesion c, and angle of dilatancy Ψ were all held

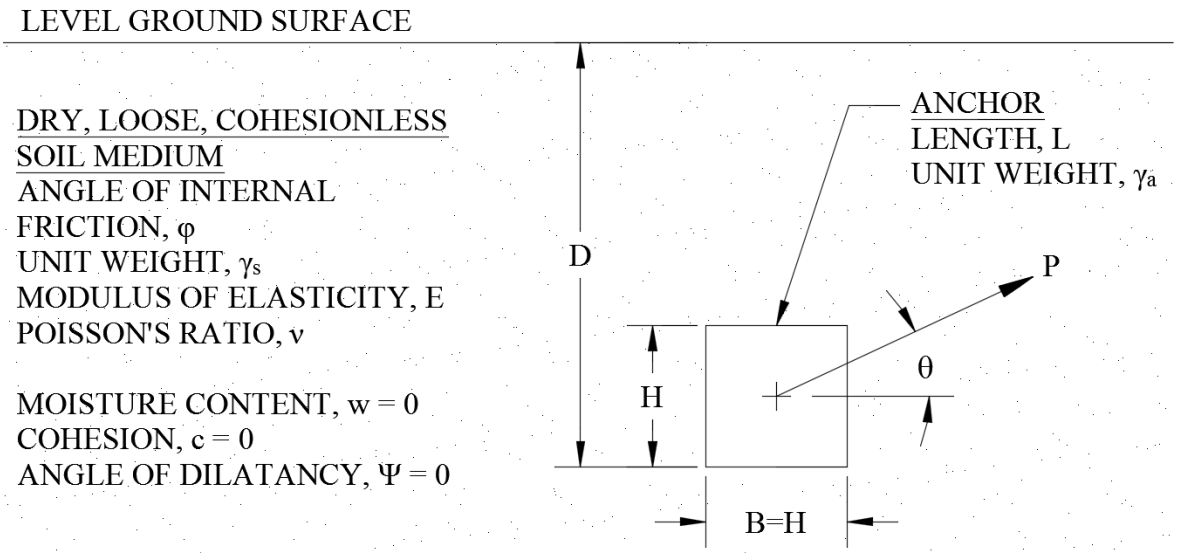

Figure 30 – Problem Definition for Deadman Anchor in Cohesionless Soil Medium.

constant at 0. The anchor has a length L, unit weight γ_a, and an interface angle of friction between the soil and anchor material of δ.

2.0.1 Theoretical Solutions

2.0.1.1 Bridges to Prosperity (B2P) Solution

The design procedure outlined in B2P's *Bridge Builder Manual, Volume 3* (2016) was re-formatted in Equations (7) through (21) to calculate pullout force, P, as a function of friction angle φ, of anchor H tall by H wide, with length L at embedment D, and soil and anchor of their own unit weights γ_s and γ_a, respectively. The design procedure as outlined by B2P does not consider the variables of E, ν, or Ψ. Cohesion and moisture content can be considered in the B2P design procedure as components of active and passive earth pressures and soil unit weights but are not included in this analysis. The solution for P is broken into two components, horizontal (sliding resistance) and vertical (uplift resistance), and a final P_{ult} is taken to be the lesser of the two. The derivation of forces is as follows for the horizontal direction (refer to Figures 3 and 4):

$$\sum F_x = P_{active} + P_x - P_{passive} - F_f = 0, \tag{7}$$

where P_{active} is the resultant force of the active earth pressure, $P_{passive}$ is the resultant force of the passive earth pressure, and P_x is the x-component of the cable force. F_f is the frictional force developed between the bottom of the anchor and the soil as a result of the weight of the anchor W_{anchor}, weight of the soil above W_{soil}, the y-component of the cable force P_y which acts against the forces of anchor and soil weight, and the coefficient of static friction, tan(δ) as shown in Equation (8).

$$F_f = (W_{anchor} + W_{soil} - P_y)\tan(\delta), \tag{8}$$

$$\text{where } W_{anchor} = \gamma_a H^2 L, \tag{9}$$

$$\text{and } W_{soil} = \gamma_s HL(D - H). \tag{10}$$

The earth pressures are composed of a triangular earth pressure as well as a constant earth pressure due to surcharge of the soil above one and one-half times the anchor height (Figure 3). The active and passive pressure coefficients are determined using Rankine's theory, which simplify to Equations (11) and (12) for a level backfill and vertical anchor face:

$$K_a = \frac{1 - \sin\varphi}{1 + \sin\varphi}, \tag{11}$$

$$\text{and } K_p = \frac{1 + \sin\varphi}{1 - \sin\varphi}. \tag{12}$$

The resultant of active and passive earth pressures (which both act at a point 5H/12 above the base of the anchor in opposing directions, thus creating no net moment) are then calculated as

$$P_{active} = \frac{1}{2} K_a \gamma_s (1.5H)^2 L + K_a \gamma_s (D - 1.5H)(1.5H)L \tag{13}$$

$$\text{and } P_{passive} = \frac{1}{2} K_p \gamma_s (1.5H)^2 L + K_p \gamma_s (D - 1.5H)(1.5H)L. \tag{14}$$

Given that

$$P_x = P\cos\theta, \text{ and} \tag{15}$$

$$P_y = P\sin\theta, \tag{16}$$

solving for cable force results in P due to the limit state of friction,

$$P_{friction} = \frac{P_{passive} + W_{anchor}\tan\delta + W_{soil}\tan\delta - P_{active}}{\cos\theta + \sin\theta\tan\delta}. \tag{17}$$

Solving for vertical forces (refer to Figure 5),

$$\sum F_y = P_y - W_{anchor} - W_{overburden} = 0, \tag{18}$$

$$\text{where } W_{overburden} = \frac{H+T}{2}(D-H)L\gamma_s, \tag{19}$$

and T is the width of the trapezoid of soil overburden at the surface, determined by

$$T = H + (D-H)\tan 30°. \tag{20}$$

Therefore, solving for the cable force results in P due to the limit state of uplift,

$$P_{uplift} = \frac{W_{anchor} + \left[\frac{2H + (D-H)\tan 30°}{2}(D-H)L\gamma_s\right]}{\sin\theta}. \tag{21}$$

The controlling limit state and ultimate capacity of the system according to the B2P design procedure is the minimum of $P_{friction}$ (17) and P_{uplift} (21).

2.0.1.2 Meyerhof's Limit Equilibrium Formula

The formula for inclined plate anchors developed by Meyerhof and discussed in Section 1.2.3 showed the best correlation with experimental data. To present another potential theoretical solution that is independent of finite element modeling, Equation (1) is adapted to the geometry shown in Figure 30 and presented as Equation (22). Here, h is taken as the diagonal length of the anchor cross section, which is H√2 for a square anchor. The variable H in Equation (1) is equal to the variable D in Figure 30, and the angle Ψ is complementary to θ. Again, note that the symbol Ψ is used to signify angle of inclination of the pullout force, and not angle of dilatancy. To avoid confusion, the symbol is replaced with a conversion to angle θ as shown in Figure 30, which is the

complementary angle to Meyerhof's Ψ. Therefore Meyerhof's theoretical capacity for the B2P anchor of length L is

$$P_{Meyerhof} = L\left[\frac{1}{2}K_b\gamma_s D^2 + \gamma_s DH\sqrt{2}\cos^2(90-\theta)\right]. \quad (22)$$

The coefficient K_b is determined graphically in Figure 31 as a function of friction angle φ and pullout angle Ψ (90 - θ).

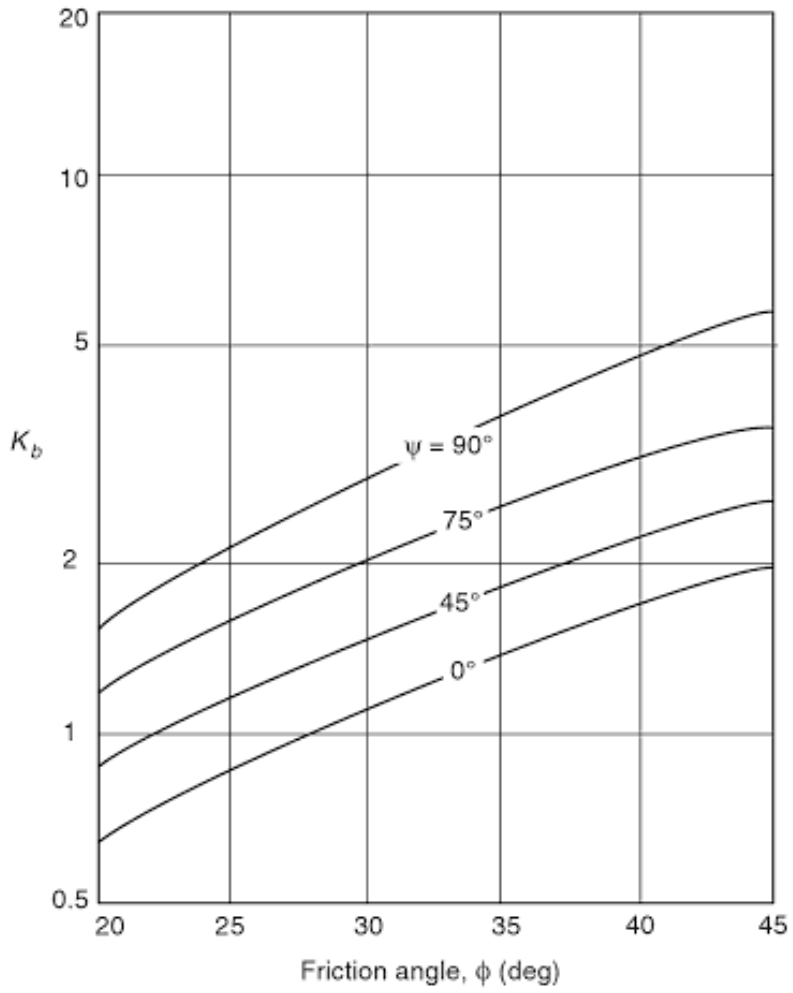

Figure 31 – Variation of Meyerhof's Earth Pressure Coefficient K_b with Soil Friction Angle φ and Pullout Angle Ψ=90-θ (Das & Shukla, 2013).

2.0.2 Qualitative Scale Modeling

A tabletop model was constructed to perform qualitative scale model tests for anchor pullout in a dry, loose, cohesionless sand to observe soil deformation and anchor rotation throughout the process of displacement and failure. The model was created to observe a cross-section of a small, square deadman anchor as it is pulled to failure. The observations made were qualitative in nature and no physical measurements were taken. Videos and images of the deformed soil during pullout were used to verify the deformed mesh of the finite element modeling.

2.0.2.1 Tabletop Model Construction

The qualitative scale model was constructed out of 3/4-inch pine wood material and 1/4-inch thick polycarbonate Plexiglas. It was assembled to create an interior box measuring 18 inches tall by 21 inches long by 2 inches deep. The short end walls used wood material with 1/4-inch thick, 1/4-inch deep slots cut into them along the height with a table saw. The Plexiglas material was cut to 18.5 inches by 21.5 inches and glued into the slots in the end pieces as well as corresponding slots on the bottom piece. Wood material was attached to the two wooden end walls of the box to act as a tension tie to resist the weight of sand placed between the Plexiglas walls. A pulley was attached to the outside of the model on one side, and the bottom piece of wood was extended out 18 inches beyond the end of the box on the other side in order to provide area to place counterweights. A second pulley was attached to a small piece of wood with pre-drilled holes that lined up with holes drilled into the top of the box that allowed a 1/4-inch bolt to pass through and clamp the wood together. Finally, wooden feet were cut to aid in the

stability of the frame during testing. Figure 32 shows a picture of the completed model. A 2-inch by 2-inch by 2-inch scale model of a B2P anchor was made out of bubinga wood, which has a higher dry density than most hardwoods. Three such blocks of wood were cut, and screw eyes were inserted at angles of 25, 35, and 45 degrees from the horizontal and directed through the centroid of the shape. The experiment was originally planned to test angles of 25, 30, 35, 40, and 45 degrees but after running a few tests it became apparent that the differences between 5 degrees were hard to distinguish on this scale and differences of 10 degrees would suffice to illustrate the results.

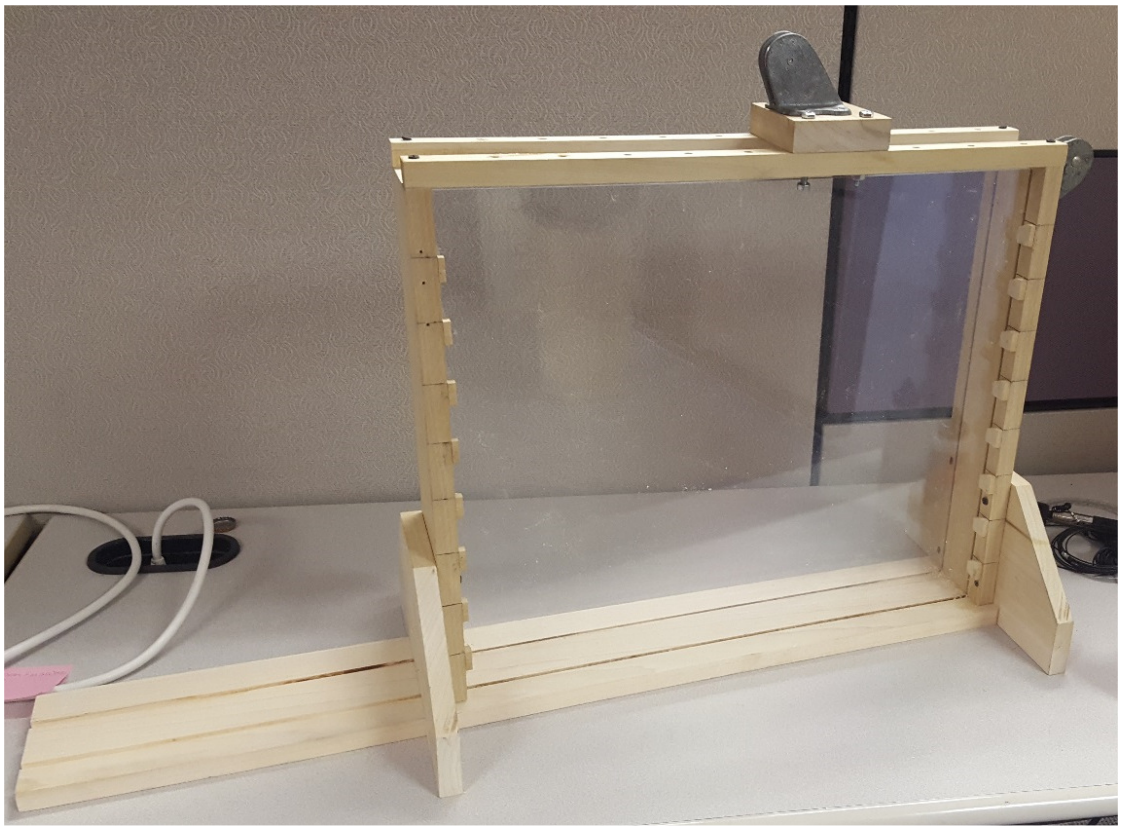

Figure 32 – Qualitative Scale Model Constructed by the Author.

2.0.2.2 Experimentation

One-sixteenth-inch diameter steel cable was threaded through the eye screw in the scale anchors and clamped to itself with soft aluminum couplers. The anchors were buried in pool filter quartz sand at various embedments, and 2-inch layers of sand above the anchor were marked using copper BB's. The BB's were laid on the surface of the sand every 2 inches of height in order to create a deformable plane that would be visible through the Plexiglas. The cable was run through the soil above the anchor, over the first pulley that is clamped to the top of the box, then over the second pulley and down the side of the box. The anchor was pulled out of the sand by pulling down on the cable by hand. Measurements of force in the cable or in-line displacement of the cable were not taken for this scale model. Pullout angles of 25, 35, and 45 degrees were tested at embedment ratios of 2, 3, 4 and 5 for a total of 12 tests.

2.0.3 Quantitative Scale Modeling

After the completion of qualitative scale model testing, the model used during that testing was modified to collect load and displacement data for the same scale model anchors pulled to failure by a test frame. It was modified to stiffen the Plexiglas sides to control flexing during pullout and to allow for a small amount of compaction of the sand. It was also modified to change the direction of the pullout cable as it left the sand: the first pulley remained unchanged, but the second pulley attached to the outside of the box was rotated in order to direct the cable upwards to attach to the pulling actuator.

2.0.3.1 Tabletop Model Modification

Three-quarter-inch thick by 2-inch wide wood slats were glued in the strong direction to the outside of the Plexiglas surface and attached at the top and bottom to the wood frame with screws. This reinforcement was placed every 3 inches along the length of the Plexiglas surface. Figure 33 shows a picture of the modified tabletop model. The bubinga wood blocks were changed slightly to help eliminate some of the problems observed during qualitative scale model testing. The blocks were sanded to be 2 inches tall by 2 inches wide by 1 7/8-inch thick, and felt material was glued to the sides that had been sanded down. This was done in order to fill the space between the blocks and the

Figure 33 – Qualitative Scale Model Modified by the Author to Run Quantitative Scale Model Tests.

Plexiglas that had previously been infiltrated by sand during pullout. The felt material was slightly compressible and provided a constant seal with a small amount of frictional resistance. The soil material used was also changed to one for which engineering properties were known: a sand used for fine aggregate in concrete mixes in the Construction Sciences Lab at MSOE with particle sizes larger than #16 (0.0469 inches/1.18 millimeters) filtered out. This sand has been used in the Direct Shear Lab of the MSOE Geotechnical Engineering course and has been verified to have an average internal angle of friction of approximately 34 degrees.

2.0.3.2 Set-Up and Experimentation

The anchors were embedded in the sand similarly to the qualitative scale model testing but omitting the layer of BB's every 2 inches in height. Instead, the sand was lightly compacted using a flat 2-inch-wide plate to ensure consistency in the soil throughout the entire volume. The cable was again run through the sand at the pullout angle for the trial up over the first pulley but then underneath the second pulley, so the resultant direction of the cable was upwards. This cable then attached to an electronic load cell that was in turn attached to the actuator screw of the test frame. The test frame had a capacity of 10,000 pounds tensile or compressive force, and the orientation used was in the tensile direction. The actuator screw was driven hydraulically by the counterclockwise rotation of a wheel for upward (pullout) displacement. The actuator screw attached directly to a coupler manufactured by the author that attached to the electronic load cell on the other side. The load cell had an eyebolt threaded through its center that held the cable attached to the buried anchor. As the actuator screw was raised by the counterclockwise rotation of the

wheel, the load cell registered force on the eyebolt as the anchor was pulled through the sand. Displacement was measured using two LVDT linear position sensors with magnetic bases and adjustable arms. The bases were magnetized to the steel test frame and the sensors were positioned equidistant from the center on the face of the load cell. As the load cell was pulled upwards by the screw actuator, the vertical displacement was measured, which corresponds directly to the in-line displacement of the anchor through the sand because there is no mechanical advantage in the system and everything is set 1:1. Pictures of the quantitative scale model testing are shown in Figures 34 through 36. The data collection software used was National Instruments LabVIEW 2011 on an HP Elitebook 8570w laptop computer. The program was written to read and record calibrated load from the load cell and an average displacement from the two LVDT sensors. Load and displacement data were collected by the LabVIEW software and exported to Excel. The tests were run under constant-strain, whereby the displacement of the anchor as dictated by the upward motion of the load cell was controlled by the author and corresponding force measurements were taken. For the quantitative scale model tests, a constant displacement rate of 1/4-inch per minute was applied for all embedment depths and pullout angles.

2.0.4 Two-Dimensional Finite Element Modeling

Representative quantitative scale models and full-scale models were both created within GEOSLOPE SIGMA/W to analyze stresses and displacements. The representative scale models were used to verify the results of the quantitative scale model tests, while the full-scale models were used to create the design charts for pullout capacity.

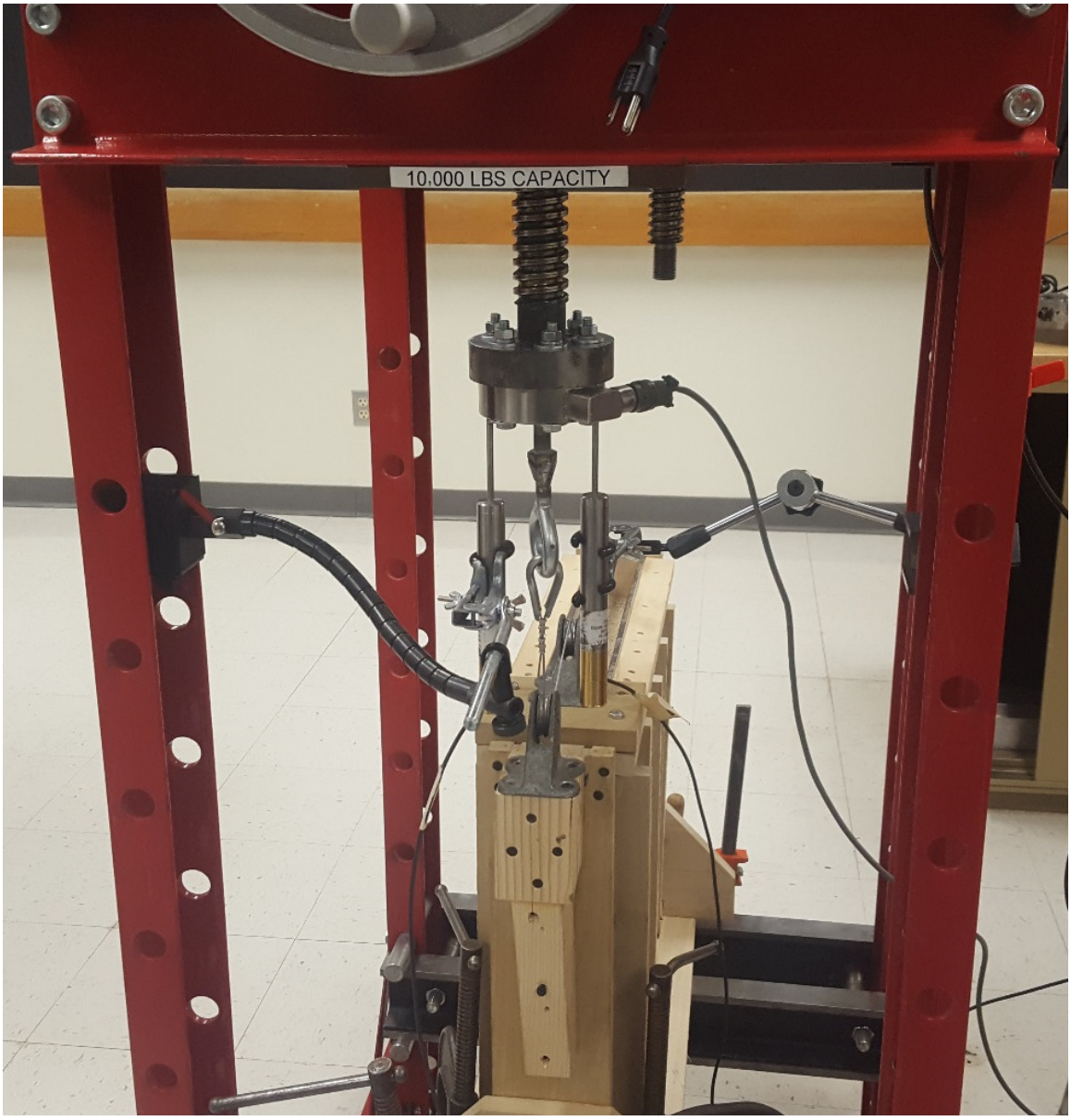

Figure 34 – Picture of Quantitative Scale Model Test Set-Up.

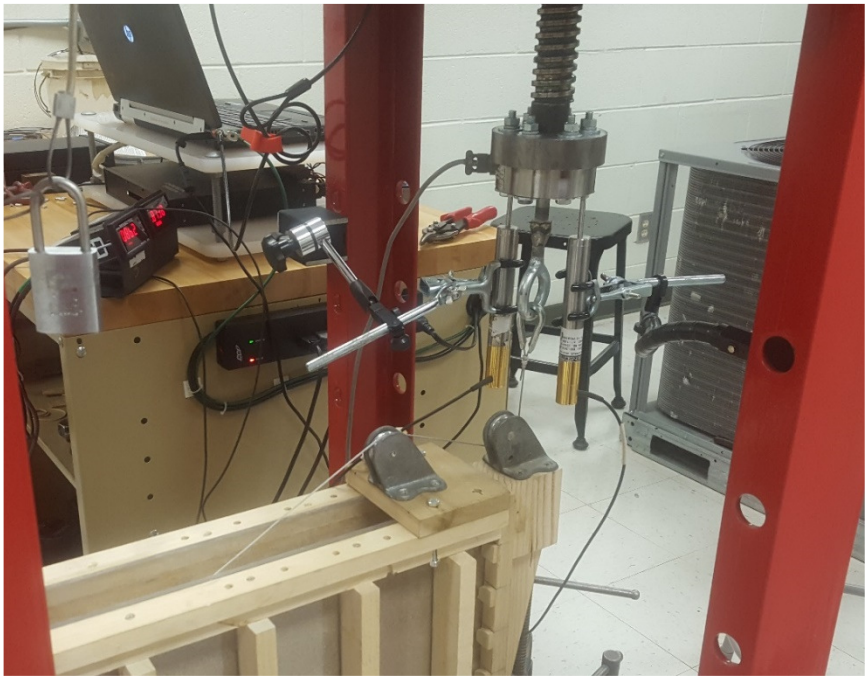

Figure 35 – Picture of Quantitative Scale Model Test Set-Up.

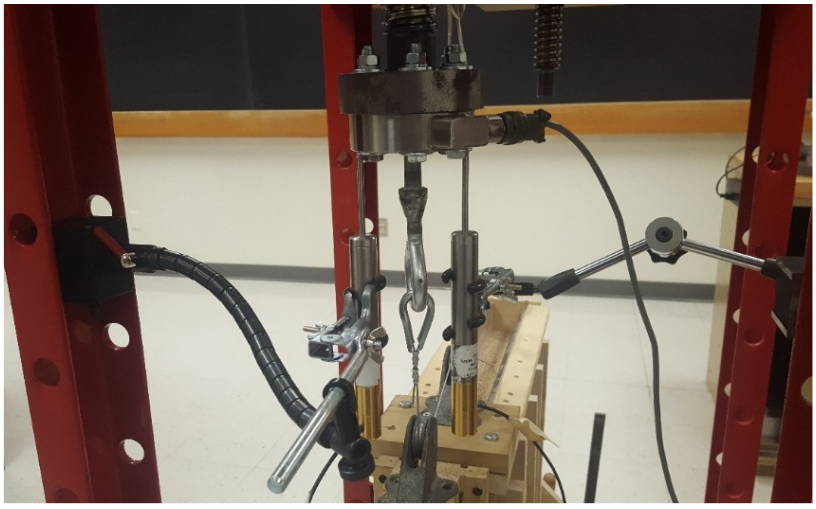

Figure 36 – Detail Picture of Electronic Load Cell and LVDT Sensors Used to Measure Force and Displacement.

2.0.4.1 Modeling Methodology

The finite element analysis used a two-stage process to analyze the anchor models. First, in-situ stresses were calculated and applied to the anchor. The in-situ stresses were the result of the surrounding soil acting on the buried anchor as well as the soil itself to create effective vertical stresses in the soil. The weight of the anchor was also applied during this stage, which imparted an increased vertical effective stress to the soil below due to the higher unit weight. After these stresses were established, the load and/or displacement was applied to the anchor in a number of increasing steps specified in the analysis. At each step, the program would apply the force or displacement, apply the self-weight of the anchor, apply the self-weight of the soil, and create results as specified by the user. The soil was modeled as elastic-plastic Mohr-Coulomb material with effective-drained parameters. Choosing these inputs in SIGMA/W gave the ability to model expected elastic-plastic behavior of soil based on common parameters: effective modulus of elasticity, effective cohesion, effective angle of internal friction, Poisson's ratio, unit weight, and angle of dilatancy. It also gives the option of defining many pore pressure-related parameters, which were not applicable to this research. Figure 37 shows an image of the material definition window for the soil used in the finite element modeling. These parameters were also used in the definition of a concrete material, but the only applicable value to be inputted was unit weight as the anchor was modeled to be a rigid body. Rigid bodies are not an option to insert as objects in SIGMA/W analyses, so the model had to make use of structural beams instead. SIGMA/W allows for the creation and analysis of bar and beam members much like most other finite element analysis programs. For this application, beams with near-infinite flexural and axial stiffness were created and applied

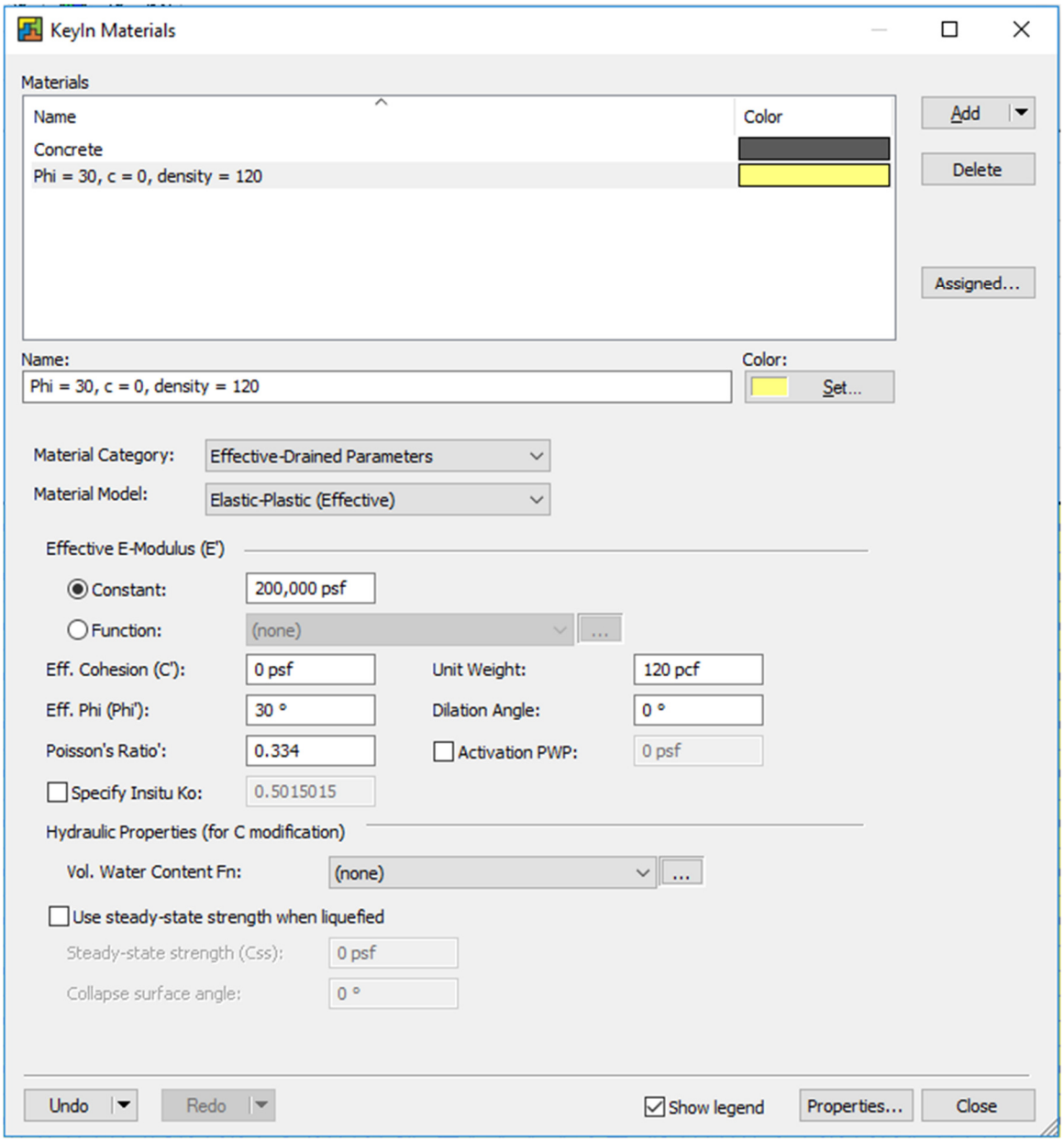

Figure 37 – SIGMA/W Soil Material Parameter Definition Window.

to the perimeter of the anchor shape (Figure 38). This effectively created a frame, inside which the concrete material was placed to give the anchor its weight. The pullout force, modeled either as a force or a displacement, was applied to a node on this frame in the

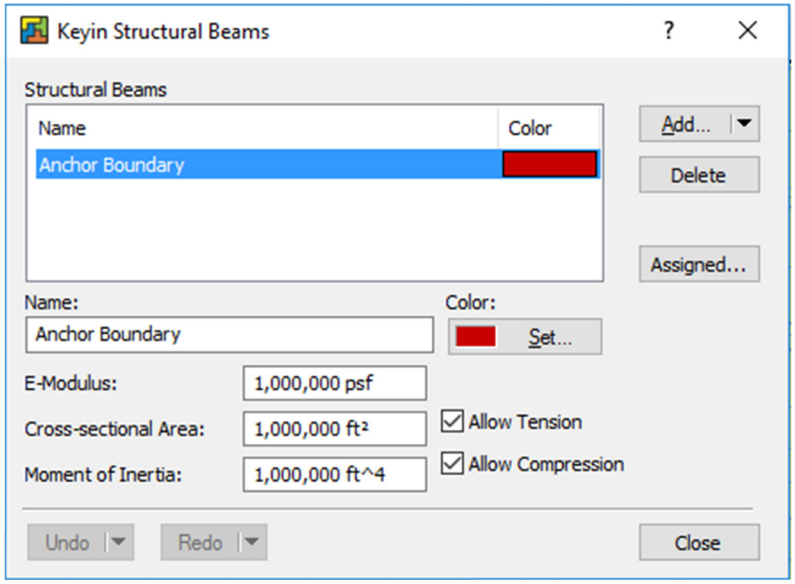

Figure 38 – SIGMA/W Structural Beam Parameter Definition Window.

direction of pullout via x and y-components. It was expressed as a boundary condition in SIGMA/W, example definitions of which can be seen in Figures 39 and 40.

2.0.4.2 Assumptions and Model Overview

The representative scale model used a 2-inch square anchor of bubinga wood material with a 2-inch element thickness (anchor length). The wood material was modeled with a unit weight of 56 pounds per cubic foot. The soil medium was held at a constant angle of friction of 34° throughout all trials to represent the filtered concrete sand used in the quantitative scale model tests, while the soil density was varied depending on the measured weight and volume of the soil inside the quantitative scale model. This was done to accurately provide a direct comparison between the quantitative scale model test results and the finite element model results. Modulus of elasticity and Poisson's ratio

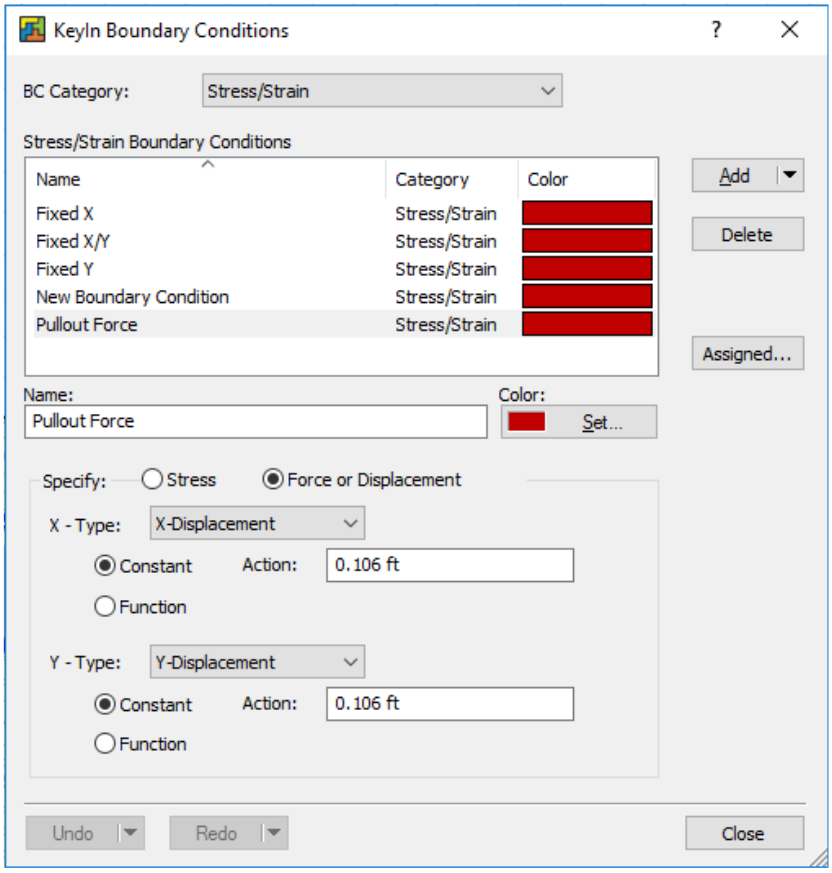

Figure 39 – SIGMA/W Boundary Condition Parameter Definition Window for Pullout Load Modeled as a Displacement.

were also kept constant at values of 200,000 tons per square foot and 0.334, respectively, as these are common values for loose, medium dense sand. The moisture content, cohesion, and angle of dilatancy were held constant at zero. The full-scale models used a 3-foot square anchor of concrete material with a 1-foot element thickness (anchor length) and a concrete material density of 150 pounds per cubic foot. The soil medium was adjusted for friction angle for the different trials, while the soil density was held constant at 120 pounds per cubic foot. Modulus of elasticity and Poisson's ratio were also kept

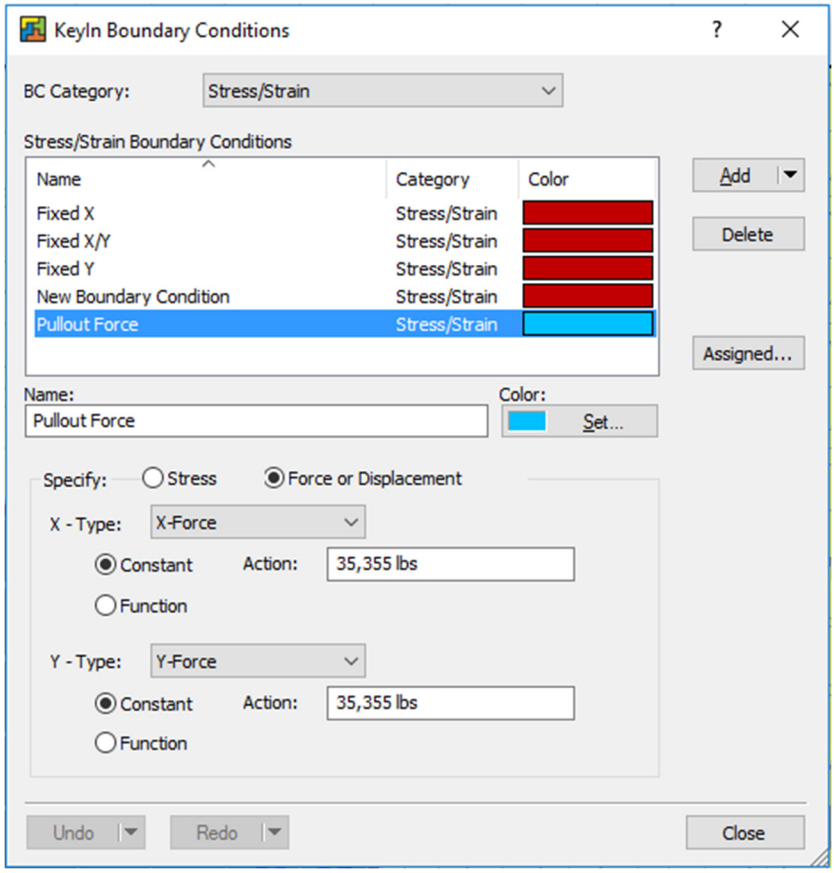

Figure 40 – SIGMA/W Boundary Condition Parameter Definition Window for Pullout Load Modeled as a Force.

constant at values of 200,000 tons per square foot and 0.334, respectively. The moisture content, cohesion, and angle of dilatancy were held constant at zero. Figure 41 shows an example image of the domain that was created for each trial. The bottom edge of the domain is constrained in the x and y direction (pinned), while the sides are constrained only in the x-direction (rollers in the y-direction) and the top edge is unconstrained and free to deform. The domain was sized to ensure shear stresses would not interact with the side boundaries, so displacement of or stresses in the soil at those locations were

Figure 41 – Domain of the Problem as Modeled in SIGMA/W.

negligible with respect to how they might impact pullout capacity. Figure 42 shows a detail of the anchor as well as the mesh that was applied to the soil material. The mesh was chosen to have triangular elements with secondary nodes, meaning that results were calculated at the midpoints of the element sides as well as the corners. The red lines on the edges of the anchor are the stiff structural beams, and the grey meshed material is the concrete. No stresses were ever applied to the concrete itself, only the beams, so the mesh remained undeformed in the analysis. The pullout force was applied at a node located at the point at which the cables coming out of the anchor would cross the anchor face. The actual construction of the B2P anchor includes a concrete member that extends from the face of the anchor to the surface, called the transition arm. The transition arm contains rebar reinforcement that connects to the anchor reinforcement (Figure 43). The cables that support the bridge deck actually attach at the ground surface and not underground at

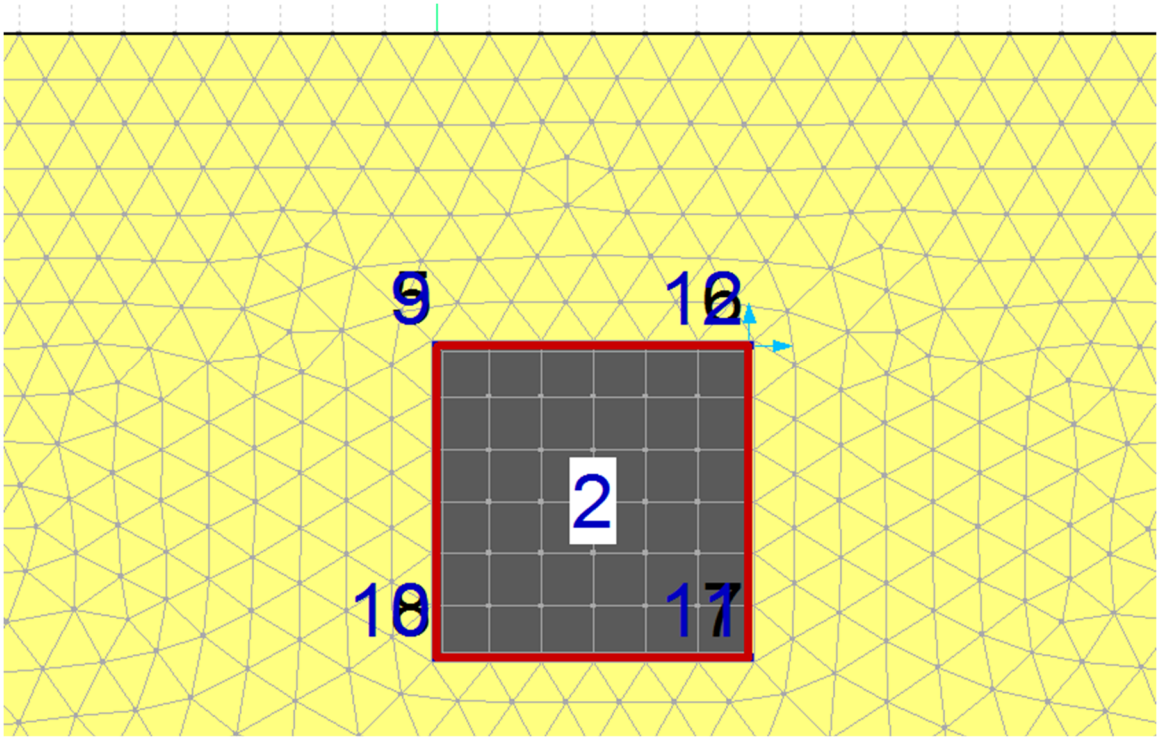

Figure 42 – Detail of Anchor Modeled in SIGMA/W and Surrounding Meshed Soil.

the anchor. However, B2P does not recommend that the anchor and transition arms be poured together, meaning that in most cases there will be a cold joint between the anchor and transition arm that can only transfer axial force through the reinforcement and cannot transfer moment. It is therefore assumed that the cable force can be applied directly at the face of the anchor and that it is free to rotate about that point if the transition arm was poured after the anchor. This is a conservative assumption, consistent with recommended B2P practices for design: to effectively ignore the contribution of the transition arm to any pullout capacity of the deadman anchor and assume the cable force is applied directly to the anchor itself. Therefore, the force or displacement was applied to a node on the anchor face in SIGMA/W that was free to rotate, allowing the anchor to rotate as it was

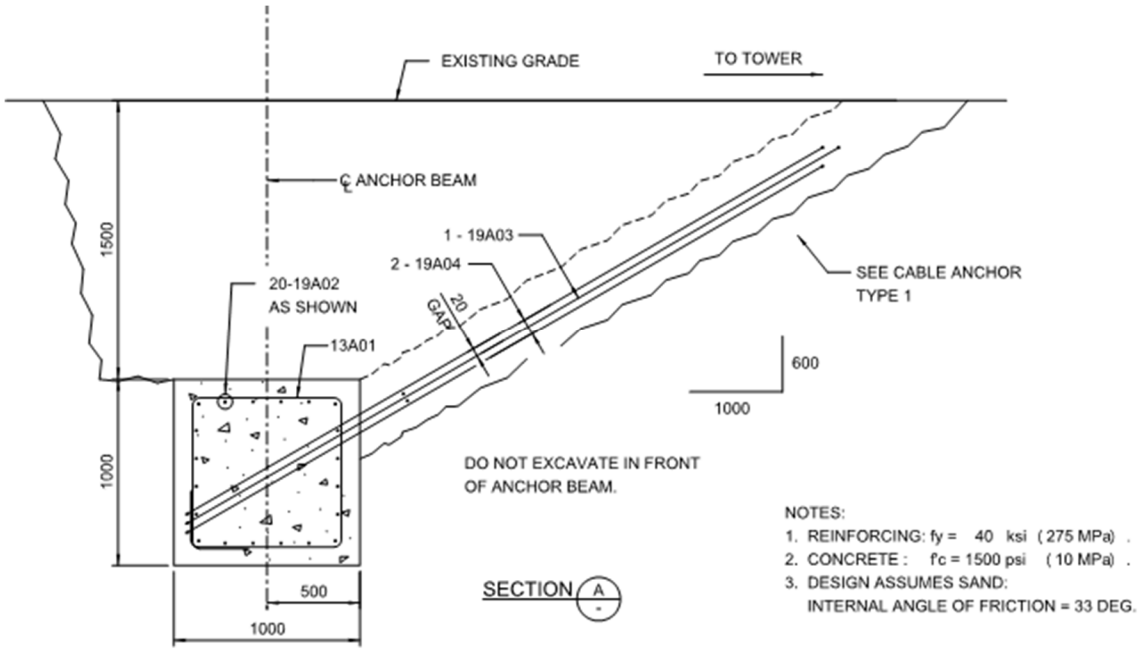

Figure 43 – Typical Anchor/Transition Arm Construction Detail (Bridges to Prosperity, 2016).

pulled through the soil. The node location changed for varying pullout angles to reflect the actual location at which the transition arm will connect to the anchor face. The force or displacement was applied in x and y components consistent with the pullout angle. Figure 44 shows a sample detail of the pullout force as well as the interface mesh. The interface mesh is a thin layer of meshed material that was added to all four surfaces of the anchor and given properties for a soil-concrete angle of static friction (δ) of 29 degrees[10]. This defined the frictional resistance of the anchor, or rather the structural beams, on the surrounding soil. The interface mesh is automatically applied to both the inside and the

[10] AASHTO LRFD Bridge Design Specifications, 6th ed. (2012), Table 3.11.5.3-1: mass concrete on clean, medium sand

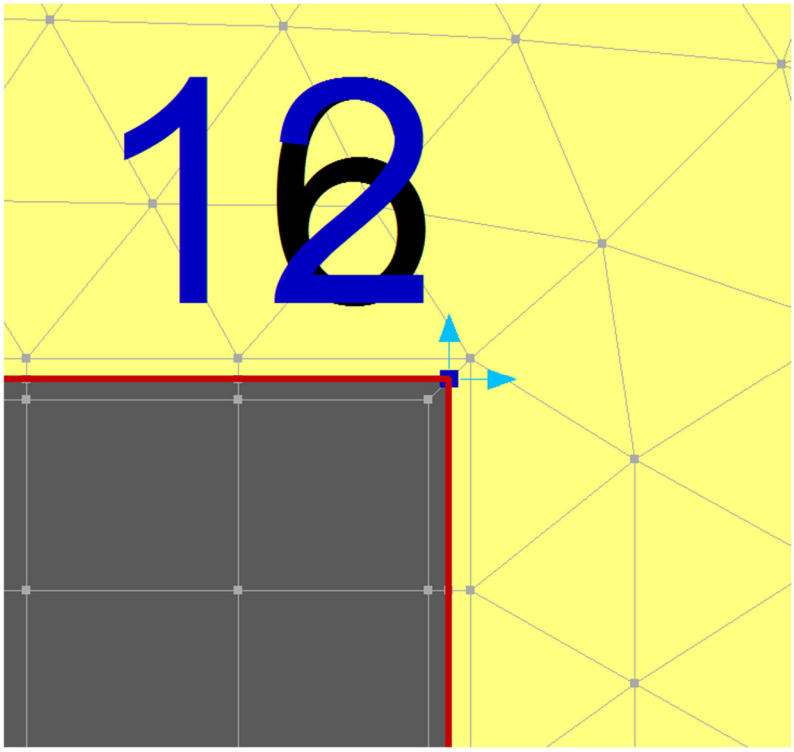

Figure 44 – Detail of Pullout Force and Interface Mesh Applied to the Anchor in the SIGMA/W Models.

outside face of the anchor, but because there are no stresses in the concrete material inside the anchor only the mesh on the outside provides frictional resistance.

For the representative scale SIGMA/W models (2-inch anchors, consistent 34-degree angle of friction, variable unit weight), the pullout load boundary condition was applied as a force. This force was increased incrementally and load-displacement graphs of the node at which the force was applied were created. The force was increased until the load-displacement graphs began to show a bi-linear curve for elastic and plastic behavior. The ultimate pullout load for that embedment ratio and pullout angle was then taken to be the maximum load before plastic behavior can be anticipated.

For the full-scale SIGMA/W models (3-foot square anchors, variable angle of friction, consistent 120 pounds per cubic foot soil density), the pullout load boundary condition was applied as a displacement. Preliminary analyses of these full-scale models revealed that the displacement at the upper bound of elastic behavior did not vary greatly from an embedment ratio of 2 to 5. This is consistent to some extent with the findings of Murray and Geddes – larger differences in failure displacements occurred for much deeper embedments (deep anchor behavior). Therefore, rather than determining a failure load and a corresponding displacement for each trial of embedment depth, pullout angle, and angle of friction, the same in-line displacement was applied to each model and the corresponding force was determined. This eliminates the need to report the displacement for each capacity, which would be necessary for a displacement-sensitive system such as this. Instead, the same displacement is applied that is within the elastic range for all combinations of embedment, pullout angle, and friction angle. Using this, designers of bridges in the future would be able to prorate an expected displacement at some design load by using the capacity from the design charts and the displacement used in the SIGMA/W models. Without using the same displacement, the displacement at the ultimate load would need to be reported for each data point and would complicate the design process to determine an expected displacement. This method also makes for a more conservative design with the higher-capacity anchors.

Chapter 3: Results and Discussion

3.0 Results

For all results presented herein, the pullout capacity is expressed in terms of a dimensionless load coefficient as defined in Equation (23):

$$\text{Dimensionless Load Coefficient} = \frac{P_{ult}}{\gamma_s LH^2}. \tag{23}$$

In order to determine the ultimate pullout capacity (P_{ult}) for a given embedment, pullout angle, and friction angle, the dimensionless load coefficient should be multiplied by $\gamma_s LH^2$. Not only is this in keeping with the style of the research discussed in the Literature Review section, but this also allows for the direct input of either metric or imperial units so long as they are consistent with the following: γ_s = [Force / Length^3]; L = [Length]; H = [Length].

3.0.1 Theoretical Solutions

3.0.1.1 Bridges to Prosperity Design Procedure

Equations (17) and (21) were graphed to illustrate the relationship between embedment depth, pullout angle, and friction angle. The results were organized into five graphs, one for each considered pullout angle, with each graph having seven curves corresponding to the seven friction angles considered. The results are presented in Figures 45 through 49.

3.0.1.2 Meyerhof's Limit Equilibrium Equation

Equation (22) was graphed to illustrate the relationship between embedment depth, pullout angle, and friction angle. The results were organized into five graphs, one for

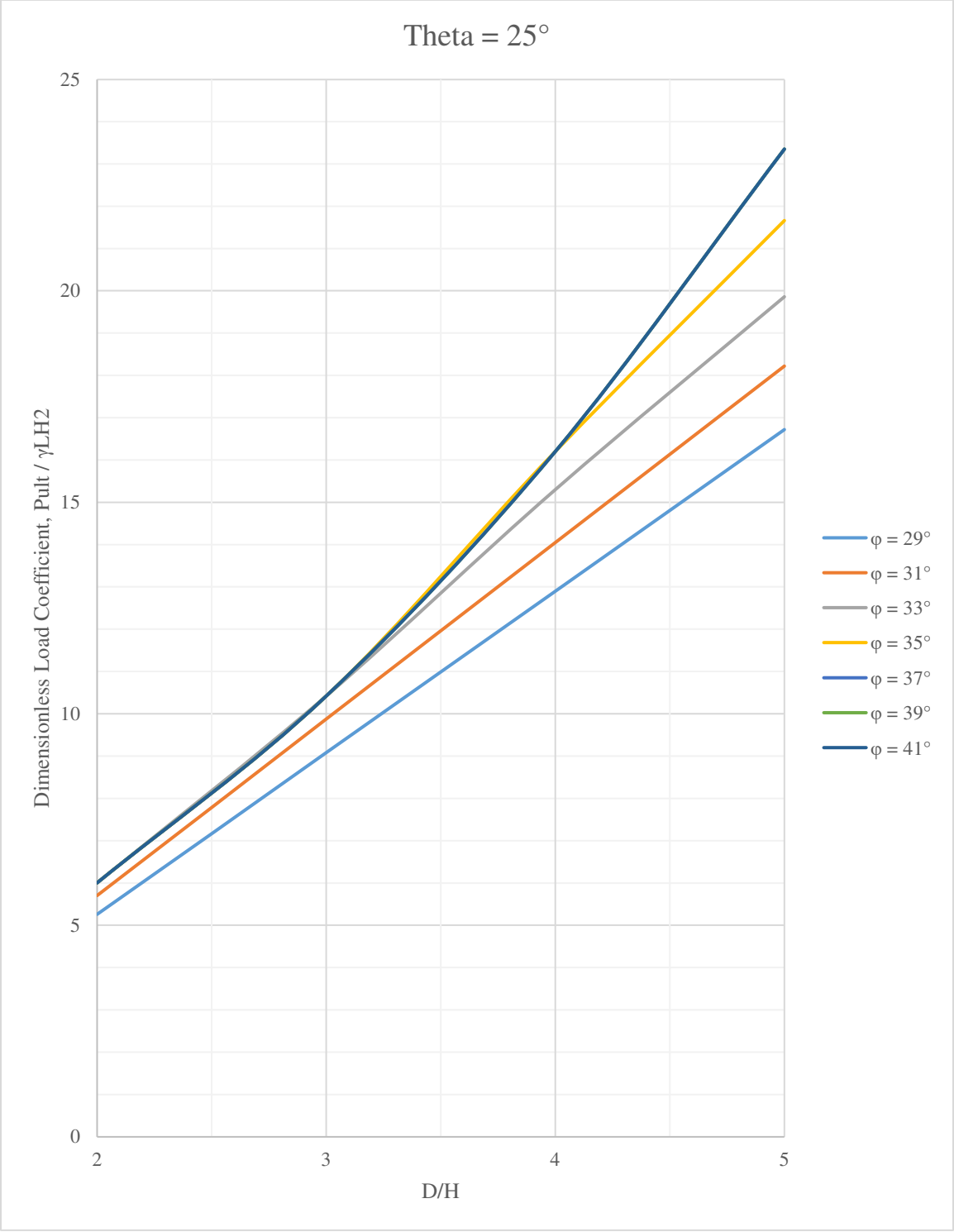

Figure 45 – B2P Design Results for a Pullout Angle of 25 Degrees.

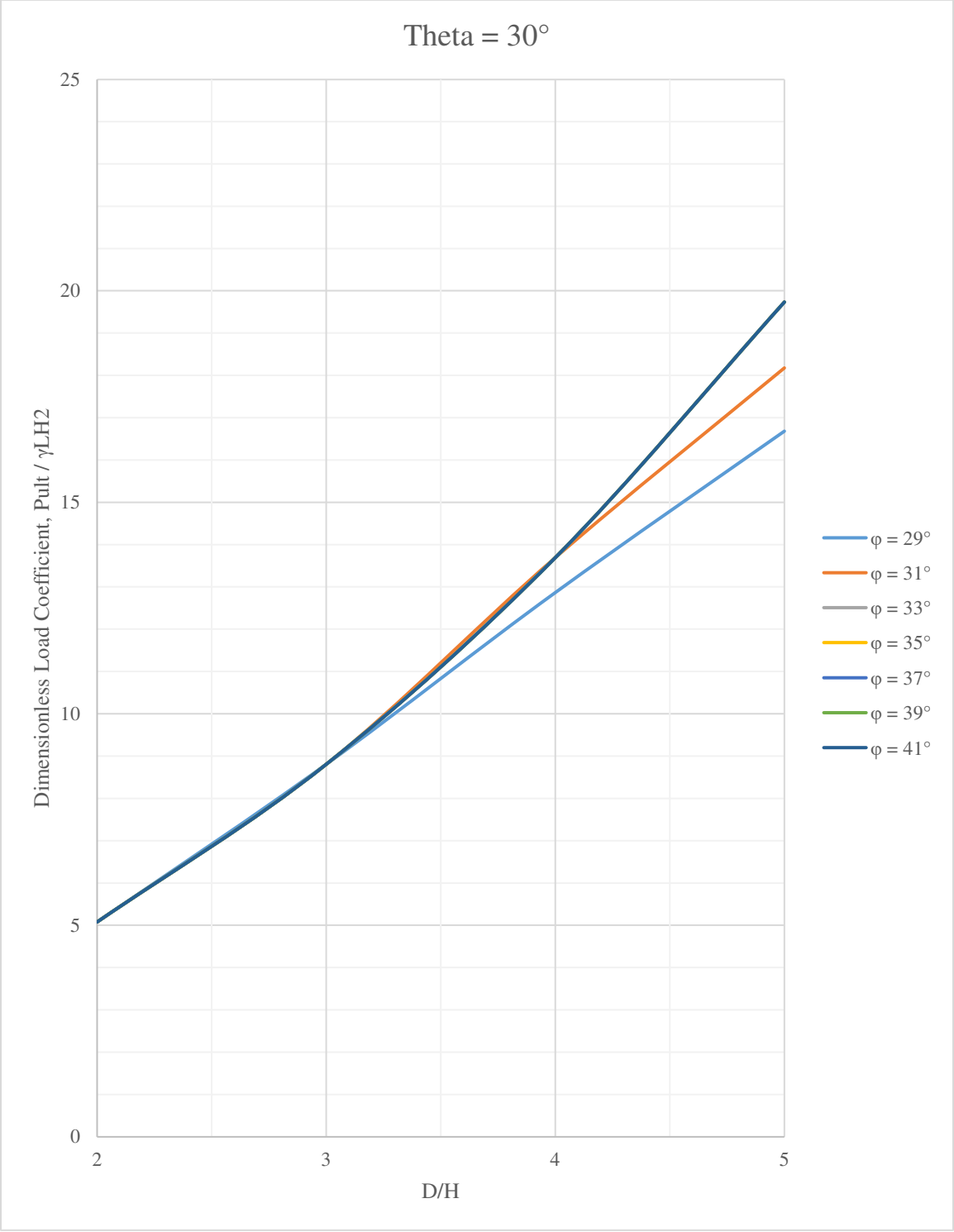

Figure 46 – B2P Design Results for a Pullout Angle of 30 Degrees.

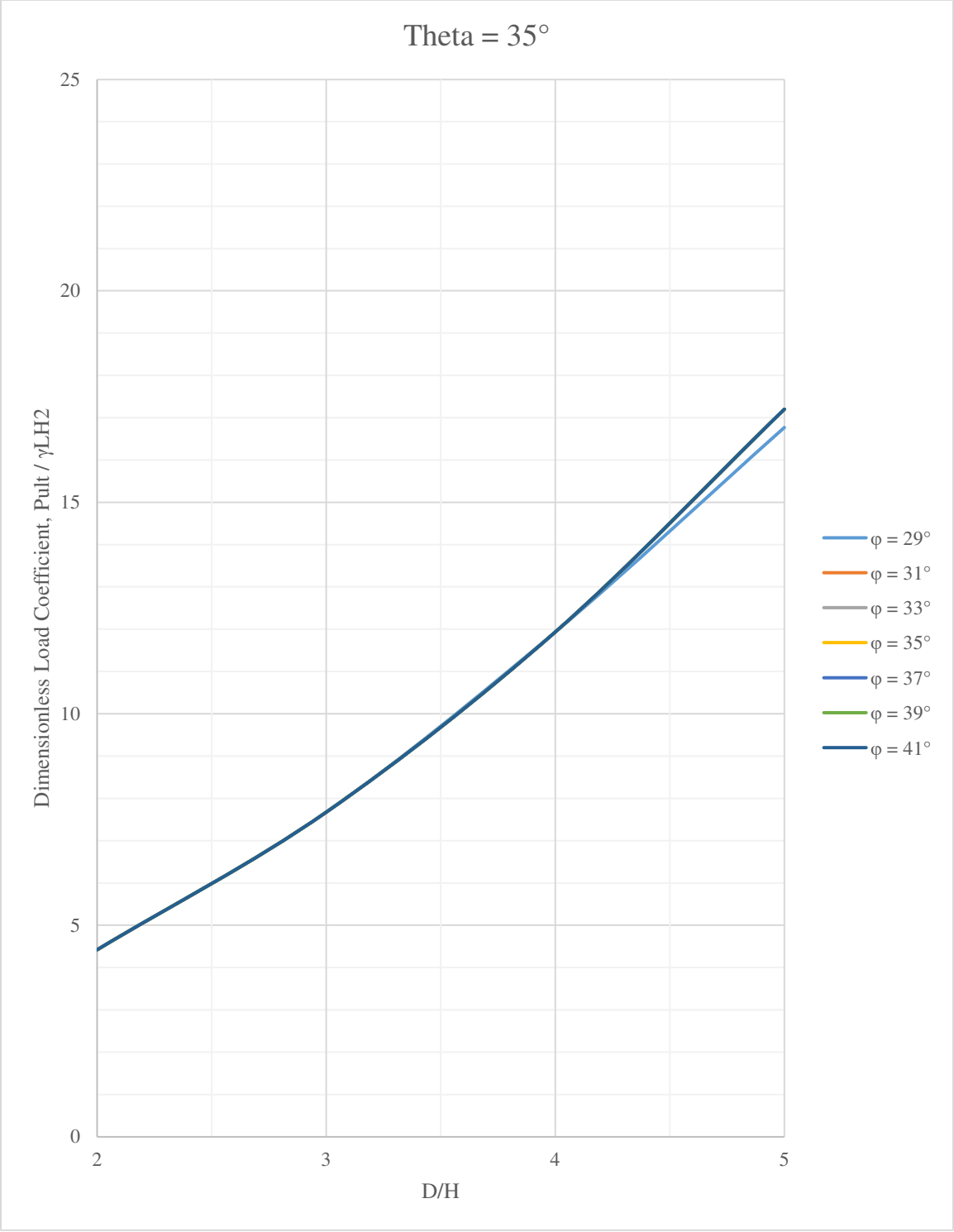

Figure 47 – B2P Design Results for a Pullout Angle of 35 Degrees.

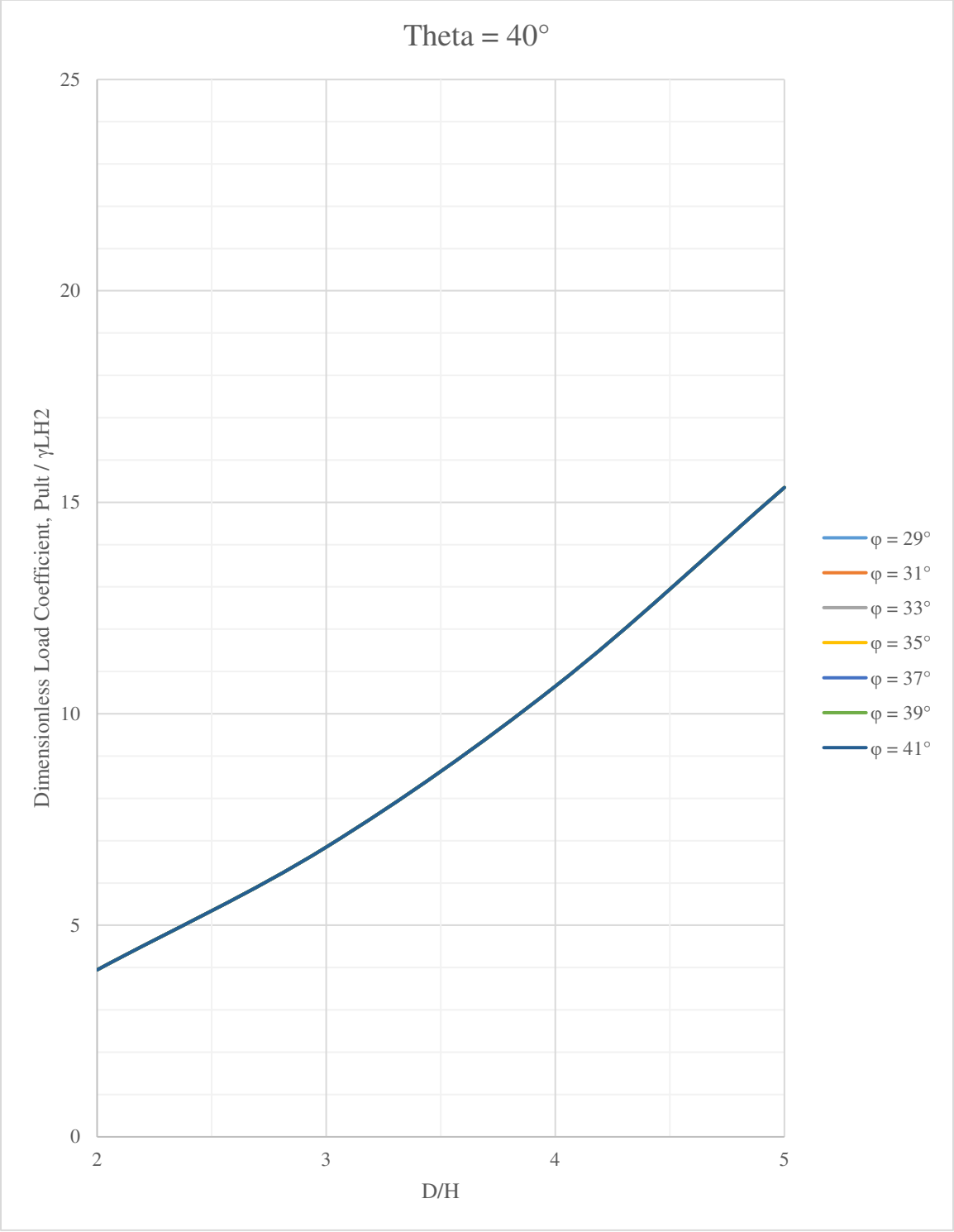

Figure 48 – B2P Design Results for a Pullout Angle of 40 Degrees.

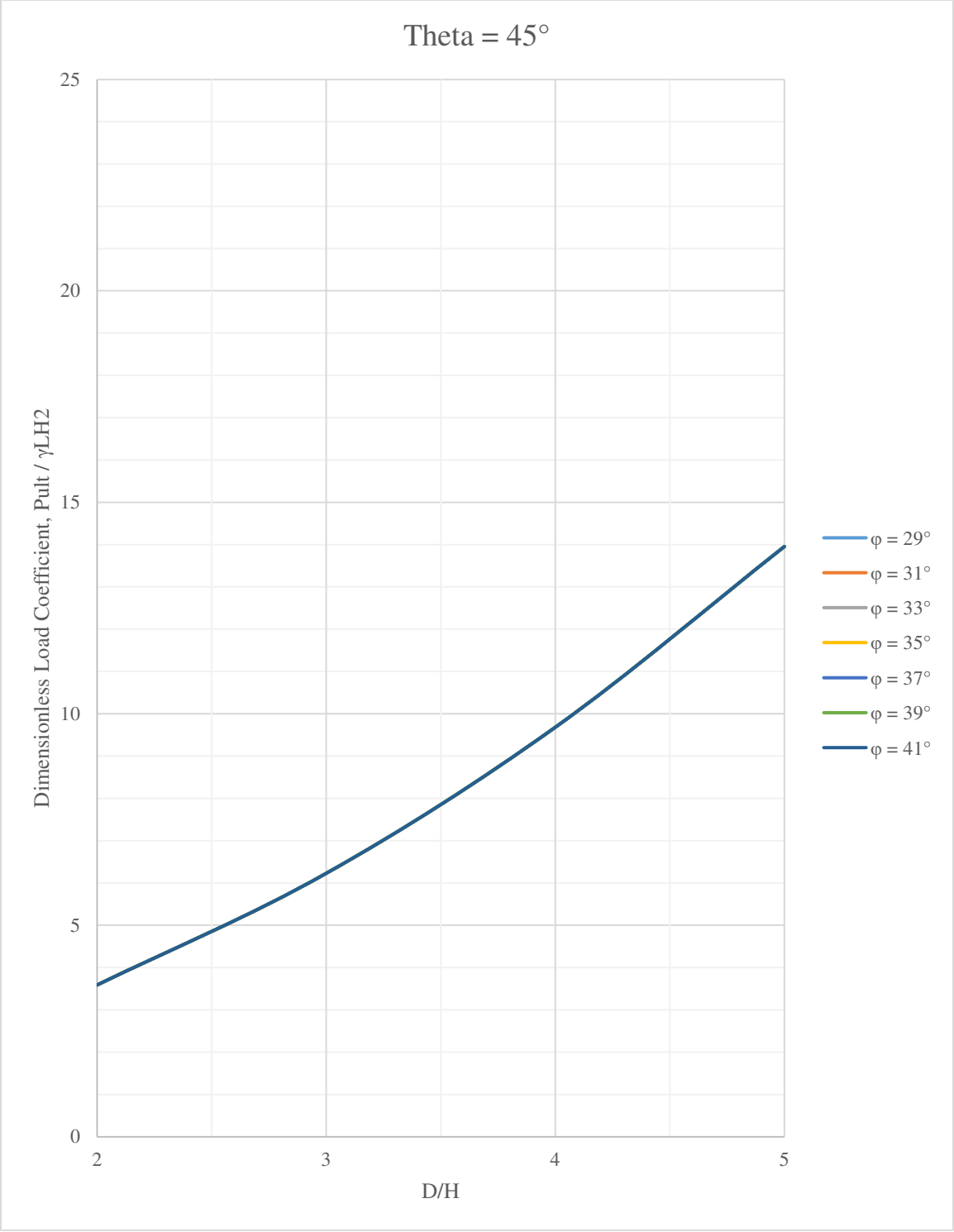

Figure 49 – B2P Design Results for a Pullout Angle of 45 Degrees.

each considered pullout angle, with each graph having seven curves corresponding to the seven internal friction angles considered for the soil. The results are presented in Figures 50 through 54.

3.0.2 Qualitative Scale Modeling

The images presented in Figures 55 through 57 are taken from video footage of three sample trials run with the qualitative scale model. These sample trials are indicative of the sand deformation shown when pulling the model anchor blocks, and how it changed with depth and inclination angle.

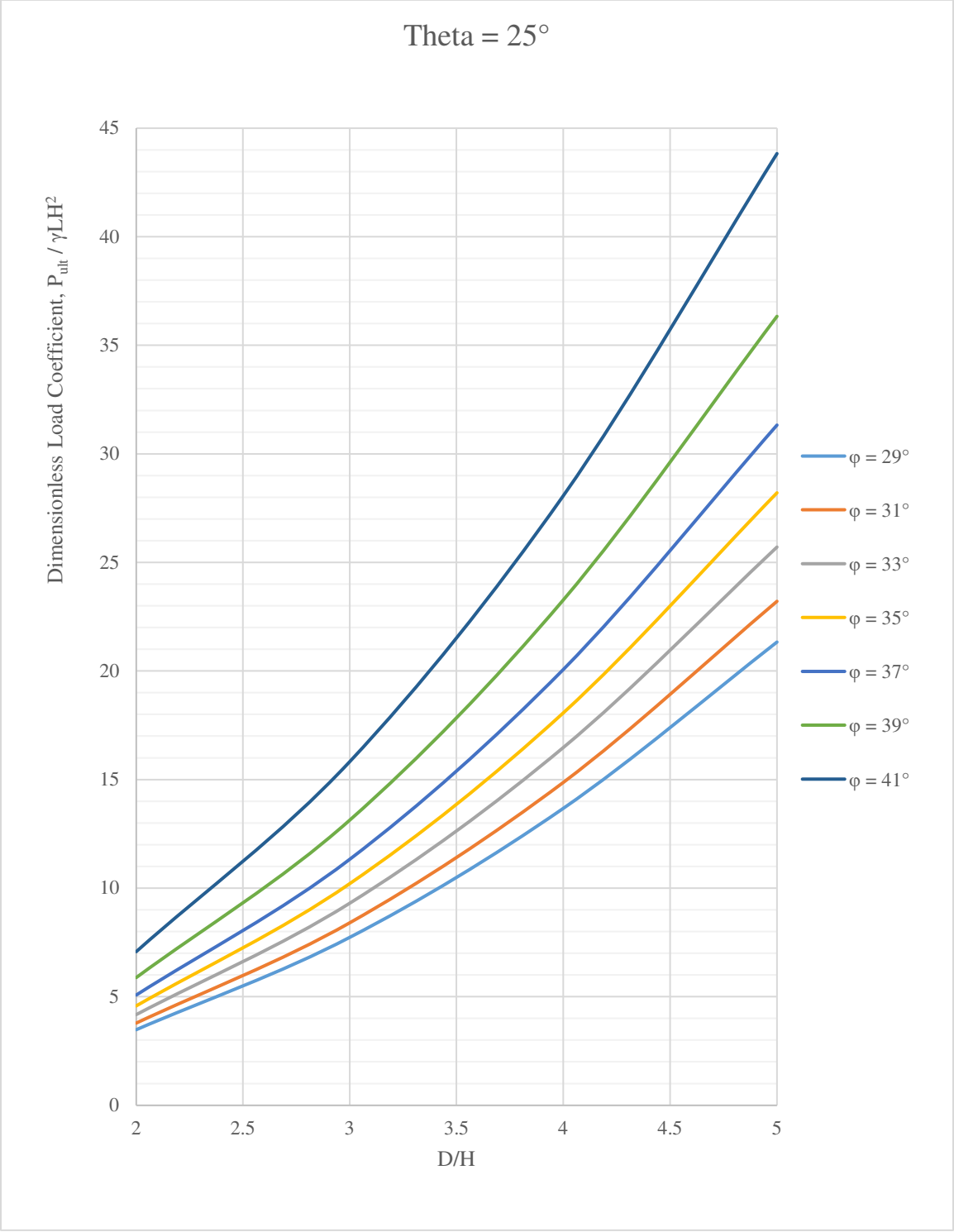

Figure 50 – Meyerhof's Equation Results for a Pullout Angle of 25 Degrees.

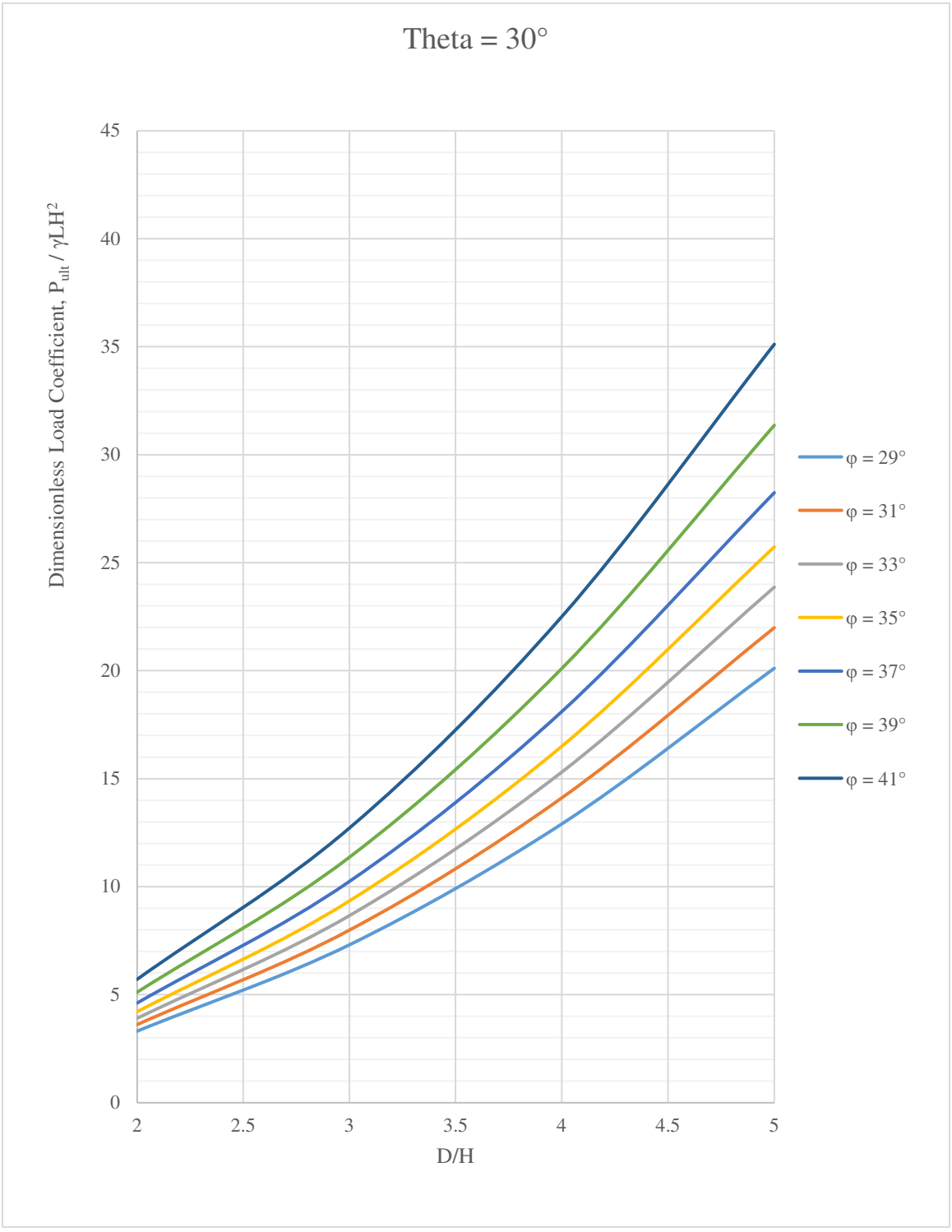

Figure 51 – Meyerhof's Equation Results for a Pullout Angle of 30 Degrees.

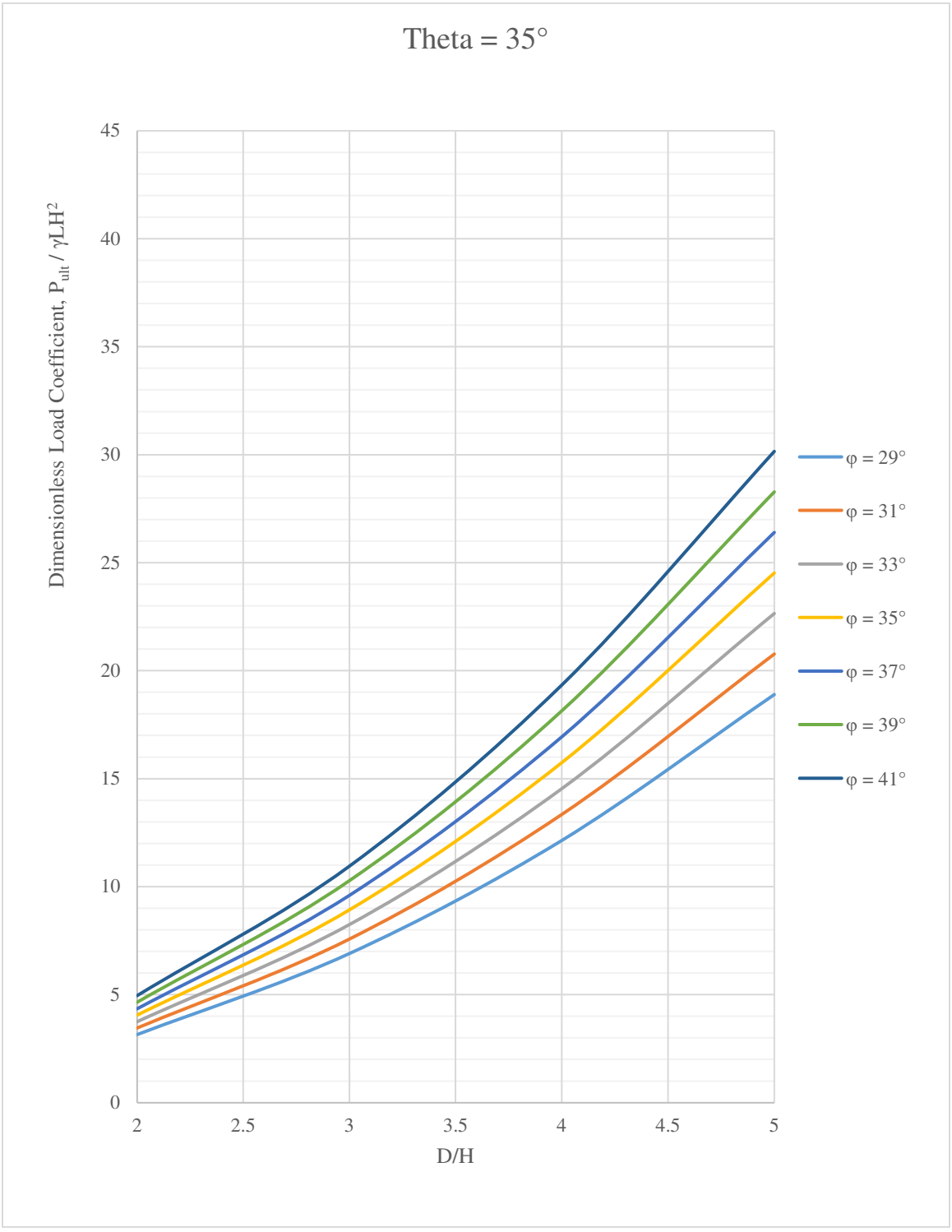

Figure 52 – Meyerhof's Equation Results for a Pullout Angle of 35 Degrees.

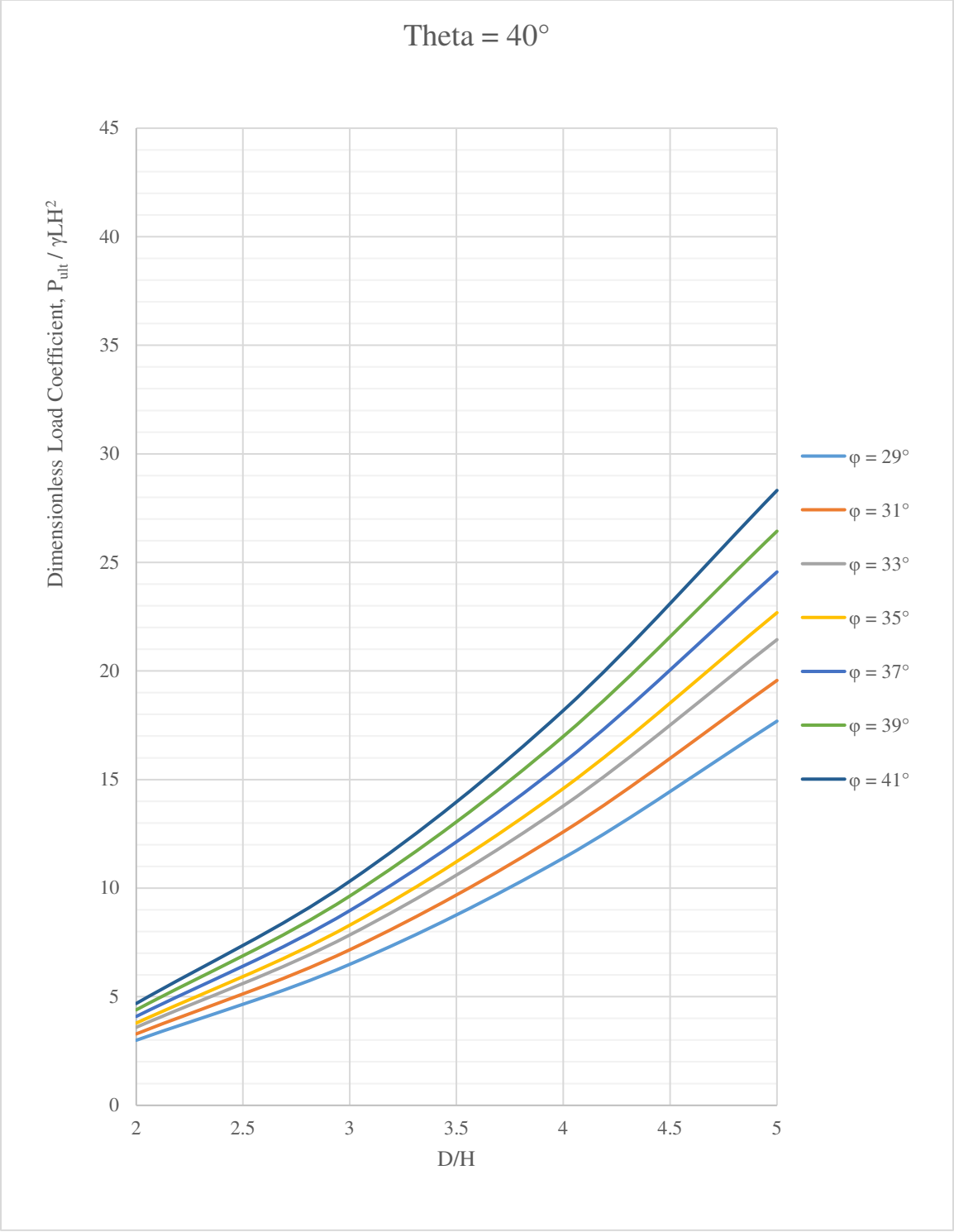

Figure 53 – Meyerhof's Equation Results for a Pullout Angle of 40 Degrees.

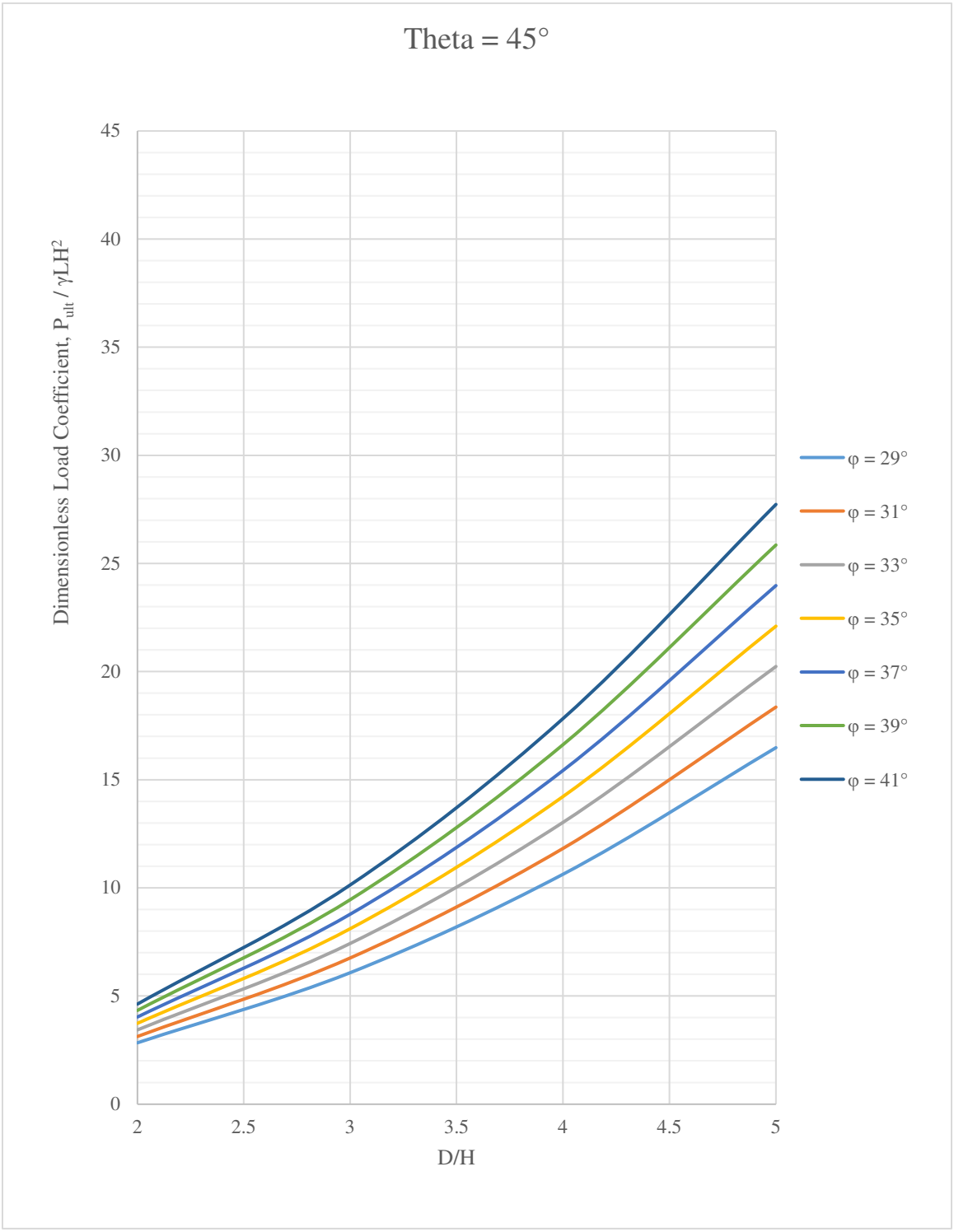

Figure 54 – Meyerhof's Equation Results for a Pullout Angle of 45 Degrees.

Figure 55 – Results of Qualitative Scale Model Testing for an Embedment Ratio of 2 and a Pullout Angle of 45 Degrees.

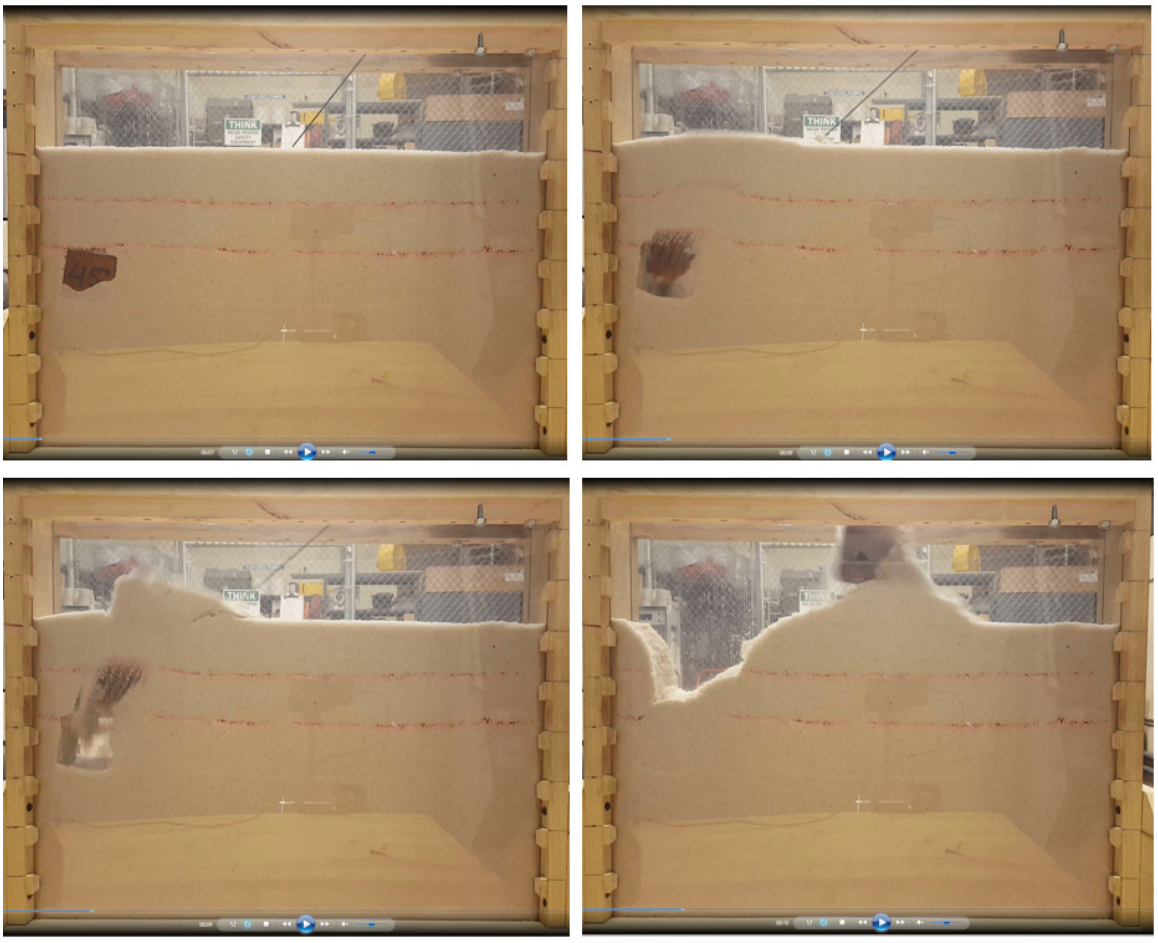

Figure 56 – Results of Qualitative Scale Model Testing for an Embedment Ratio of 3 and a Pullout Angle of 45 Degrees.

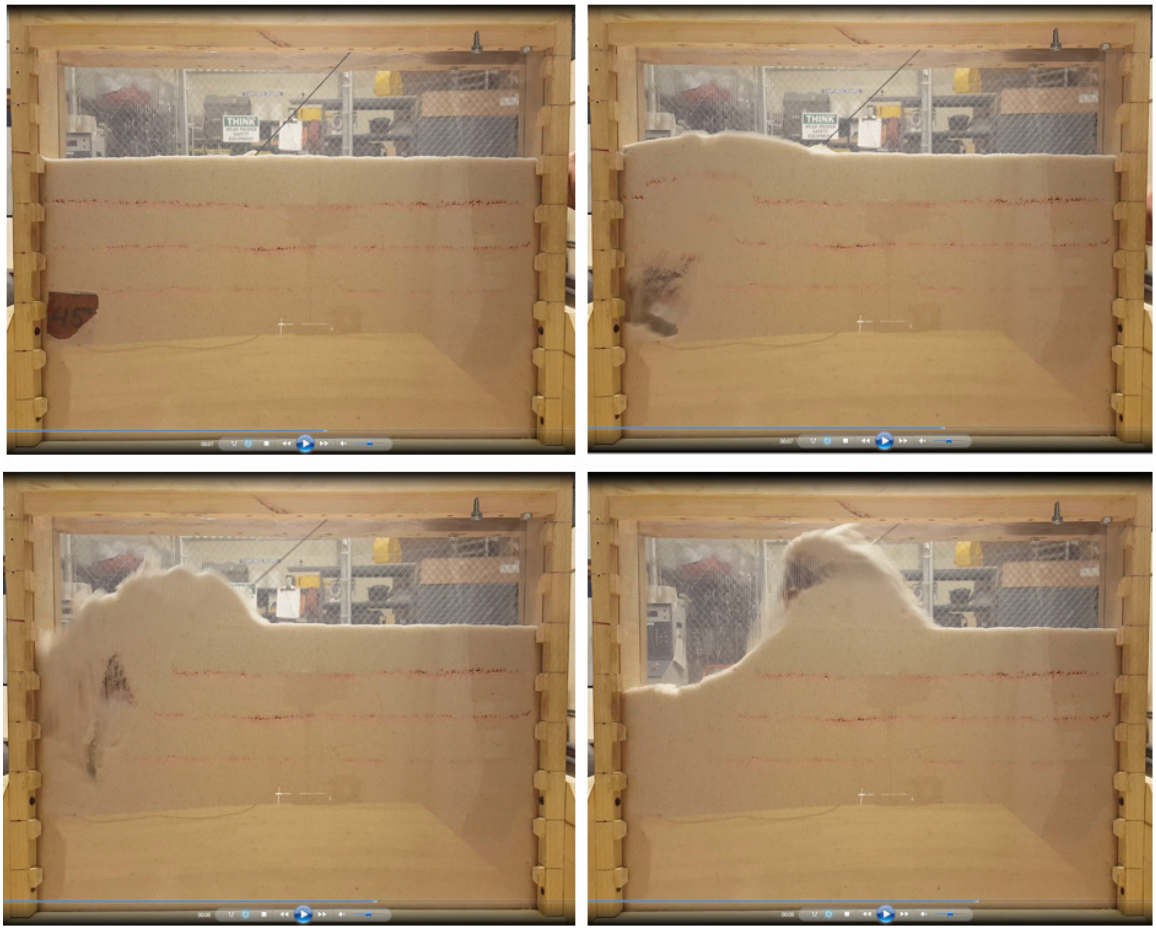

Figure 57 – Results of Qualitative Scale Model Testing for an Embedment Ratio of 4 and a Pullout Angle of 45 Degrees.

3.0.3 Quantitative Scale Modeling

Five trials were conducted using the modified tabletop model for quantitative scale model testing. The five trials covered embedment ratios of 2, 3, 4, and 5, and pullout angles of 25, 35, and 45 degrees from the horizontal with overlap at the upper and lower limits to check empirical relationships. The five trials conducted are listed in Table 1.

Table 1 – Experimental Trials Run for Quantitative Scale Modeling.

Trial	Embedment Ratio (D/H)	Pullout Angle (θ)
1	2	35
2	2	25
3	3	35
4	4	45
5	5	45

The raw load-displacement data captured by the LabVIEW software are presented for all five trials in Figure 58. Each trial was also conducted without sand in order to quantify the frictional resistance between the felt material and the Plexiglas. In each trial the wood block was still positioned to the embedment and pullout angle to capture as much as possible the friction that the block actually experienced during the experimental trials. The raw load-displacement data for these “no soil” iterations are presented in Figure 59. The raw data from Figure 58 was then excluded after reaching the maximum elastic load, and the friction loads were subtracted from the raw loads based on the data in Figure 59. The adjusted experimental data are presented in Figure 60.

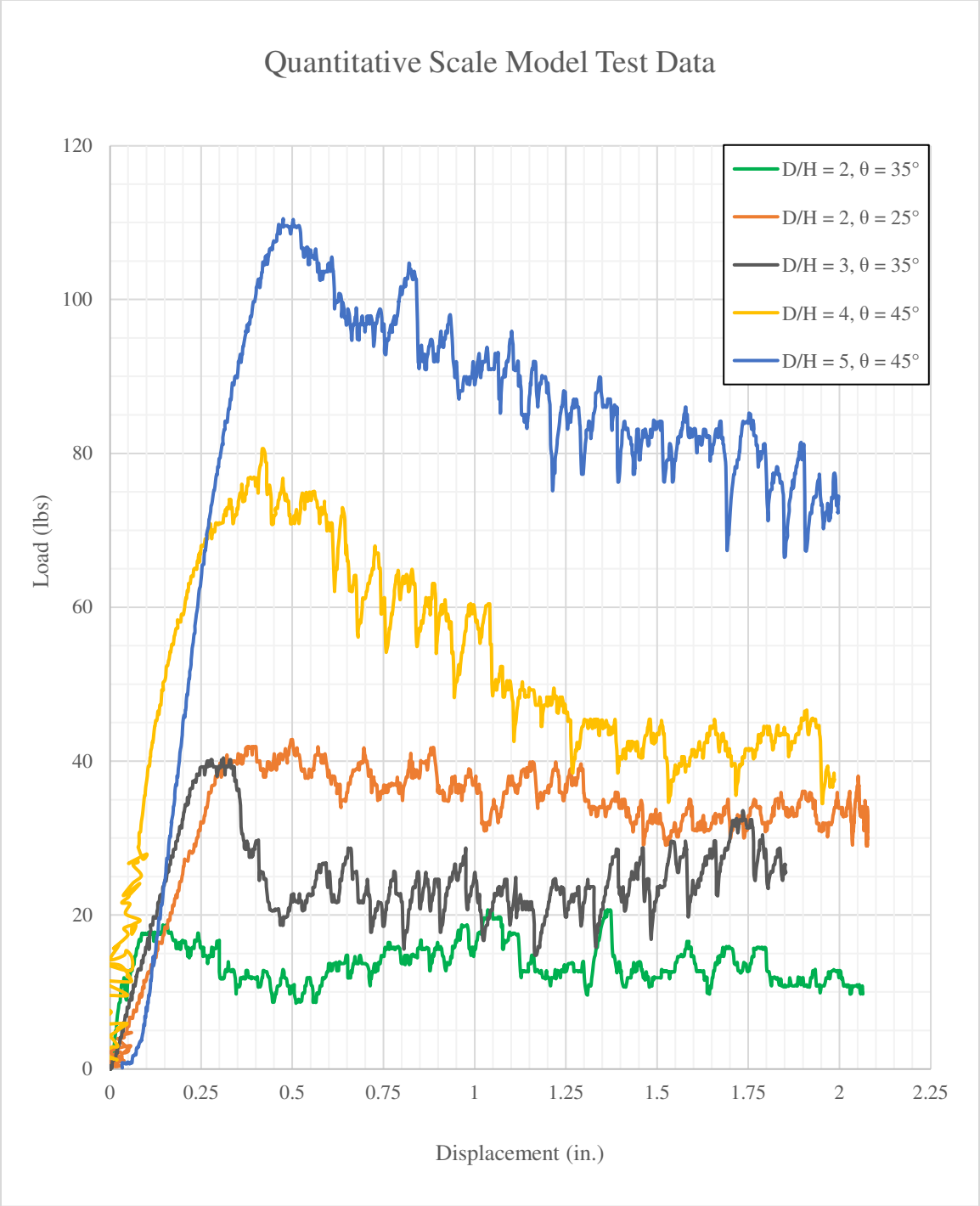

Figure 58 – Raw Experimental Data for all Five Trials as Described in Table 1 for the Quantitative Scale Model Testing.

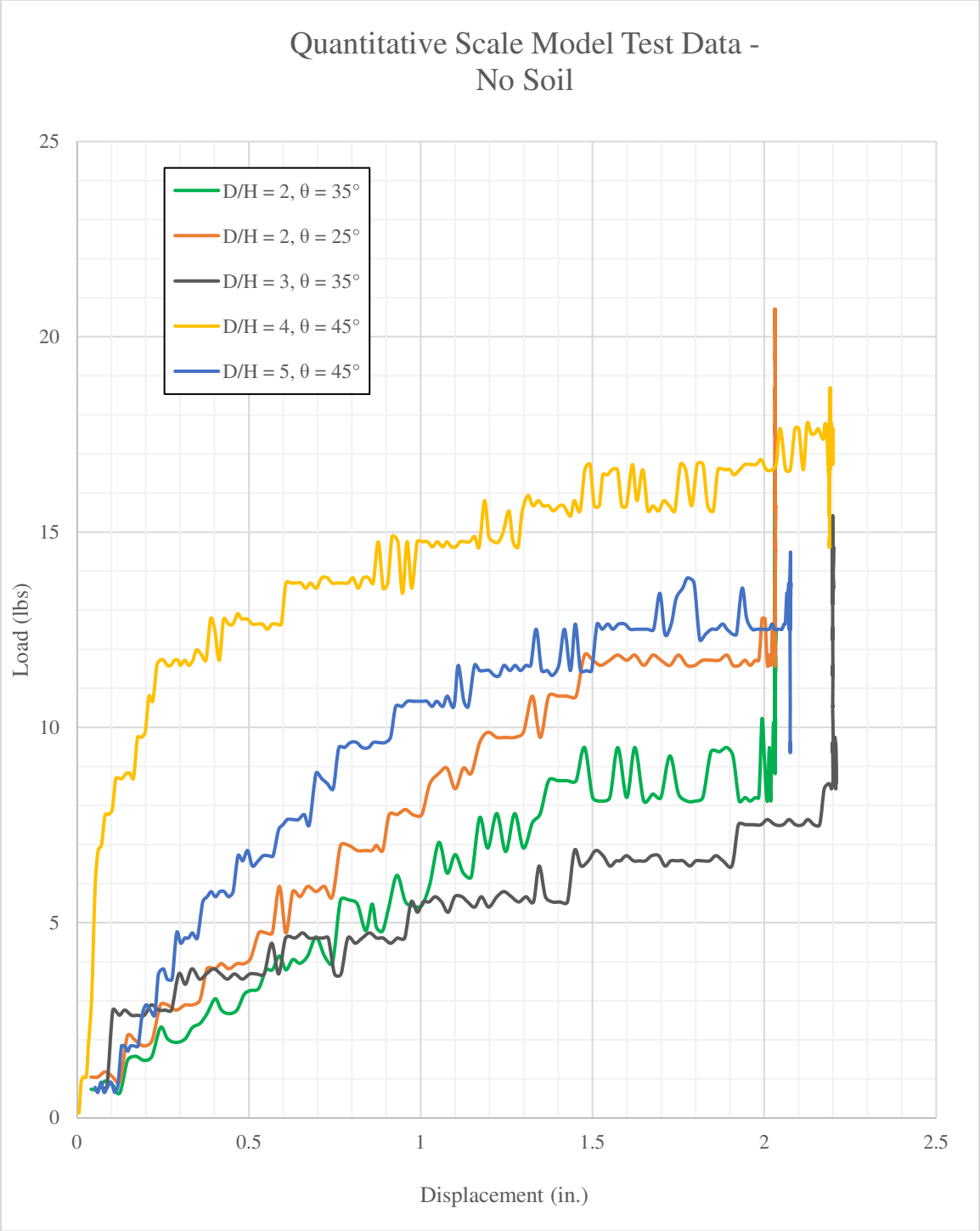

Figure 59 – Raw Experimental Data for all Five Trials Without Soil for the Quantitative Scale Model Testing.

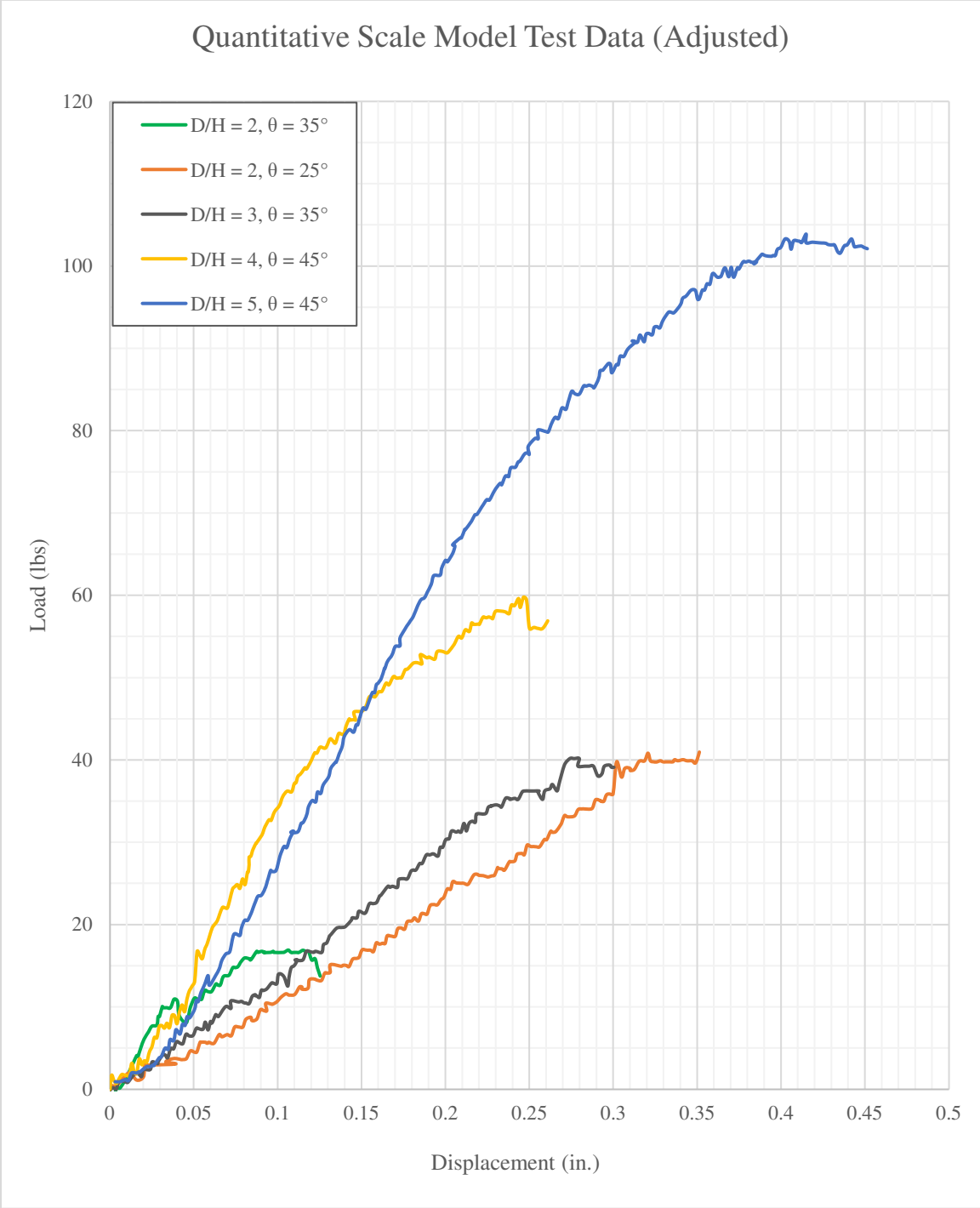

Figure 60 – Adjusted Experimental Data for all Five Trials for the Quantitative Scale Model Testing Showing Only Linear Elastic Portion.

3.0.3.1 Comparison of Test Results to Finite Model

For each of the five trials, a SIGMA/W model was created with a soil medium matching the measured density of the soil above the anchor, with a consistent angle of friction and modulus of elasticity between all models. The elastic limit for each trial configuration was determined and is plotted in Figures 61 through 65 along with the test data.

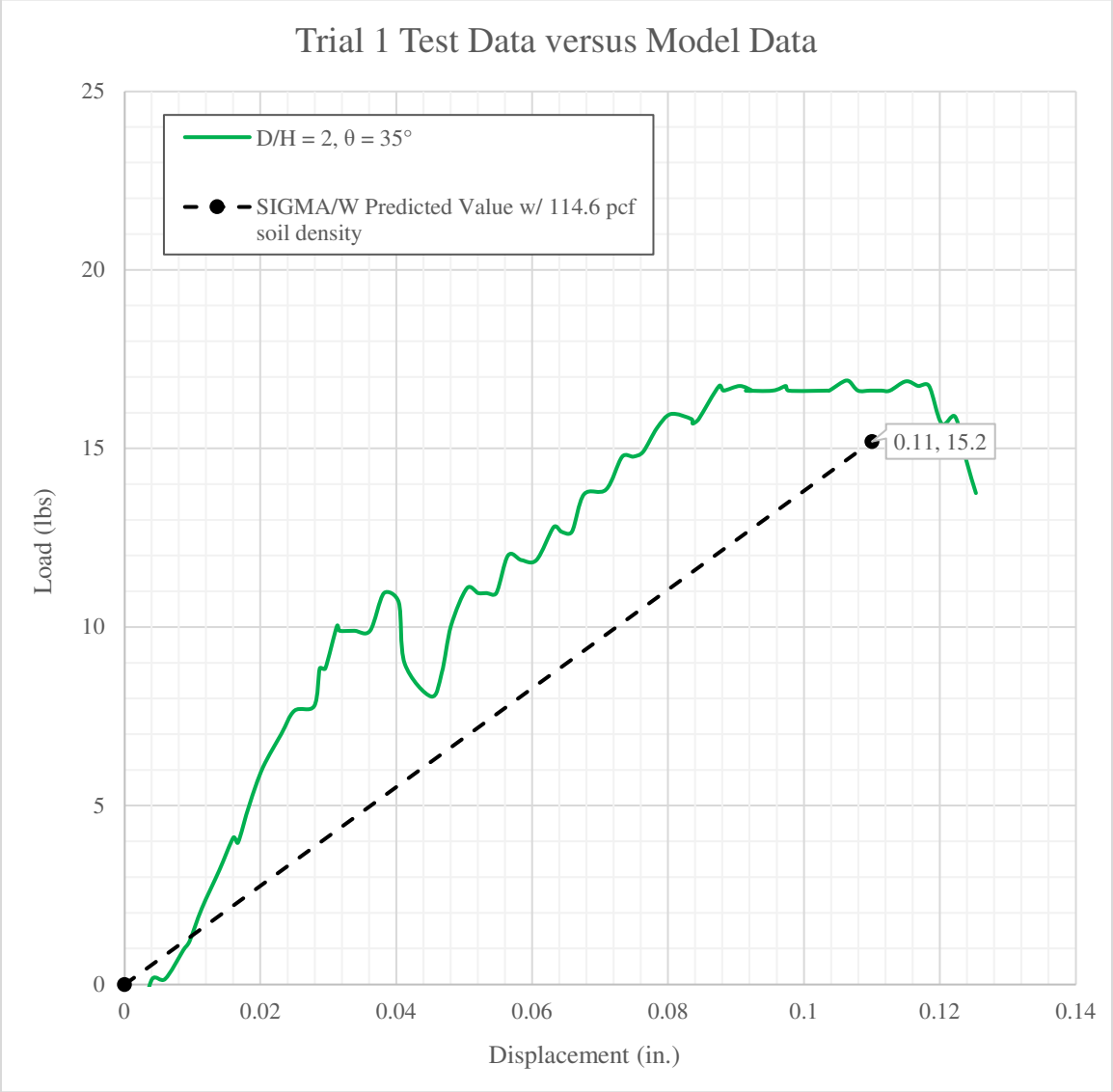

Figure 61 – Quantitative Test Data Compared to SIGMA/W Results for Trial 1.

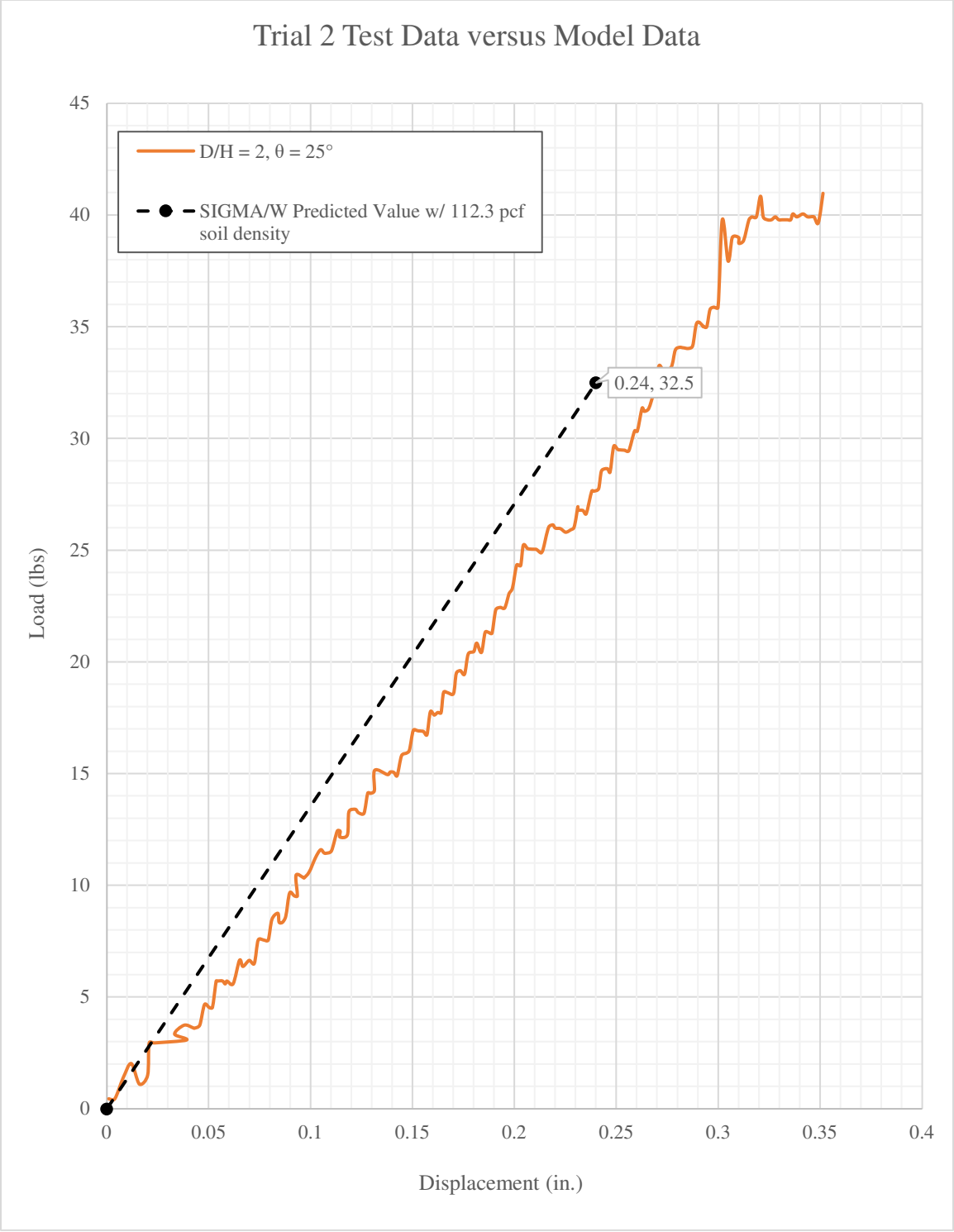

Figure 62 – Quantitative Test Data Compared to SIGMA/W Results for Trial 2.

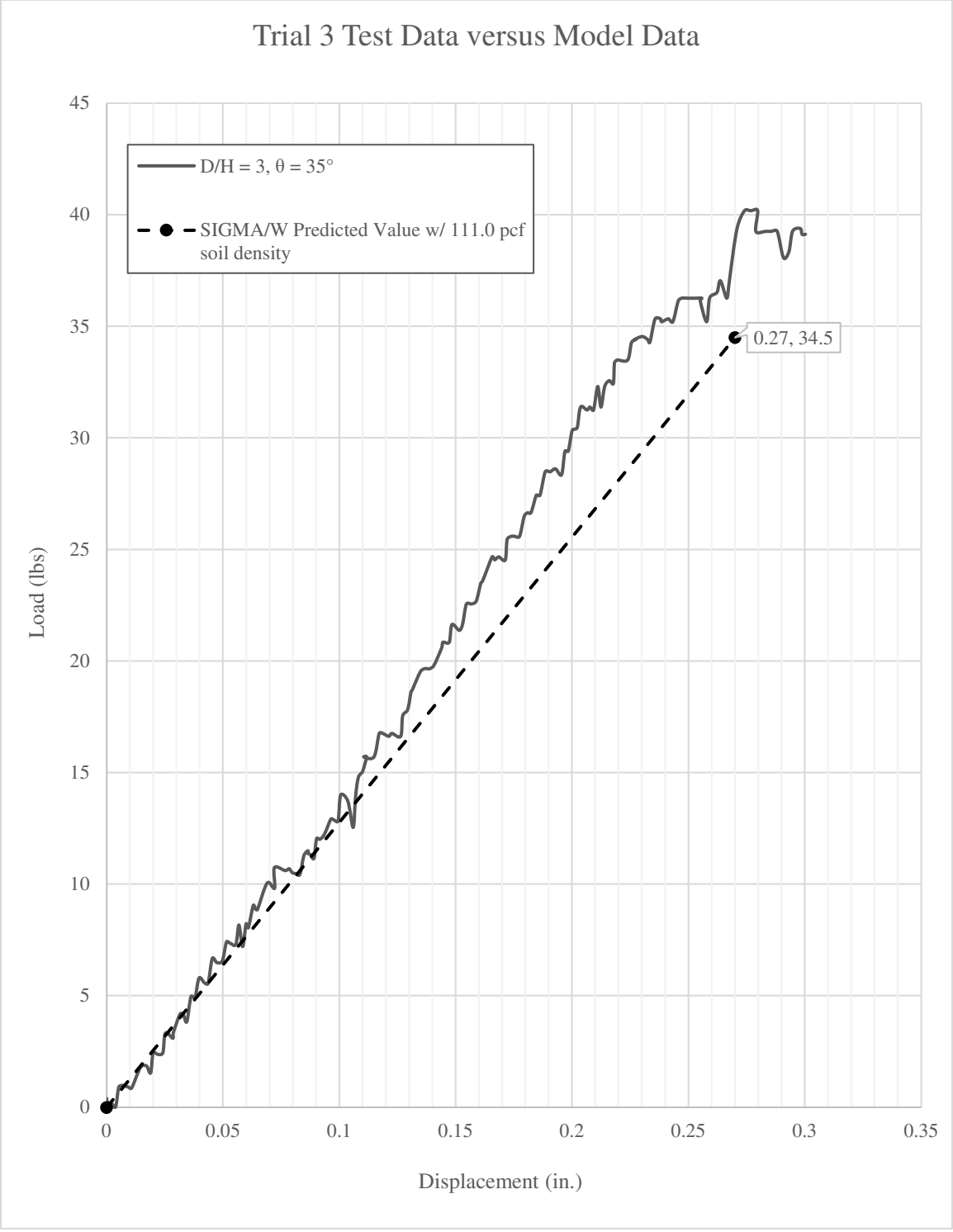

Figure 63 – Quantitative Test Data Compared to SIGMA/W Results for Trial 3.

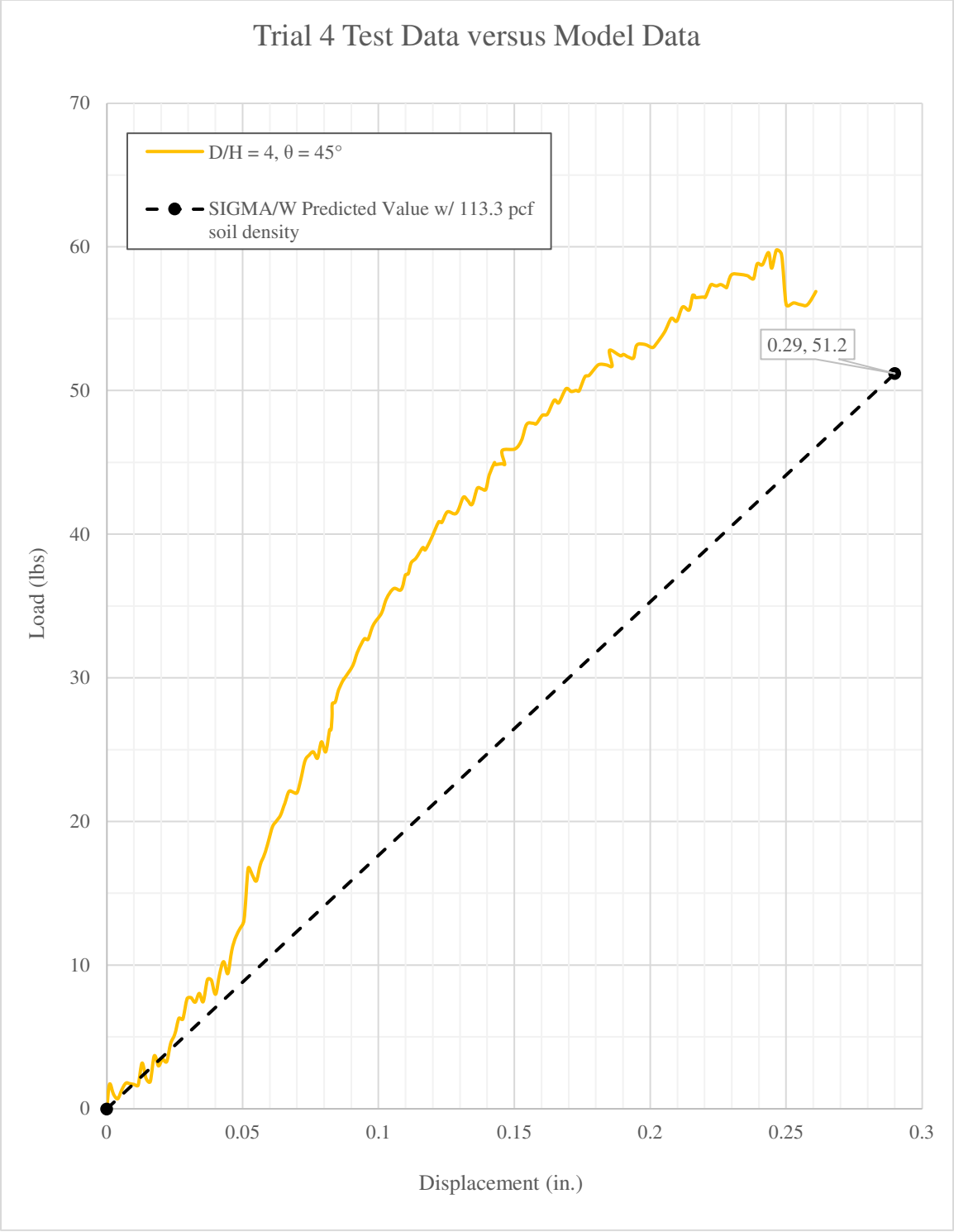

Figure 64– Quantitative Test Data Compared to SIGMA/W Results for Trial 4.

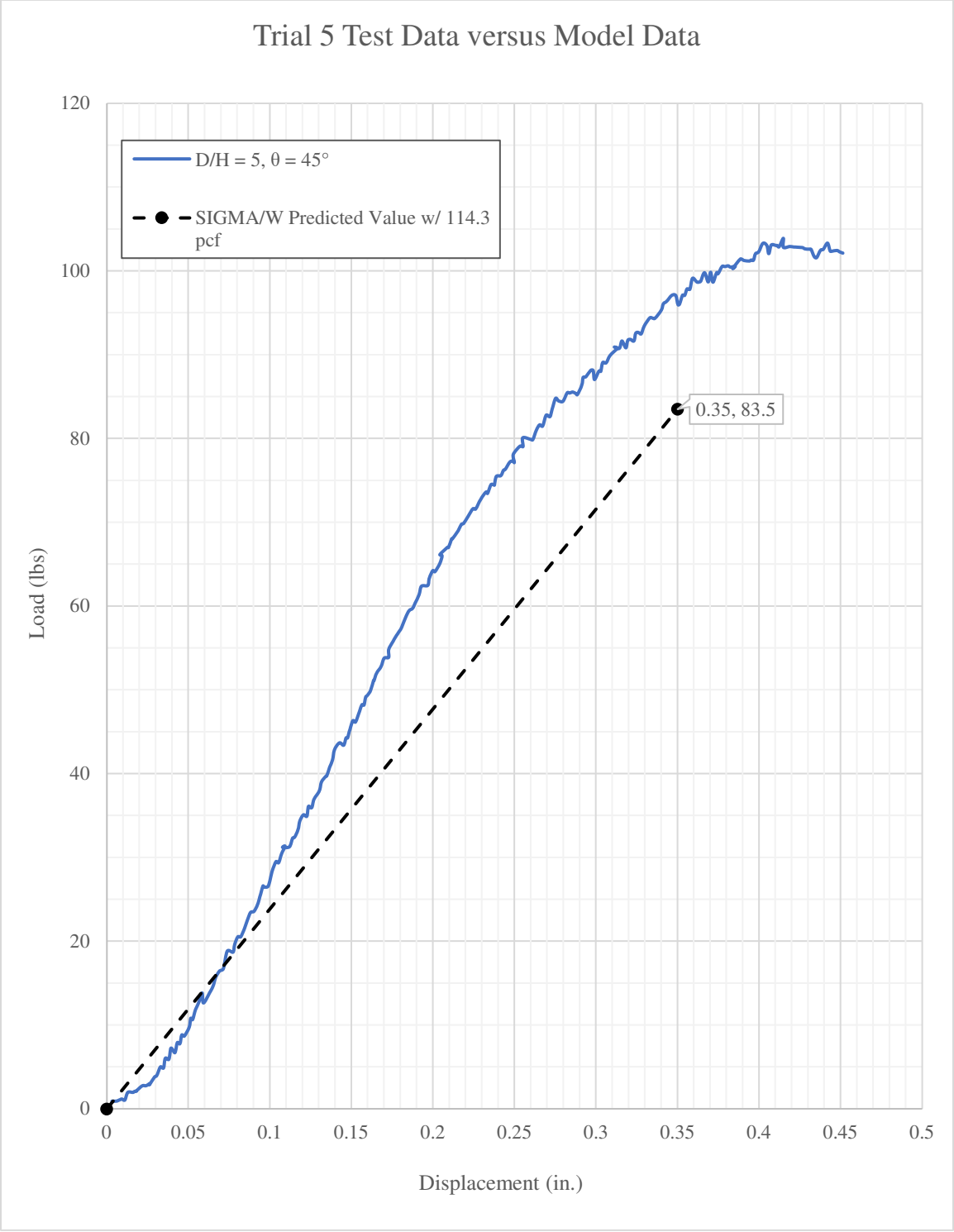

Figure 65– Quantitative Test Data Compared to SIGMA/W Results for Trial 5.

3.0.4 Two-Dimensional Finite Element Modeling

Twenty separate SIGMA/W models were created for full-scale (3-foot tall by 3-foot wide anchors) models for each combination of embedment depth and pullout angle. The soil medium around the anchor was then modified to values between 29- and 41-degrees internal friction angle every 2 degrees, for a total of 140 data points. Each analysis was conducted using a boundary condition of 0.015 feet (1.8 inches/45.7 mm), which was chosen because it was the largest elastic displacement in the weakest-capacity configuration (D/H = 2, $\theta = 45°$). All other maximum elastic displacements were larger, so all the calculated values are within the elastic range. The difference between maximum values was not that large considering the size of the anchor: the largest displacement for the highest capacity anchor (D/H = 5, $\theta = 25°$) was only 0.2 feet (2.4 inches/60.9 mm). The results of the SIGMA/W analyses are displayed in the design graphs in Figures 66 through 70.

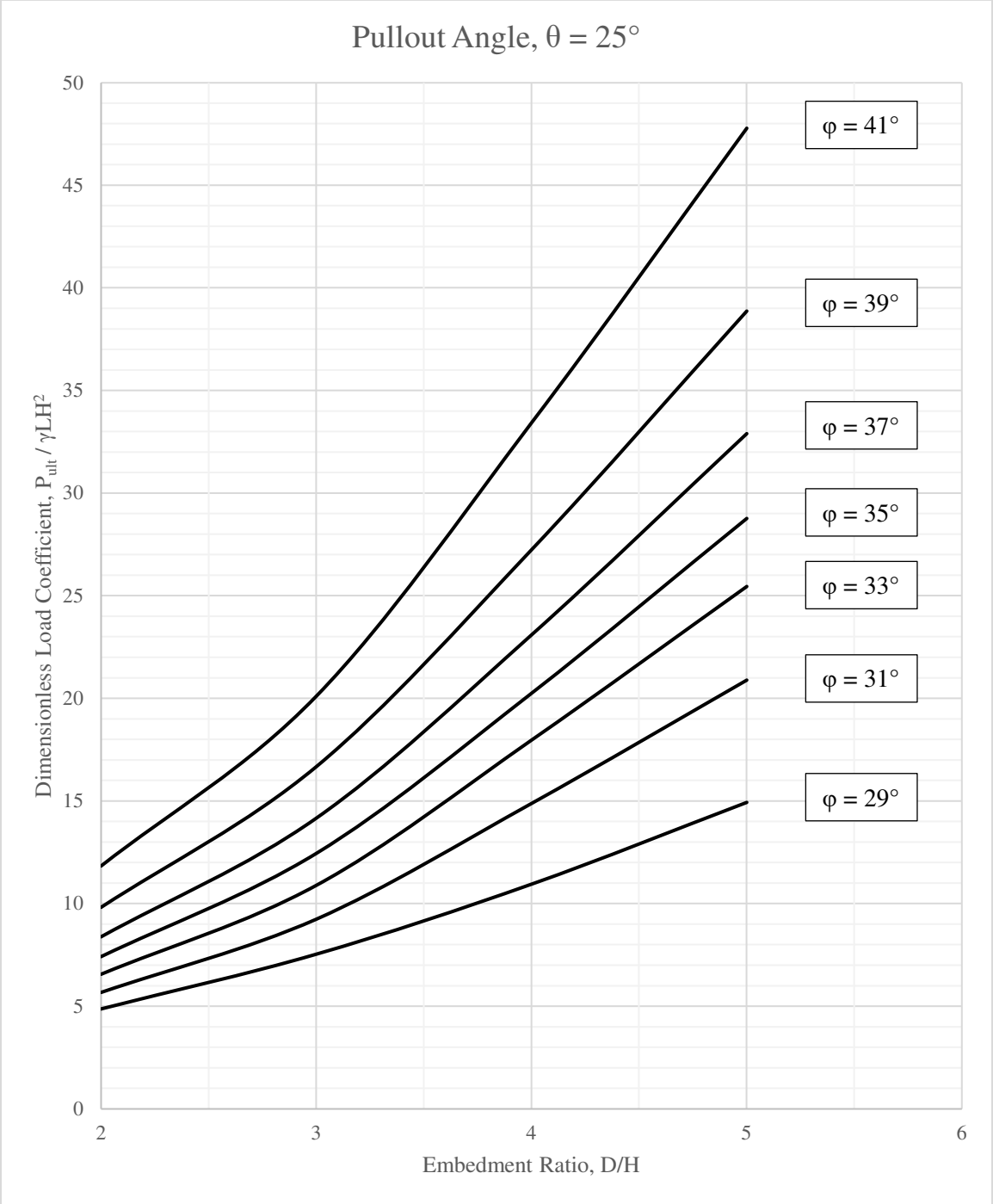

Figure 66 – Uplift Capacity Design Chart for Pullout Angles of 25 Degrees. Displacements at Each Point are 0.15 feet (1.8 inches/45.7 mm).

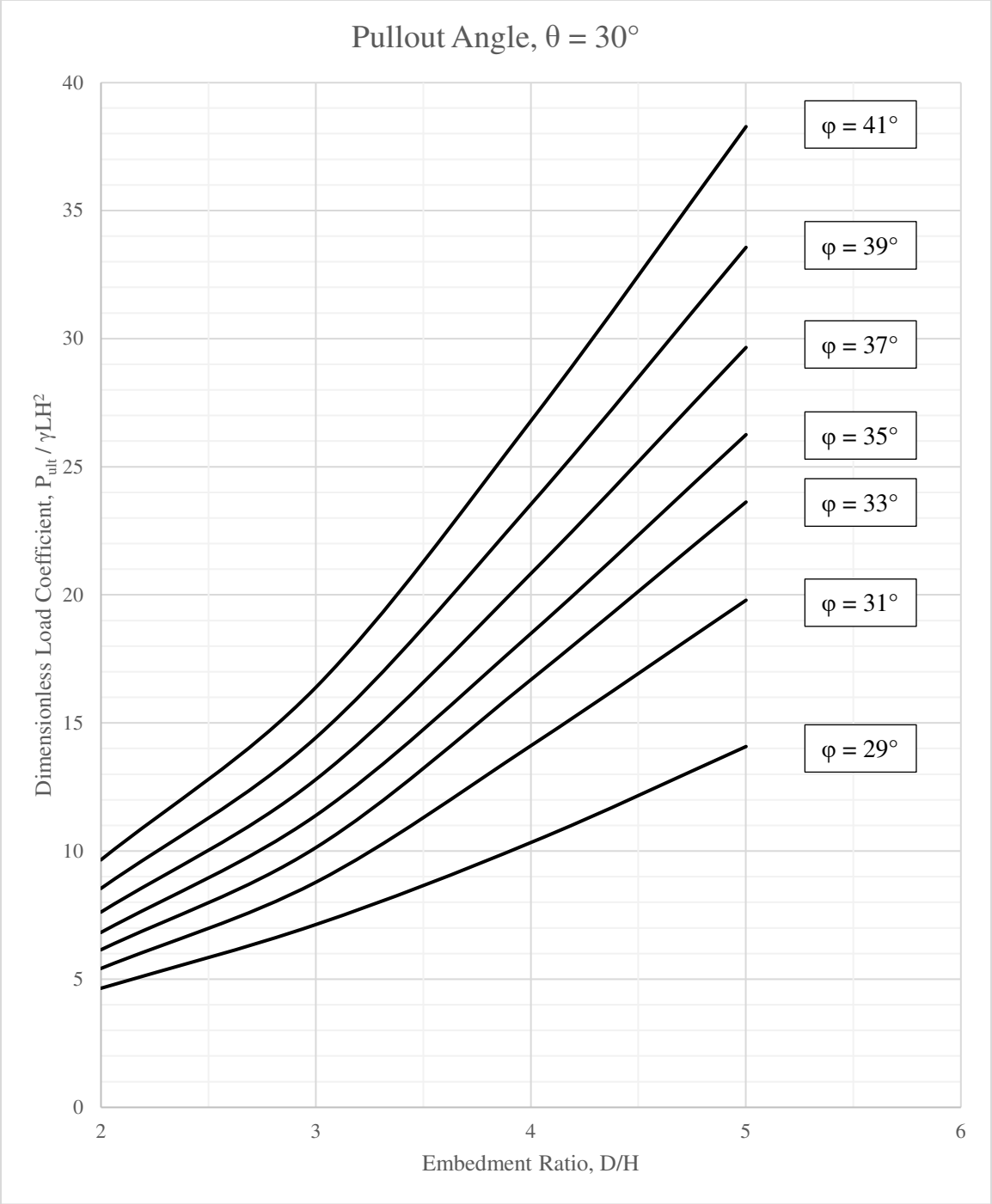

Figure 67 – Uplift Capacity Design Chart for Pullout Angles of 30 Degrees. Displacements at Each Point are 0.15 feet (1.8 inches/45.7 mm).

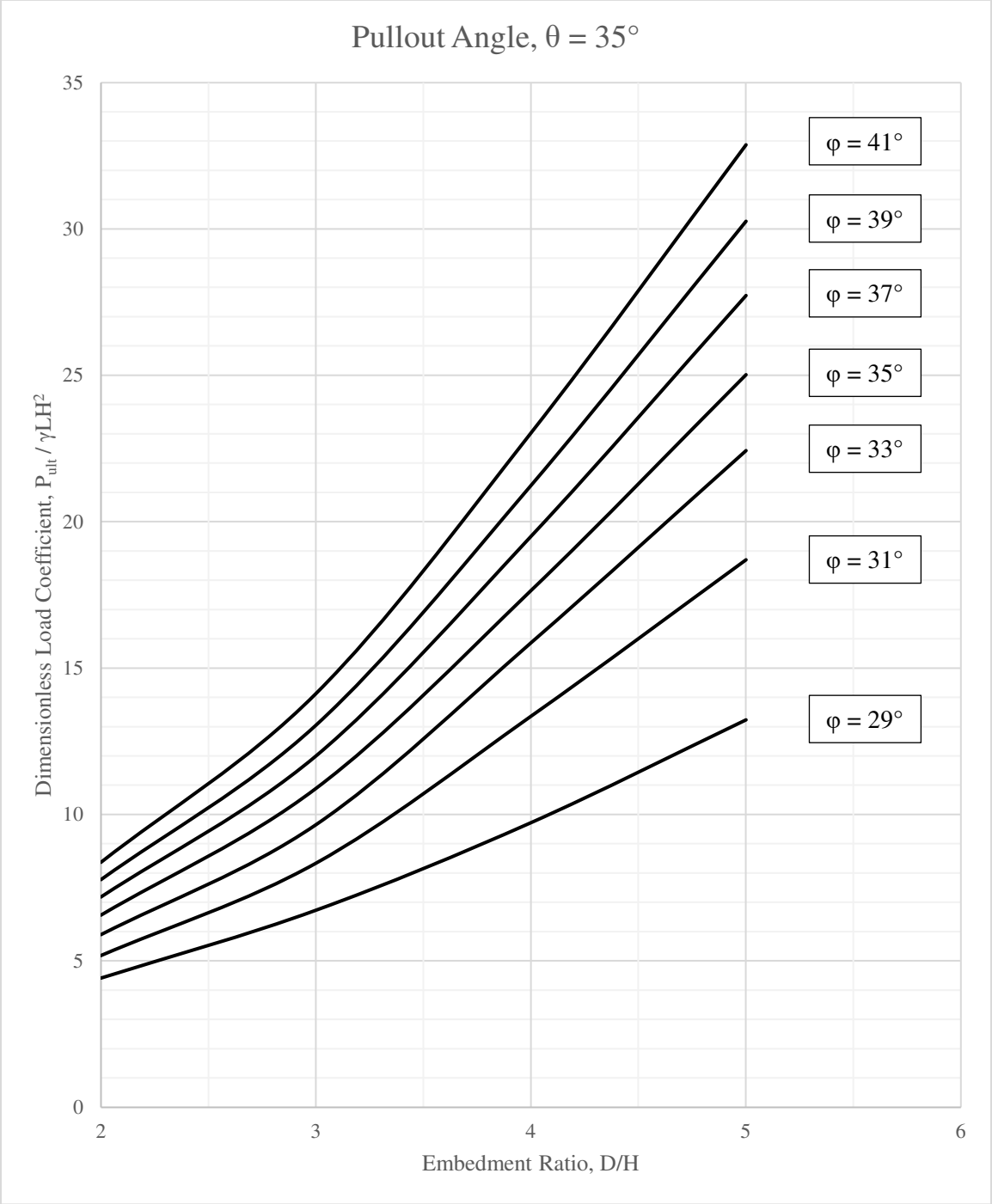

Figure 68 – Uplift Capacity Design Chart for Pullout Angles of 35 degrees. Displacements at Each Point are 0.15 feet (1.8 inches/45.7 mm).

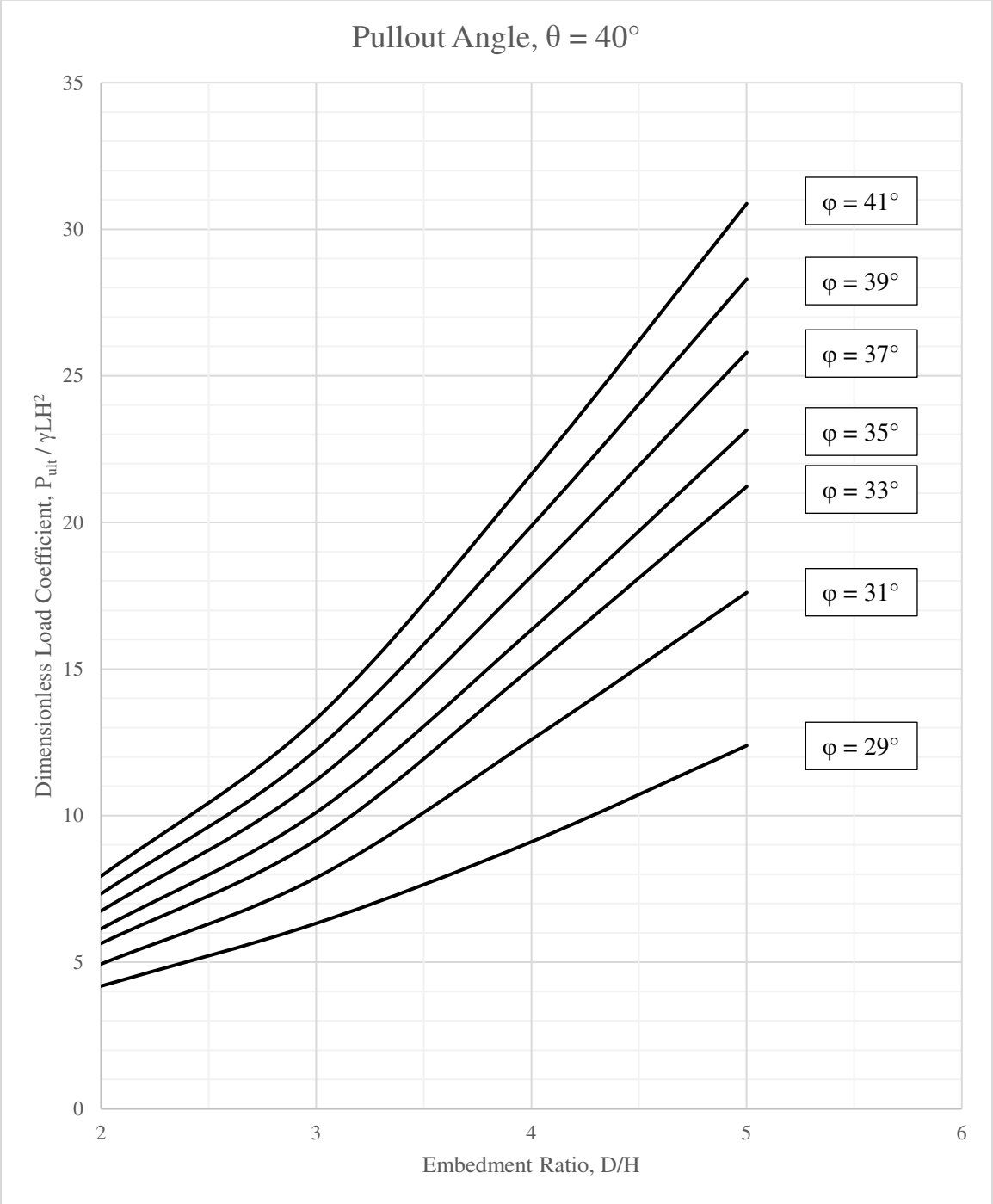

Figure 69 – Uplift Capacity Design Chart for Pullout Angles of 40 Degrees. Displacements at Each Point are 0.15 feet (1.8 inches/45.7 mm).

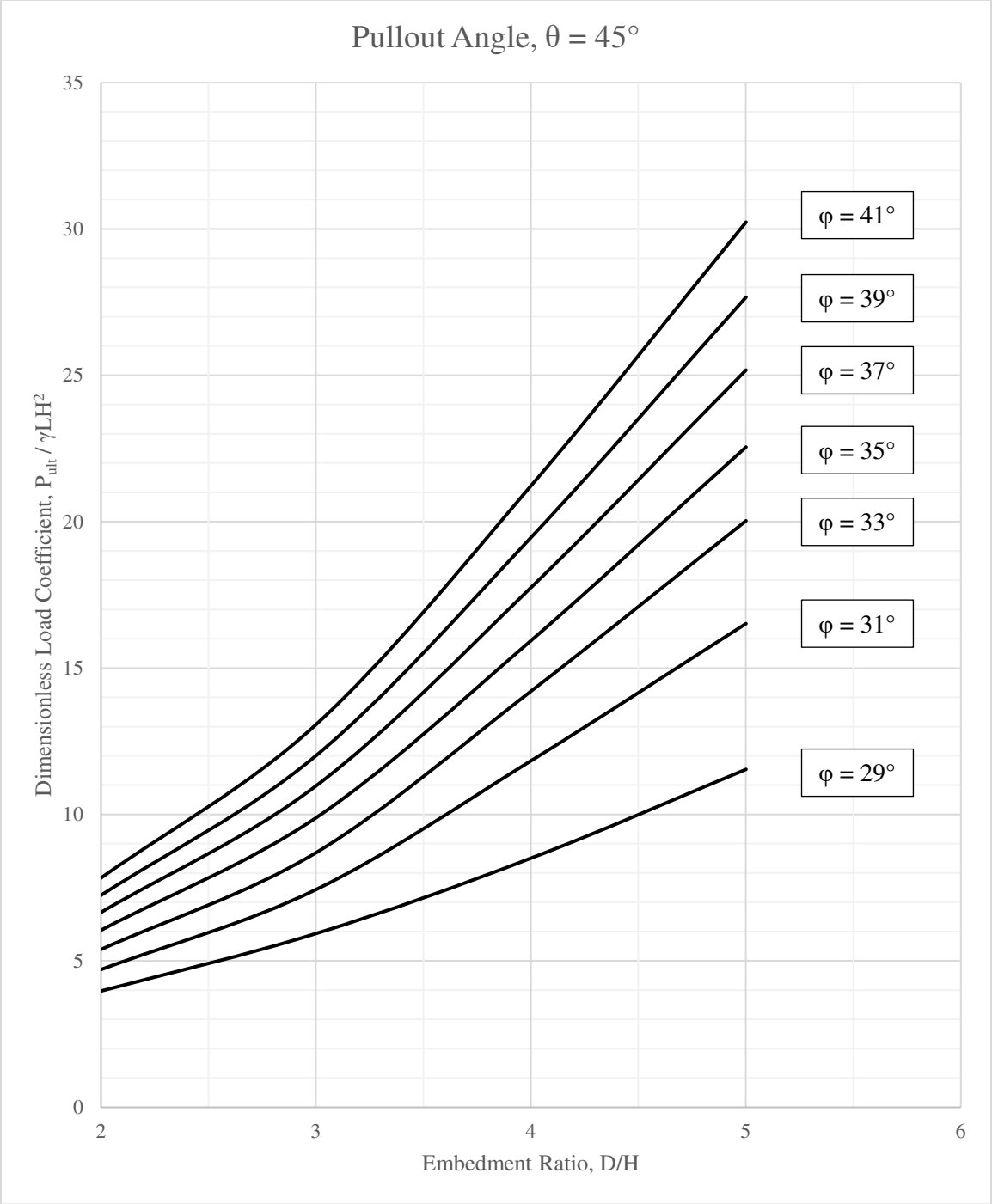

Figure 70 – Uplift Capacity Design Chart for Pullout Angles of 45 Degrees. Displacements at Each Point are 0.15 feet (1.8 inches/45.7 mm).

3.1 Discussion of Results

3.1.1 Theoretical Results (B2P and Meyerhof)

In general, the B2P design gives an expected correlation between anchor pullout and the variables considered: pullout capacity increases with embedment and with shallower pullout angles. However, for the geometries considered in this research, the B2P design solution gives a capacity that is more dependent upon uplift resistance than sliding resistance. This is illustrated by the curved line that begins to truncate the straight lines in Figure 45 and continues to define the controlling capacity for all soil friction angles as the angle of pullout increases. The uplift capacity calculation is independent of soil friction angle, which is why it can be shown that it is controlling over friction because the capacity is the same for all or multiple friction angles. This is part of what makes the B2P design an overly conservative methodology.

The Meyerhof solution was developed for an inclined configuration using limit equilibrium, and the results are consistent with the work of past researchers even with a modified geometry. Most pullout capacities predicted by Meyerhof's equation are significantly higher than those determined by the B2P design method, because it considers a wedge of soil above and in front of the anchor as well as frictional resistance and does not separate the two.

3.1.2 Qualitative Scale Model Testing

The 12 trials conducted for the qualitative scale model testing returned similar results prior to failure. Rotation of the anchor was negligible until the anchor had failed and the force required to pull it out had decreased. Beyond that point, the anchor did orient itself

to act as a wedge at the shallower pullout angles. But as it pertains to the magnitude of displacement that is important to the capacity of a B2P suspension-cable bridge as a system, rotation of anchors is not a concern. The general deformed shape of the soil layers was also observed for each trial – these images helped to verify that the finite element models were working correctly. Figure 71 shows a snapshot of soil displacement taken from a SIGMA/W model that compares well with the deformations observed in Figure 55 through 57.

The tabletop model created for the qualitative scale model testing had many flaws. The Plexiglas used was not stiff enough to resist outward deflection as soil was added. Especially as the anchor was pulled, the very fine filter sand filled the small space

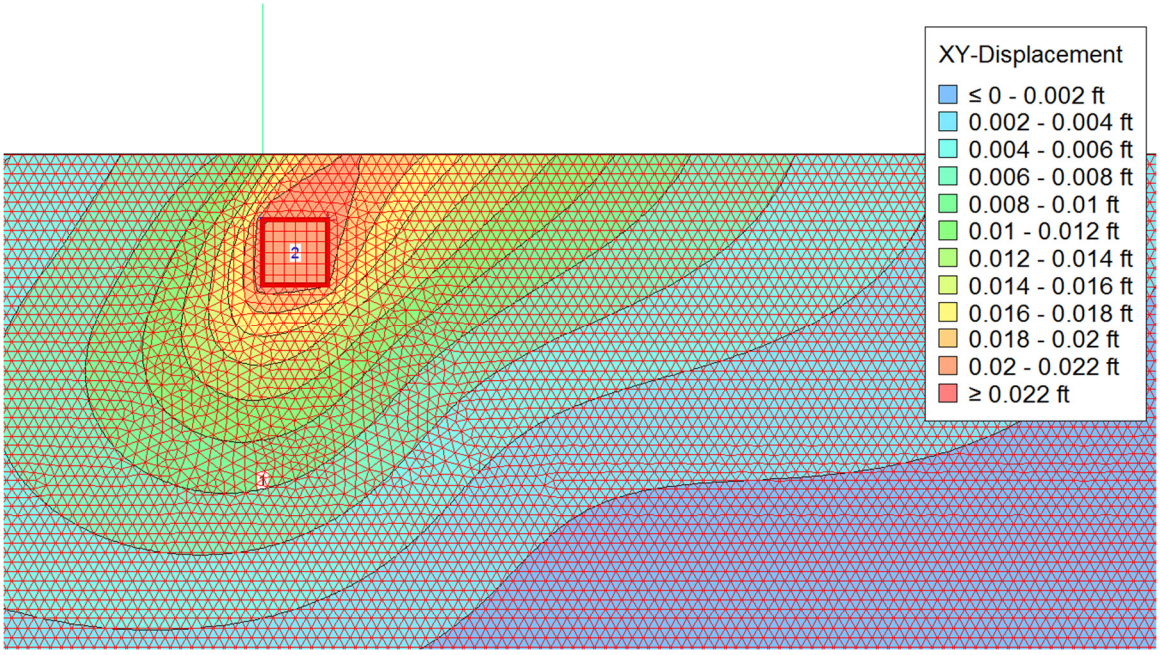

Figure 71 – Soil Displacements in SIGMA/W Finite Element Model.

between the wood block and the Plexiglas. For the purposes of observing soil movement, the model worked reasonably well, and the modifications for the quantitative scale model testing all but eliminated the soil intrusion into the space between the block and the Plexiglas. However, there are a few improvements that can be made. It would make for a simpler and shorter overall research process to make both qualitative and quantitative models into one and perform load-displacement testing with instrumentation and qualitative inspection of soil deformation. This would require the construction of a model with highly stiff, yet transparent side material, or another method not conceived by the author. This would allow for the testing of more trials to observe soil movement while still gathering data on load and displacement.

3.1.3 Quantitative Scale Modeling

The results of the quantitative scale model testing using the modified tabletop model were mixed. The ultimate theoretical values from SIGMA/W were consistently equal to 77 to 88 percent of the ultimate test values from the quantitative scale model testing. For Trials 2 and 3, the slope of the theoretical curve was close to being parallel with the slope of the experimental curve, meaning that the soil stiffness modeled by SIGMA/W was close to being accurate. However, for Trials 1, 4, and 5, the slope of the experimental data curve was not as linear as in Trial 2 and 3, and the SIGMA/W models were not configured to produce anything but a linear relationship for elastic behavior. Trials 4 and 5 had an embedment ratio of 4 and 5, respectively, but the overall shape of the curve and magnitude of the ultimate pullout value do not suggest deep anchor behavior – instead, the density of the soil in the experimental trial is most likely the reason for the non-linear

relationship in these trials as well as Trial 1. Even though the densities were on average 2 to 3 pounds per cubic foot more than in Trials 2 and 3, the change in density creates a change in modulus of elasticity as well as a change in angle of dilatancy. For the sand used, it appears that a density of 111 to 112 pounds per cubic foot is reasonably well-modeled as a loose soil with E = 200,000 tons per square foot and $\Psi = 0°$. However, increasing this density by 2 to 3 pounds per cubic foot should have prompted an increase in both of those soil parameters, but it is unknown how large. For this research it seemed best to focus on analyzing the stated variables and leave soil modulus and angle of dilatancy as a topic of future work. Those two variables probably played a role in the inaccuracy of the ultimate values in Trials 2 and 3, as well: while the slopes of the curves were similar, the ultimate values differed by 16 to 17%, most likely due to an angle of dilatancy or increased soil modulus in the sand that could not be quantified but was not on the scale of the error in Trials 1, 4, and 5.

In general, the modifications to the tabletop model worked well for quantitative testing. The Plexiglas walls did not flex during testing, and the friction between the felt and the Plexiglas was able to be quantified using a no-soil trial. Despite this, it would be the most logical improvement to combine qualitative and quantitative testing into one model as described in Section 3.1.2 and set up a camera to observe soil deformation during load-displacement testing.

3.1.4 Two-Dimensional Finite Element Modeling (SIGMA/W)

The 20 full-scale anchor models created in SIGMA/W to determine design chart values carried many of the same assumptions as the scale models used to compare to

quantitative experimental results. A soil density of 120 pounds per cubic foot was used across all trials, which given the differences in Trials 4 and 5 discussed in Section 3.1.3 might suggest that actual pullout capacities for full-sized anchors are going to be higher due to soil dilatancy and modulus of elasticity. Neither of these are variables in the determination of pullout force using Figures 66 through 70 and therefore cannot be accounted for by designers using these graphs. Soil density is a variable used to determine ultimate anchor pullout but acts in a direct relationship, as was observed through undocumented trials in SIGMA/W where all other variables were held constant and soil density was varied. A doubling of soil density leads to a doubling of anchor pullout capacity, as is the case in the results of many past researchers. In real-world applications, doubling soil density is unrealistic due to the range of optimum densities observed in most soils. However, for an angle of dilatancy above zero that appears to present naturally with higher soil densities, the effect on anchor pullout capacity is unknown and requires further research. It should be noted that an angle of dilatancy of zero is a conservative assumption, as an increase in that angle will only result in higher anchor pullout capacities.

The actual results presented in Figures 66 through 70 show a consistent overall relationship with the considered variables that is consistent with the work of past researchers. Anchor pullout capacity increases with embedment depth, angle of internal friction, and shallower pullout angles as predicted. The shape of the curves is similar to those shown in Meyerhof's solution, getting progressively steeper with embedment depth. The results also suggest an overly conservative B2P design procedure, as shown in Figures 72 through 76. It should be noted that for clarity, the line labels for varying soil

internal friction angle φ are not included in Figures 72 through 76. To interpret these results, the soil internal friction angle for both the SIGMA/W results and the B2P theoretical results are shown in increments of 2 degrees varying from 29- to 41-degrees. For comparison, the SIGMA/W data are the exact same as shown in Figures 66 through 70, and the B2P data are the exact same as shown in Figures 45 through 49. The two data sets are simply superimposed for comparison. The results from SIGMA/W are almost all larger than the B2P values, and on the order of 30 to 200%. SIGMA/W results are consistently smaller than B2P for an internal angle of friction of 29 degrees, which would be a weak soil that is perhaps not applicable to soil found in the world without other parameters that would affect anchor pullout capacity, such as cohesion and moisture content. The shape of the curves are similar as well, which is interesting given that the B2P solutions are controlled by uplift for the most part. The sliding resistance curves are all linear, but the uplift resistance curves have a slightly increasing slope as embedment depth increases, similar to that of Meyerhof and the SIGMA/W results. This would suggest that a greater proportion of the resisting forces in the Meyerhof and SIGMA/W capacities are controlled by resistance to uplift and would in part explain the capacity increasing with a lower pullout angle. As the limiting component of uplift resistance is decreased with a shallower pullout angle, the gain in overall capacity becomes larger.

A similar comparison was made with the SIGMA/W results and the Meyerhof results in Figures 77 through 81. The internal friction angle labels were also omitted for clarity, but the SIGMA/W data still match that of Figures 66 through 70 and the Meyerhof data are the exact same as shown in Figures 50 through 54. The two data sets are simply superimposed for comparison. Meyerhof's equation gives a much better

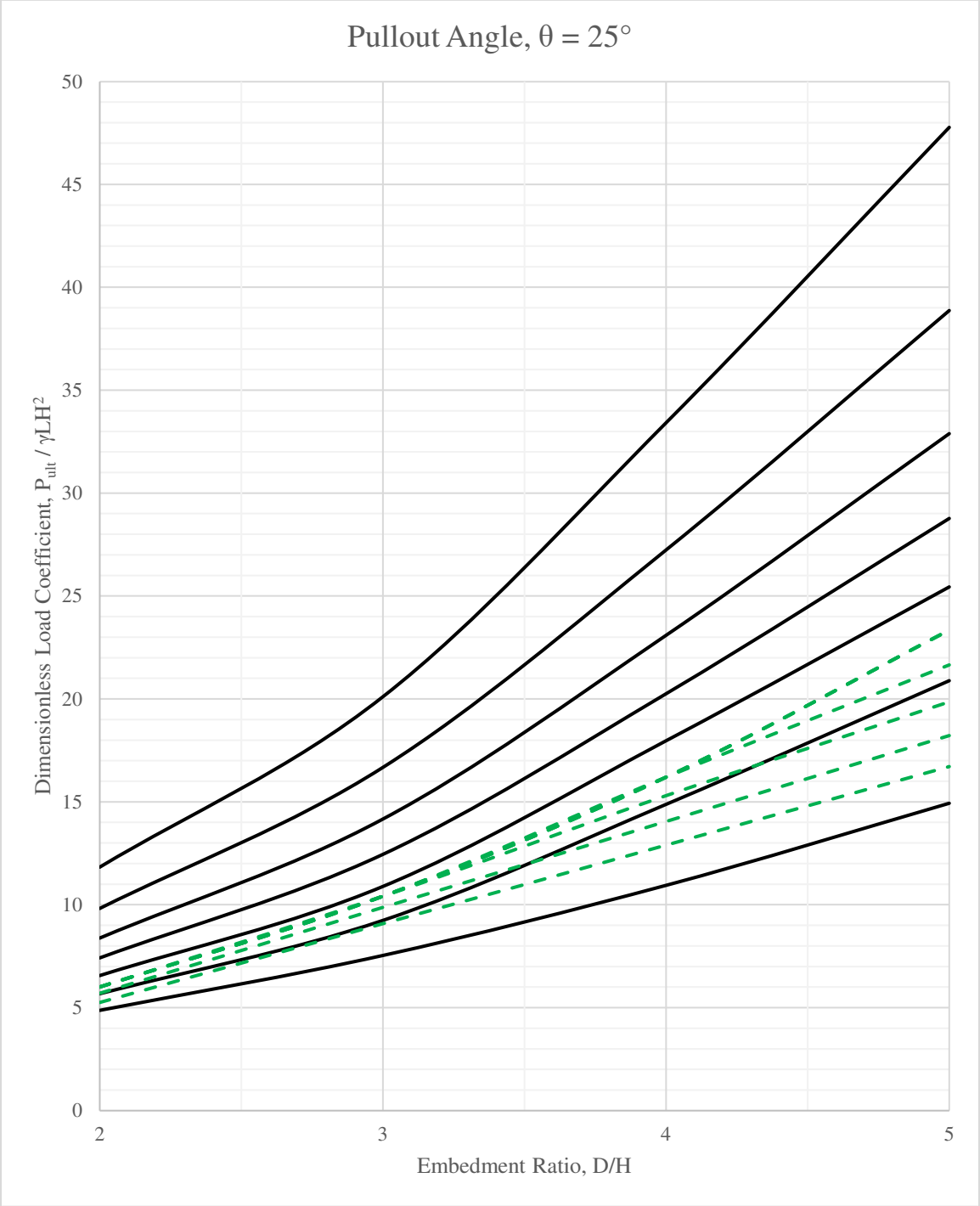

Figure 72 – Comparison of SIGMA/W Results (Black Solid Lines) to B2P Results (Green Dashed Lines) for a Pullout Angle of 25 Degrees.

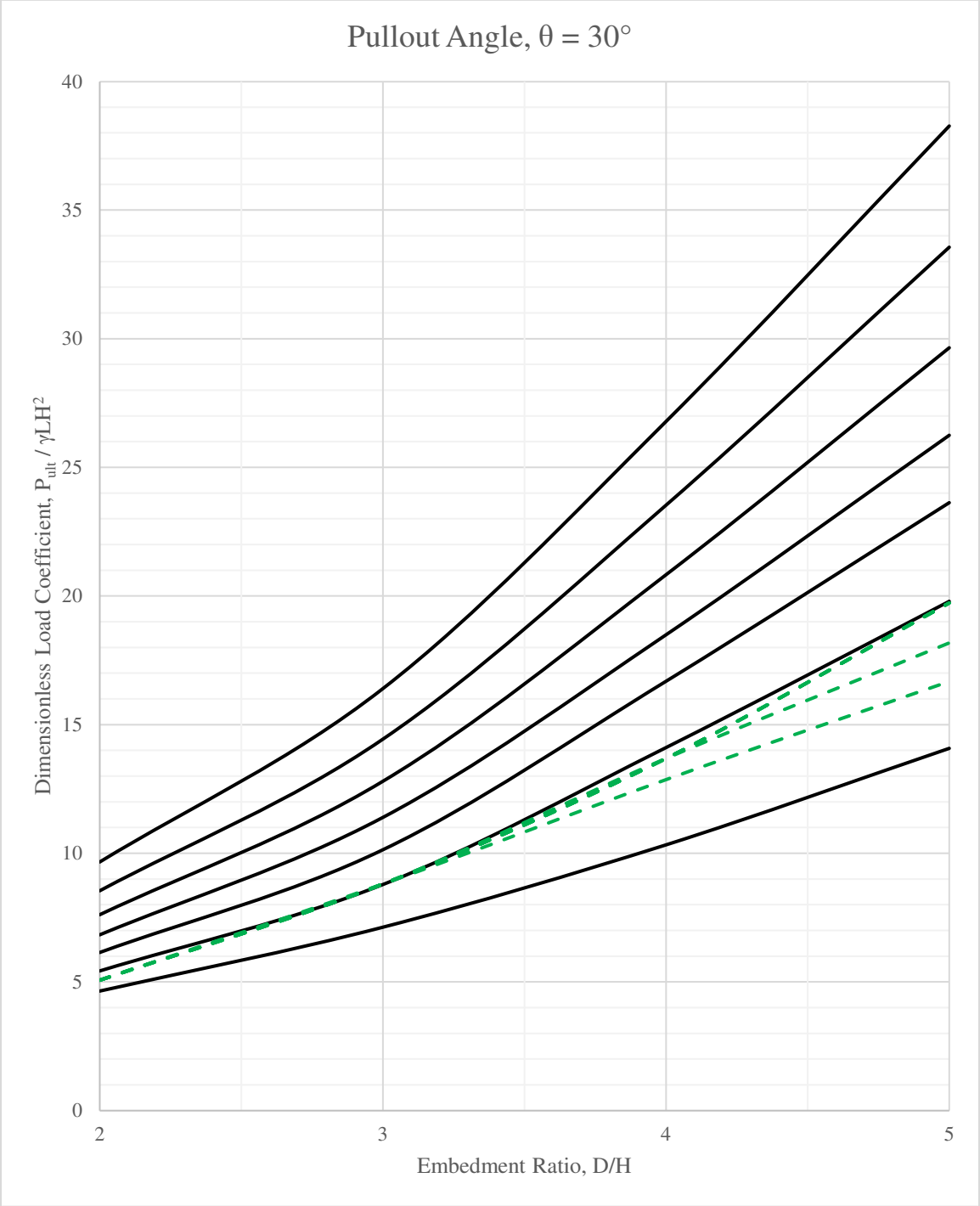

Figure 73 – Comparison of SIGMA/W Results (Black Solid Lines) to B2P Results (Green Dashed Lines) for a Pullout Angle of 30 Degrees.

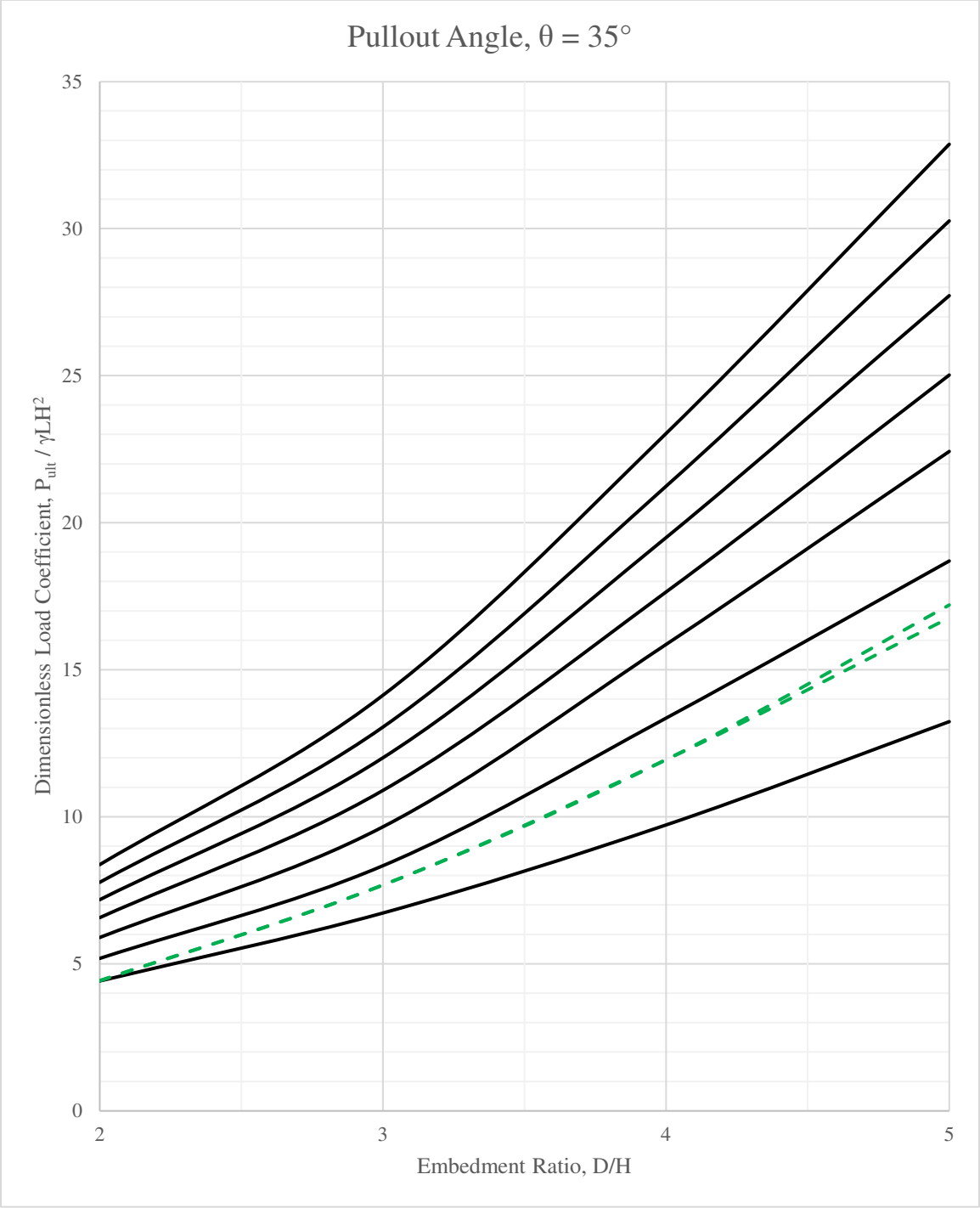

Figure 74 – Comparison of SIGMA/W Results (Black Solid Lines) to B2P Results (Green Dashed Lines) for a Pullout Angle of 35 Degrees.

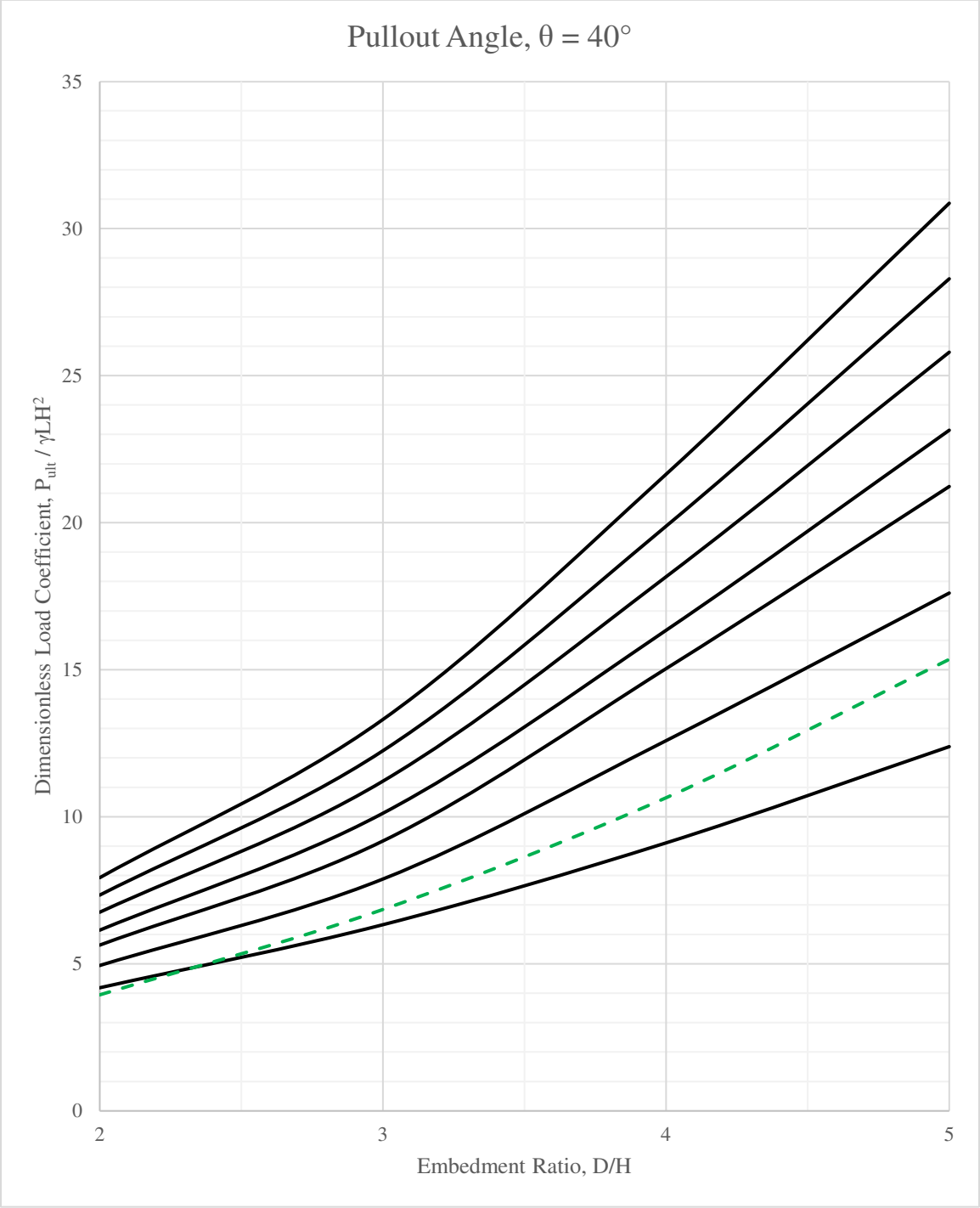

Figure 75 – Comparison of SIGMA/W Results (Black Solid Lines) to B2P Results (Green Dashed Lines) for a Pullout Angle of 40 Degrees.

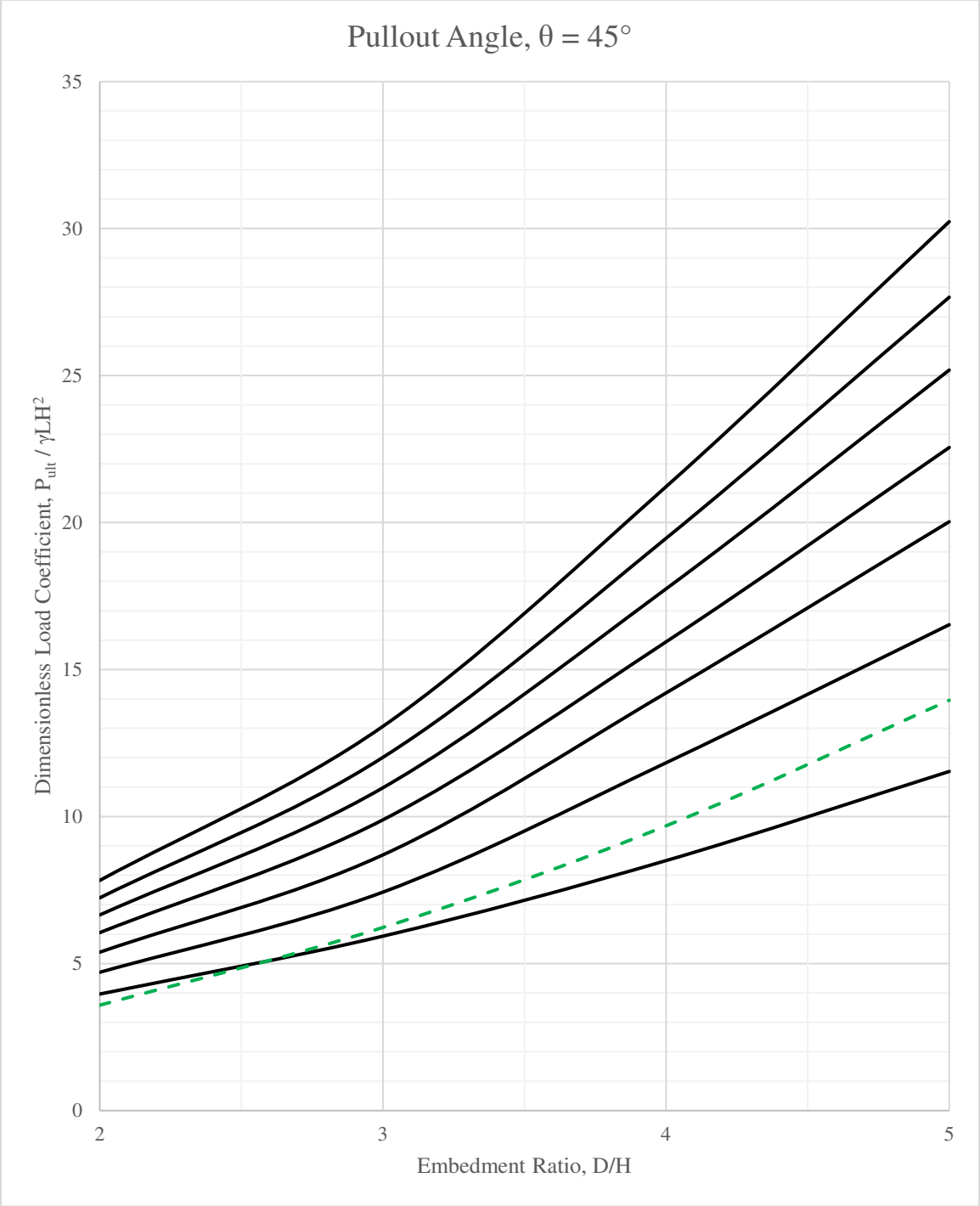

Figure 76 – Comparison of SIGMA/W Results (Black Solid Lines) to B2P Results (Green Dashed Lines) for a Pullout Angle of 45 Degrees.

prediction of the results determined by SIGMA/W, as evidenced in Figures 77 through 81. The shapes of the curves do not match as well as B2P to SIGMA/W but the magnitudes are much closer. The difference in shape is most easily explained by the shape of the anchor and how Meyerhof's equation was adapted for the B2P anchor geometry: the anchor face area used is not orthogonal to the direction of pullout except for when the pullout angle is 45 degrees, and even in that case the results are not consistent. Another explanation would be the anchor weight that is accounted for by SIGMA/W with body forces but not by Meyerhof for plate anchors. Also not accounted for by Meyerhof is friction between the anchor and the soil, which is considerable for concrete and not so considerable for steel, the material used by Meyerhof for plate anchors. What these data suggest is that limit equilibrium analysis might be the answer to a theoretical solution if it can be derived for this particular anchor style. If that is the case, Meyerhof also developed equations to account for cohesion that could be analyzed for comparison (Das & Shukla, 2013).

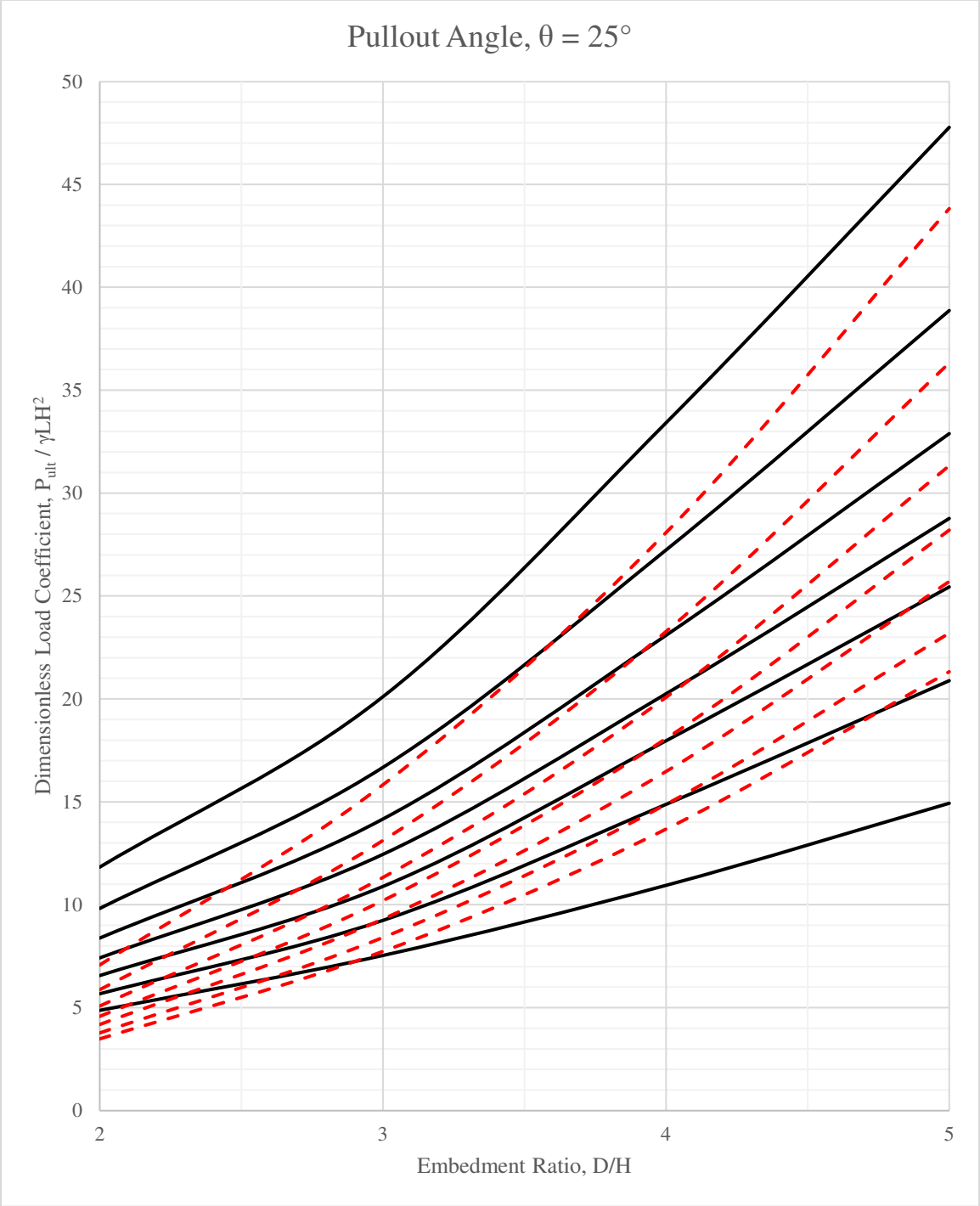

Figure 77 – Comparison of SIGMA/W Results (Black Solid Lines) to Meyerhof Results (Red Dashed Lines) for a Pullout Angle of 25 Degrees.

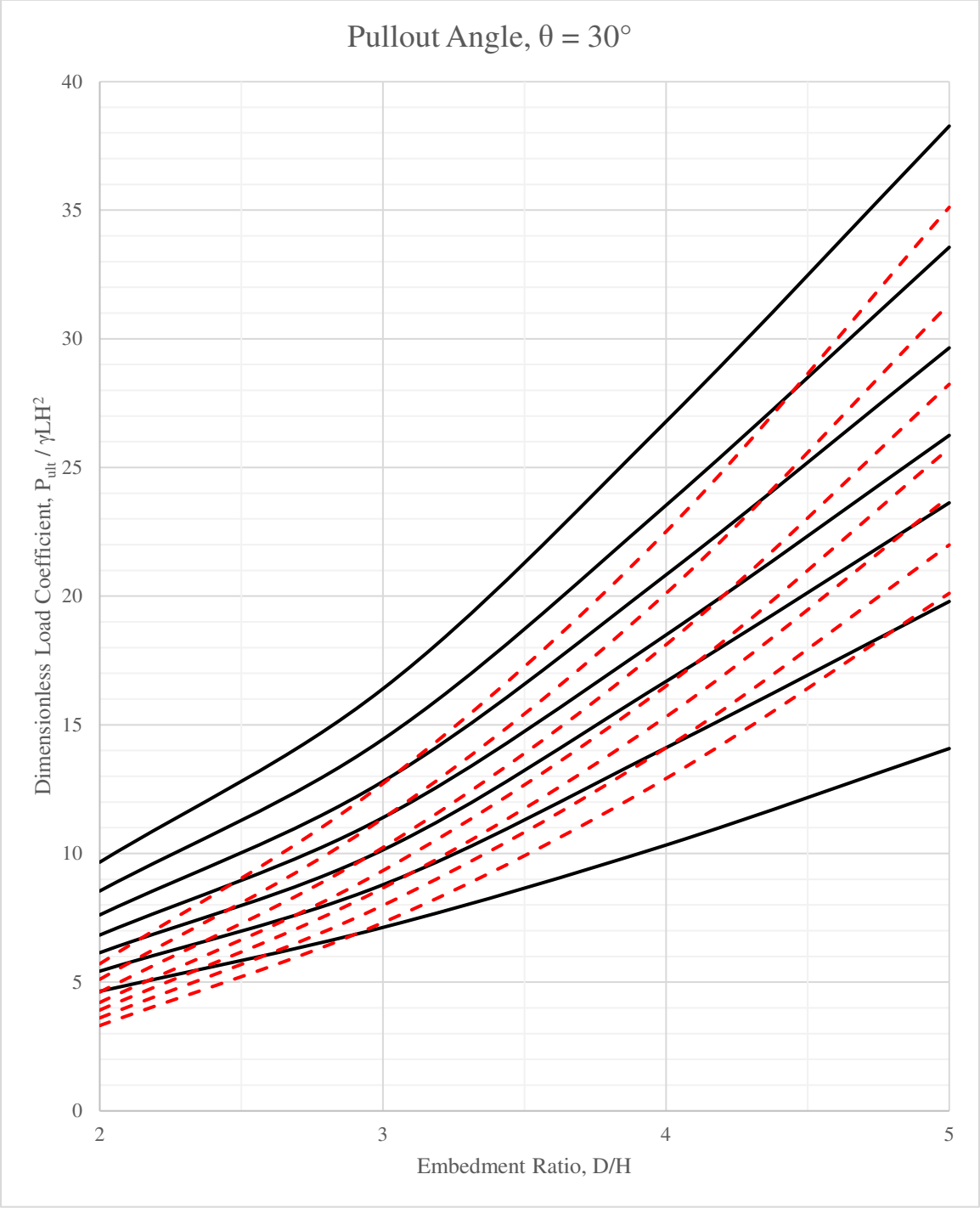

Figure 78 – Comparison of SIGMA/W Results (Black Solid Lines) to Meyerhof Results (Red Dashed Lines) for a Pullout Angle of 30 Degrees.

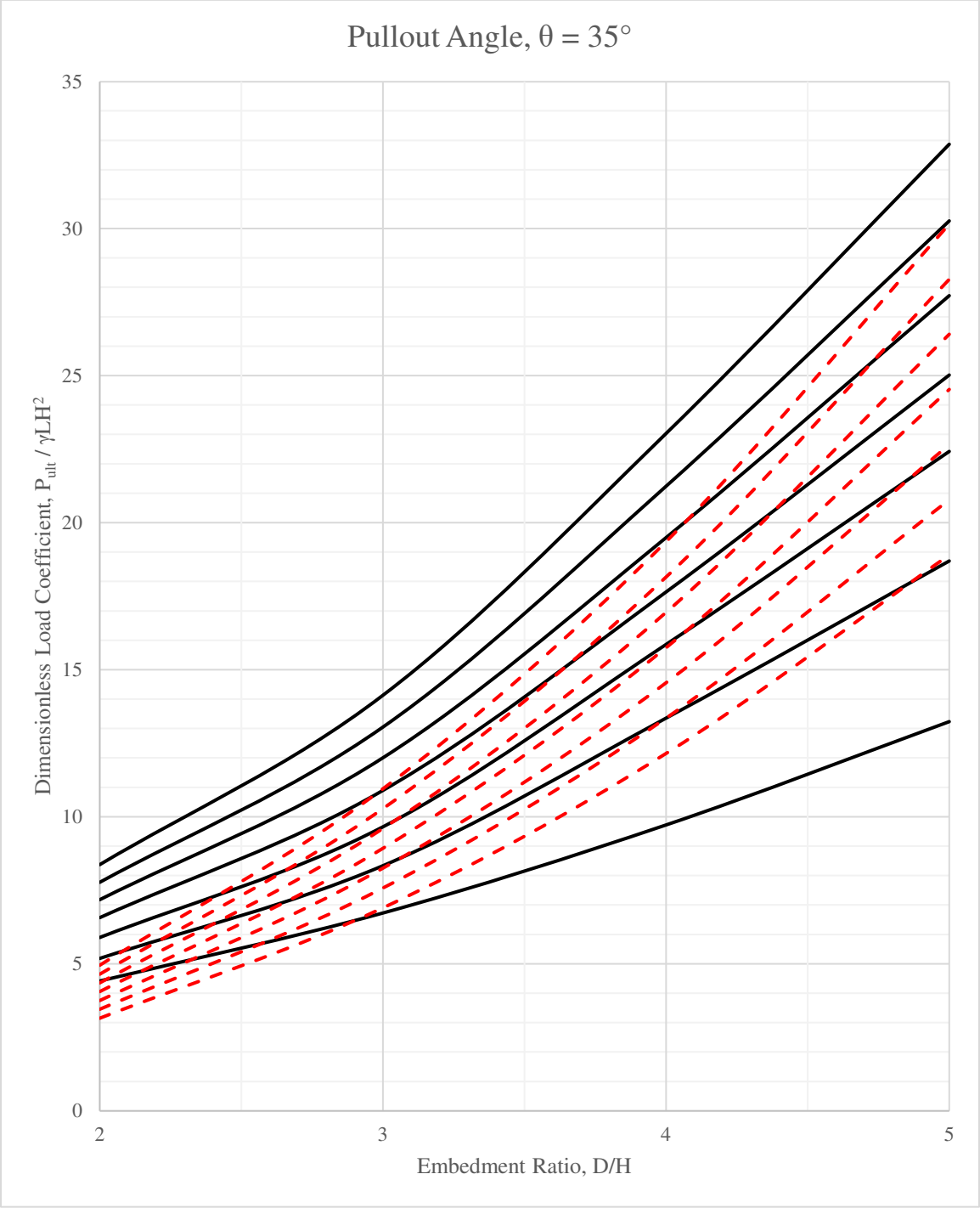

Figure 79 – Comparison of SIGMA/W Results (Black Solid Lines) to Meyerhof Results (Red Dashed Lines) for a Pullout Angle of 35 Degrees.

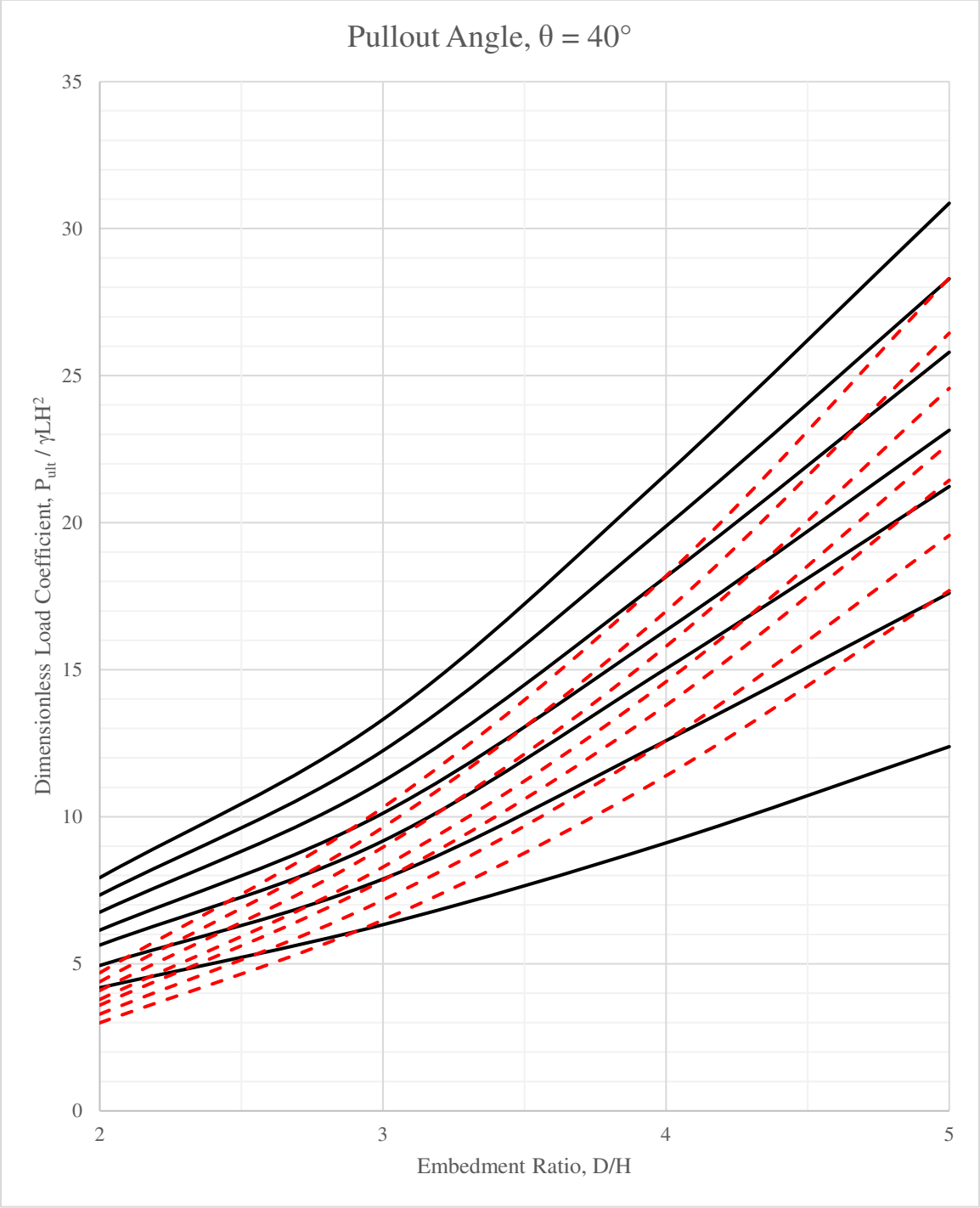

Figure 80– Comparison of SIGMA/W Results (Black Solid Lines) to Meyerhof Results (Red Dashed Lines) for a Pullout Angle of 40 Degrees.

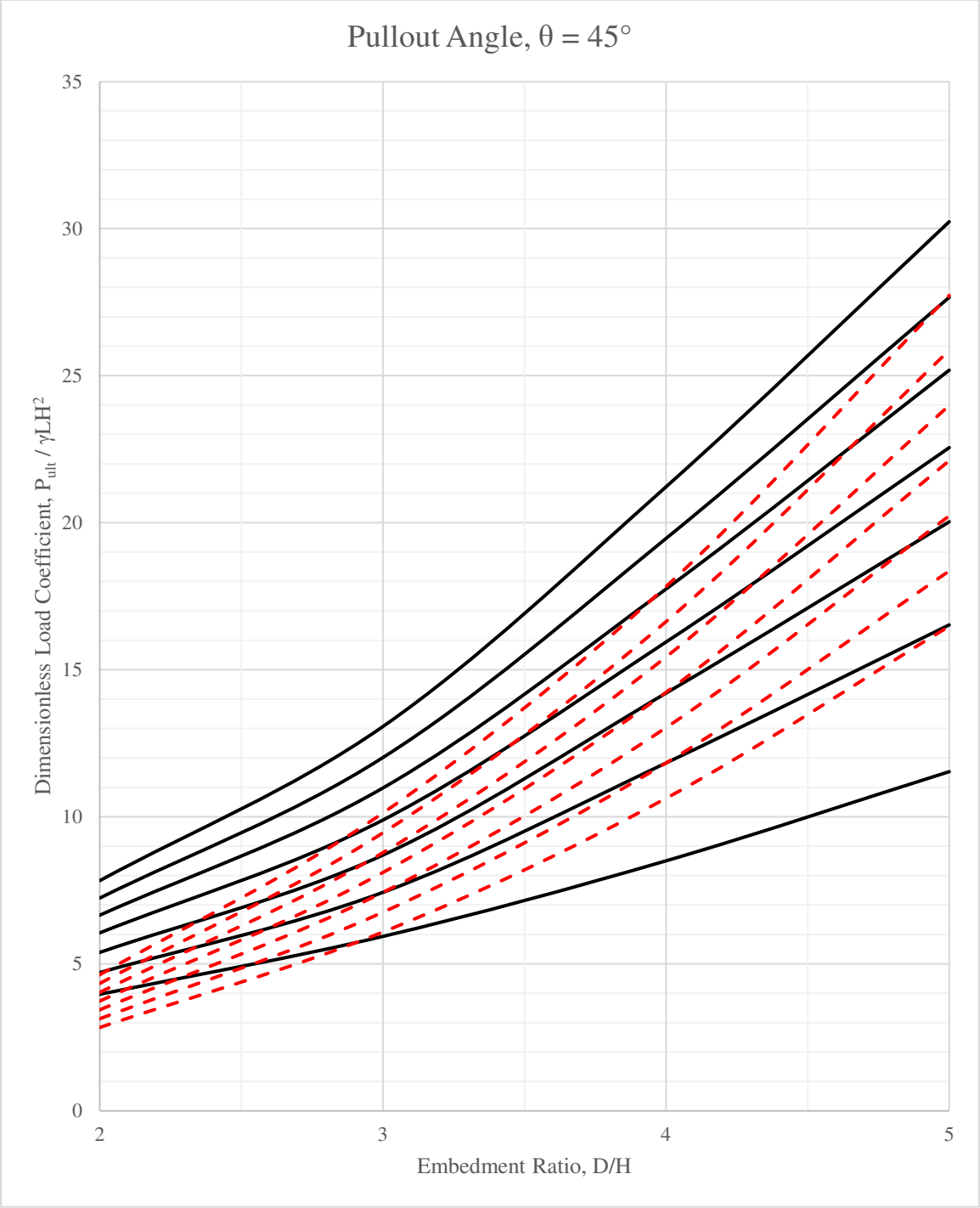

Figure 81 – Comparison of SIGMA/W Results (Black Solid Lines) to Meyerhof Results (Red Dashed Lines) for a Pullout Angle of 45 Degrees.

Chapter 4: Conclusions and Recommendations

4.0 Conclusions

The intention of this research was to determine a more accurate prediction of B2P suspension-cable bridge deadman anchor pullout capacity using theoretical and experimental modeling. Two methods explored suggest that the B2P design procedure is overly conservative as it exists today: Meyerhof's equation for inclined plate anchors in cohesionless sand and 2-D finite element modeling in GEOSLOPE SIGMA/W. The latter is mostly supported by experimental results, though there are many soil parameters not considered by this research that could play a large part in calculating anchor capacity. Because both methods looked at highly idealized conditions for the anchors and found promising results, there is much more work that must be performed to verify the findings of this research and determine relationships for the unconsidered variables if any of the findings presented here will ever be used by B2P in the future. Considering the two methods presented here that suggest there is considerable capacity to be accounted for in the construction of suspension-cable bridges, it is highly recommended to investigate further and with broader scope. If these results can be verified or refined while still showing considerably more capacity than has been used by B2P, it would be at their discretion to adopt these methods and allow student and professional chapters to construct bridges closer to their ultimate capacity.

4.0.1 Factors of Safety

All the results presented in this report reflect unfactored values. B2P suggests a factor of safety of 1.5 against their ultimate capacity determined by either uplift or sliding

resistance. None of the researchers mentioned in the Literature Review section suggest a factor of safety against uplift for vertical, horizontal, or inclined anchors. It is a subject that might warrant future research into code recommendations and intentions, or simply the opinion of the engineers at B2P. At this time, the author is not prepared to recommend a factor of safety to be used in design without verification from more research, particularly full-scale load testing.

4.1 Recommendations

4.1.1 Verification of Research Results

4.1.1.1 Full-Scale Testing

The results presented in Figures 65 through 70 for anchor uplift capacity as a function of anchor height and length, soil density, soil friction angle, embedment ratio, and pullout angle can all be verified by full-scale testing. This would involve excavating and trench pouring a reinforced concrete anchor with a transition arm and pulling it to failure using heavy equipment while monitoring load and displacement. The size of the anchor would be as close to full-size as possible, on the order of 1 meter x 1 meter x 3 meters. This test would also analyze the accuracy of end effects as determined by Ovesen for this configuration and geometry. This kind of experimentation was considered at the beginning of this research, but it was decided to instead explore theoretical options first. The challenges to this testing are mostly logistical, in terms of finding heavy equipment large and powerful enough to pull a full-sized anchor to failure. For example, the weakest capacity anchor ($D/H = 2$, $\theta = 45°$) in a 33° internal soil friction angle, 120 pounds-per-cubic-foot cohesionless sand, at the dimensions of 1 meter x 1 meter x 3 meters, would

require 68,523 pounds of force to be pulled to failure according to Figure 70. Conversely, the strongest anchor (D/H = 5, θ = 45°) in a 33°, 120 pounds-per-cubic-foot cohesionless sand, at the dimensions of 1 meter x 1 meter x 3 meters, would require 323,331 pounds of force to be pulled to failure according to Figure 66. Both of those values are also not considering end effects, which would imply a multiplier of 1.5 and 1.8, respectively, by Ovesen's theory. Additionally, the test would require a large, strong frame to both control the angle of pullout as well as convert a horizontal pulling force by the heavy equipment into the necessary angle. Finally, there is the question of soil medium used for a full-scale test. It would be difficult to find soil conditions in nature to reflect the idealized conditions used in the SIGMA/W analysis, especially if the soil used is allowed to naturally consolidate and compact over time as the anchor cures, or if there is a change of season between pouring and testing. A purely cohesionless, dry sand with no dilatancy whatsoever would need to be created in a lab environment, which complicates the heavy equipment logistics. The effects of cohesion, dilatancy, and moisture content would almost certainly need to be quantified prior to a full-scale test in a realistic environment. Despite all these challenges, a full-scale test would give researchers the best opportunity to analyze load and displacement of a real anchor that would be used to support bridges constructed by B2P chapters.

4.1.1.2 Scale-Model Testing

Testing scale model anchors would be much easier than full-scale anchors, especially if they can be tested in a lab with controlled soil conditions. However, scaling effects are usually an area of concern with geotechnical testing that sometimes require the use of a

centrifuge to modify gravitational acceleration. Scaling effects were not researched or considered for this particular report, as the scale models that were used in testing were analyzed at real dimensions in a SIGMA/W model. If scale model testing were to be used to verify the results presented in this report, it would be necessary to analyze the applicable scaling effects and design experiments accordingly. References on previous geotechnical scale model testing collected during Literature Review are included in the Bibliography.

4.1.2 Investigation of other Controlling Variables

This research analyzed only some of the controlling variables that have been shown by past researchers to affect pullout capacity. The decision to investigate the following variables will depend on the magnitude of their effect, as well as the applicability to B2P suspension-cable bridges, but they are all outlined herein to give future researchers a starting point.

4.1.2.1 Dilatancy

The angle of dilatancy seems to be the most important variable that will affect B2P anchor pullout. This engineering property of soil is not as prevalent in other geotechnical design derivations because it is entirely a function of shear stress application and helps determine deformation. Standard equations for settlement or consolidation of soils will only use the modulus of elasticity to approximate the deformation of soil because the settlement of, for example, a footing will usually not ever reach the plastic range in which dilation begins to describe volume change. However, for a buried anchor pulled to failure

this is precisely the mechanism in action. Angle of dilatancy was not considered by this research to simplify the analysis and attempt to keep soil deformation in the elastic range with a conservative design. However, in order to understand the total picture of B2P anchor pullout dilation should be better understood and should be researched further as it relates to this particular subject. One area to consider is that it might be difficult for B2P designers to quantify the angle of dilatancy for a soil sample at a potential bridge site. It would require multiple direct shear tests of representative soil taken from the site, and existing geotechnical survey techniques currently suggested and practiced by B2P are mostly field tests and do not require laboratory work. In order to truly determine its effect on capacity, it would require a small paradigm shift in the way B2P chapters normally construct a bridge. Therefore, it would be prudent to determine if including angle of dilatancy into capacity calculations is worth the additional effort, and if its exclusion will only lead to more conservative designs. If it is the case that its exclusion would lead to more conservative designs it is likely that for the vast majority of bridges designed by B2P chapters, analysis of plastic deformation would be unnecessary, and dilation should be excluded. Again, multiple references collected during Literature Review on soil dilation as a geotechnical engineering property are included in the Bibliography.

4.1.2.2 Modulus of Elasticity and Poisson's Ratio

There exist many correlations for Young's Modulus of Elasticity and Poisson's Ratio for differing soil types based on friction angle, cohesion, USCS classification, and many more field-tested parameters. However, because they were not varied in this analysis for simplicity, they should be included as variables in any future research. There are many

correlations for these two variables that can be found in any soils mechanics textbooks based on soil parameters easily determined during a field survey by a B2P chapter.

4.1.2.3 Cohesion

Cohesion is the most prevalent soil parameter that could be of concern with regards to anchor pullout capacity, because there are so many potential bridge sites with cohesive native soils. It is reasonable to assume that the inclusion of cohesion would only lead to higher anchor pullout capacity, but this should certainly be verified by further research. Plate anchors in cohesive soils has been the subject of many researchers' work alongside purely granular soils, though their results are not described here. For a theoretical solution, Meyerhof also determined an equation for anchor pullout capacity including cohesion, which is:

$$Q'_u = cK_c H + \frac{1}{2} K_b \gamma H^2 + \gamma h H \cos^2 \Psi, \tag{24}$$

where c is cohesion, K_c is an empirical net earth pressure constant much like K_b but dependent on cohesion and pullout angle as opposed to soil internal friction angle and pullout angle, and the remainder of the variables are the same as defined in Figure 17 and Equation (1). However, experimental research is strongly recommended to accompany any theoretical solutions in the future.

4.1.2.4 Moisture Content

Moisture content impacts anchor pullout capacity largely through an increased soil unit weight, but the decreased effective stress due to pore water pressures will concurrently

reduce the shear stress required for failure. Given the application of these anchors with bridges often crossing waterways, it is certainly reasonable to define the impact moisture content will have on anchor pullout capacity. Moisture content will also affect cohesion for most clayey soils, and the two should be analyzed together.

4.1.2.5 Slope of Ground Surface

When used to cross a valley, suspension-cable bridges will often have no choice but to bury the anchor in a sloping hillside. Oftentimes it is conservative to assume a level ground surface at the lowest point within the trapezoid of soil above the anchor, but in some cases that may not be feasible or possible. Therefore, it would be a worthwhile investigation to understand if the anchor failure begins to become more of a slope stability problem, where capacity is predicted by a circular failure surface and a rotation about some center point.

4.1.2.6 End Effects

Ovesen's theory as presented in Section 1.2.5 was developed for deadman anchors pulled horizontally from behind a retaining wall. Even when adjusting for pullout angle by the cosine of θ, the multipliers for end effect are extreme and almost all get curtailed at 2.0 following a recommendation by the California Department of Transportation. Further research should really determine if the end effects on an inclined beam anchor <u>not</u> oriented orthogonal to the pullout force are as significant, especially for the deeper embedments where Ovesen predicts a multiplier of anywhere from 3 to 6. Performing either full-scale or scale-model testing should be performed in large areas where

sidewalls or underground structures will not come into contact with the soil deformation and provide any additional resistance or slip surfaces.

References

Balla, A. (1961). The resistance to breaking out of a mushroom foundation for pylons. *Proceedings of the 5th ICSNFE, Paris, Vol. I*, 569–576.

Bridges to Prosperity. (2016). *Bridge Builder Manual, 5th Edition*. https://www.bridgestoprosperity.org/bridgebuildermanual/

California Department of Transportation. (2011). Offices of Structure Construction. *Trenching and shoring manual, Rev. 1*. https://dot.ca.gov/-/media/dot-media/programs/engineering/documents/structureconstruction/201906-sc-trenchingshoring-a11y.pdf

Das, B.M. & Shukla, S.K. (2013). *Earth anchors* (2nd ed.). J. Ross Publishing.

Emirler, B., Tolun, M. & Laman, M. (2016). Numerical investigation of the uplift capacity of inclined anchor plates in sand. *Proceedings of the 4th International Conference on New Developments in Soil Mechanics and Geotechnical Engineering, North Cyprus.* https://www.researchgate.net/publication/309634876_Numerical_Investigation_of_the_Uplift_Capacity_of_Inclined_Anchor_Plates_in_Sand

Goel, S., Shalini & Patra, N.R. (2006). Break out resistance of inclined anchors in sand. *Geotechnical & Geological Engineering, Vol. 24*, 1511–1525. https://doi.org/10.1007/s10706-005-2634-4

Macdonald, H.F. (1963). *Uplift resistance of caisson piles in sand* [Master's thesis, Nova Scotia Technical College, Canada].

Meyerhof, G.G. (1973). Uplift resistance of inclined anchors and piles. *Proceedings of the 8th International Conference on Soil Mechanics and Foundation Engineering, Moscow, Vol. II,* pp 167–172. https://www.issmge.org/uploads/publications/1/37/1973_04_0026.pdf

Meyerhof, G.G. & Adams, J.I. (1968). The ultimate uplift capacity of foundations. *Canadian Geotechnical Journal, Vol. V Issue 4,* 225-244. https://cdnsciencepub.com/doi/10.1139/t68-024

Murray, E.J. & Geddes, J.D. (1987). Uplift of anchor plates in sand. *Journal of Geotechnical Engineering*, *Vol. 113 Issue 3*, 202-215. https://ascelibrary.org/doi/10.1061/%28ASCE%290733-9410%281987%29113%3A3%28202%29

Murray, E.J. & Geddes, J.D. (1989). Resistance of passive inclined anchors in cohesionless medium. *Géotechnique, Vol. 39 Issue 3*, 417-431. https://www.icevirtuallibrary.com/doi/abs/10.1680/geot.1989.39.3.417

Rowe, R.K. & Davis, E.H. (1982). The behaviour of anchor plates in sand. *Géotechnique, Vol. 32 Issue 1*, 25-41. https://www.icevirtuallibrary.com/doi/10.1680/geot.1982.32.1.25

Sutherland, H.B. (1965). Model studies for shaft rising through cohesionless soils. *Proceedings of the 6th ICSMFE, Vol. II*, 410–413.

Bibliography

Aldaikh, H., Knappett, J., Brown, M., & Patra, S. (2014). Evaluation of monotonic ultimate pullout capacity of plate anchors in sand. *Advances in Soil Mechanics and Geotechnical Engineering, Vol. III,* 291-297. https://ebooks.iospress.nl/publication/36788

Bhattacharya, P. & Kumar, J. (2016). Uplift capacity of anchors in layered sand using finite-element limit analysis: Formulation and results. *International Journal of Geomechanics, Vol. 16, Issue 3*, 04015078. https://doi.org/10.1061/(ASCE)GM.1943-5622.0000560

Dickin, E.A. (1988). Uplift behavior of horizontal anchor plates in sand. *Journal of Geotechnical Engineering*, *Vol. 114 Issue 11*, 1300-1317. https://ascelibrary.org/doi/10.1061/%28ASCE%290733-9410%281988%29114%3A11%281300%29

Foriero, A. (1985). *Pullout capacity of inclined strip anchor plates in sand.* [Master's thesis, Concordia University, Montreal, Quebec, Canada]. https://spectrum.library.concordia.ca/4042/1/ML23160.pdf

Frgic, L., Marovic, P. & Tor, K. (2004). Pullout capacity of spatial anchors. *Engineering Computations*, *Vol. 21 Issue 6*, 598-609. https://doi.org/10.1108/02644400410545182

Frydman, S. & Shaham, I. (1989). Pullout capacity of slab anchors in sand. *Canadian Geotechnical Journal, Vol. 26, Issue 3*, 385-400. https://doi.org/10.1139/t89-053

Ilamparuthi, K., Dickin, E.A., & Muthukrisnaiah, K. (2011). Experimental investigation of the uplift behaviour of circular plate anchors embedded in sand. *Canadian Geotechnical Journal, Vol. 39 Issue 3,* 648-664. https://cdnsciencepub.com/doi/10.1139/t02-005

Kumar, J. & Sahoo, J.P. (2012). Upper bound solution for pullout capacity of vertical anchors in sand using finite elements and limit analysis. *International Journal of Geomechanics, Vol. 12, Issue 3*, 333-337. https://doi.org/10.1061/(ASCE)GM.1943-5622.0000160

Kumar, J. & Subba Rao, K.S. (1994). Vertical uplift capacity of horizontal anchors. *Journal of Geotechnical Engineering, Vol. 120, Issue 7*, 1134-1147. https://doi.org/10.1061/(ASCE)0733-9410(1994)120:7(1134)

Merifield, R.S, & Sloan, S.W. (2006). The ultimate pullout capacity of anchors in frictional soils. *Canadian Geotechnical Journal, Vol. 43, Issue 8*, 852-868. https://doi.org/10.1139/t06-052

Murray, E.J. & Geddes, J.D. (1991). Passive inclined anchorages in sand. *Journal of Geotechnical Engineering*, *Vol. 117 Issue 5*, 810-814. https://ascelibrary.org/doi/abs/10.1061/(ASCE)0733-9410(1991)117:5(810)

Rowe, R.K., Booker, J.R., & Balaam, N.P. (1978). Application of the initial stress method to soil-structure interaction. *International Journal for Numerical Methods in Engineering, Vol. 12 Issue 5,* 873-880. https://doi.org/10.1002/nme.1620120511

Schanz, T. & Vermeer, P.A. (1996). Angles of friction and dilatancy of sand. *Géotechnique, Vol. 46 Issue 1*, 141-151. https://doi.org/10.1680/geot.1996.46.1.145

Singh, B. & Mistri, B. (2011). A study on load capacity of horizontal and inclined plate anchors in sandy soils. *International Journal of Engineering Science and Technology, Vol. III Issue 9,* 6914-6922. https://www.idc-online.com/technical_references/pdfs/civil_engineering/A%20STUDY%20ON%20LOAD.pdf

Singh, B., Mistri, B., & Patel, R. (2010). A study on pullout capacity of horizontal and inclined plate anchors for offshore installations. *Proceedings of The International Conference on Marine Technology, Bangladesh*, 453–458.

Tagaya, K., Tanaka, A., & Aboshi, H. (1983). Application of finite element method to pullout resistance of buried anchor. *Japanese Society of Soil Mechanics and Foundation Engineering, Vol. 23 Issue 3,* 91-104. https://doi.org/10.3208/sandf1972.23.3_91.

U.S. Naval Civil Engineering Laboratory. (1966). Bureau of Yards and Docks. Technical report R434: Deadman anchorages in various soil mediums. https://apps.dtic.mil/dtic/tr/fulltext/u2/631848.pdf

Appendix A: Sample Calculation

Problem Definition

See Figure 30 for variable definition

Geometry

Anchor embedment	$D := 9ft$		
Anchor height H = width B	$H := 3ft$	Embedment ratio	$\frac{D}{H} = 3$
Anchor length	$L := 10ft$		
Pullout angle	$\theta := 35deg$		

Material Properties

Soil:

Angle of internal friction	$\phi := 33deg$
Unit weight	$\gamma_s := 115pcf$
Modulus of elasticity	$E := 200000psf$
Poisson's ratio	$\upsilon := 0.334$

Anchor:

Unit weight	$\gamma_a := 150pcf$
Soil-concrete friction angle	$\delta := 29deg$

Bridges to Prosperity (B2P) Method

Sliding Resistance Check (Horizontal Forces)

Equation 9 $W_{anchor} := \gamma_a \cdot H^2 \cdot L = 1.35 \times 10^4 lbf$

Equation 10 $W_{soil} := \gamma_s \cdot H \cdot L \cdot (D - H) = 2.07 \times 10^4 lbf$

Equation 11 $K_a := \frac{1 - \sin(\phi)}{1 + \sin(\phi)} = 0.295$

Equation 12 $K_p := \frac{1 + \sin(\phi)}{1 - \sin(\phi)} = 3.392$

Equation 13 $P_{active} := \frac{1}{2} \cdot K_a \cdot \gamma_s \cdot (1.5H)^2 \cdot L + K_a \cdot \gamma_s \cdot (D - 1.5H) \cdot (1.5H) \cdot L = 1.03 \times 10^4 lbf$

Equation 14 $P_{passive} := \frac{1}{2} \cdot K_p \cdot \gamma_s \cdot (1.5H)^2 \cdot L + K_p \cdot \gamma_s \cdot (D - 1.5H) \cdot (1.5H) \cdot L = 1.185 \times 10^5 lbf$

Equation 17 $$P_{friction} := \frac{P_{passive} + W_{anchor}\cdot\tan(\delta) + W_{soil}\cdot\tan(\delta) - P_{active}}{\cos(\theta) + \sin(\theta)\cdot\tan(\delta)} = 1.118\times10^{5}\ \text{lbf}$$

Uplift Resistance Check (Vertical Forces)

Equation 21 $$P_{uplift} := \frac{W_{anchor} + \left[\frac{2H + (D-H)\cdot\tan(30\text{deg})}{2}\cdot(D-H)\cdot L\cdot\gamma_s\right]}{\sin(\theta)} = 8.046\times10^{4}\ \text{lbf}$$

Ultimate Pullout Resistance following B2P

$$P_{ult.B2P} := \min\left(P_{friction}, P_{uplift}\right) = 8.046\times10^{4}\ \text{lbf}$$

Meyerhof's Method (adapted) using Limit Equilibrium

From Figure 31: $K_b := 1.9$

Equation 22 $$P_{ult.Meyerhof} := L\cdot\left[\frac{1}{2}\cdot K_b\cdot\gamma_s\cdot D^2 + \gamma_s\cdot D\cdot H\cdot\sqrt{2}\cdot(\cos(90\text{deg} - \theta))^2\right] = 1.029\times10^{5}\ \text{lbf}$$

GEO-SLOPE SIGMA/W Design Charts Method

From Figure 67: $Dimensionless\_Load\_Coefficient := 10.2$

$$P_{ult} := Dimensionless\_Load\_Coefficient\cdot\gamma_s\cdot L\cdot H^2 = 1.056\times10^{5}\ \text{lbf}$$

Comparison of Results

B2P $P_{ult.B2P} = 8.046\times10^{4}\ \text{lbf}$

Meyerhof $P_{ult.Meyerhof} = 1.029\times10^{5}\ \text{lbf}$

Design Charts $P_{ult} = 1.056\times10^{5}\ \text{lbf}$

Project Approval Form

Civil Engineering

Capstone Report Approval Form

Master of Science in Civil Engineering – MSCVE

Milwaukee School of Engineering

This capstone report, entitled "Pullout Capacity of Reinforced Concrete Deadman Anchors in Cohesionless Soil," submitted by Riley Padron, has been approved by the following committee:

Faculty Advisor:_____ Date:_____

Dr. Todd Davis, Ph.D.

Faculty Member:_____ Date:_____

Dr. Douglas Stahl, Ph.D.

Faculty Member:_____ Date:_____

Dr. Richard DeVries, Ph.D.